AD

MECHANICS OF THROUGH-THICKNESS REINFORCED LAMINATES: DELAMINATION AND DYNAMIC RESPONSE

Final Technical Report

by

Roberta Massabò

(December 2002)

United States Army
EUROPEAN RESEARCH OFFICE OF THE U.S. ARMY
London, England
Contract number N68171-01-M-5909
R&D 9084-AN-01

Giovanni Solari (contractor)
University of Genova, Italy
Roberta Massabò (PI)

Approved for Public Release; distribution unlimited

REPORT DOCUMENTATION PAGE

Form Approved
OMB No. 0704-0188

1. AGENCY USE ONLY (Leave blank)	2. REPORT DATE	3. REPORT TYPE AND DATES COVERED
		FINAL - October 23, 2002 - December 23, 2002

4. TITLE AND SUBTITLE
Mechanics of through-thickness reinforced laminates: delamination and dynamic response

5. FUNDING NUMBERS
C- N68171-01-M-5909

6. AUTHOR(S)
Roberta Massabò - Principal Investigator
Giovanni Solari - Contractor

7. PERFORMING ORGANIZATION NAME(S) AND ADDRESS(ES)
Department of Structural and Geotechnical Engineering
University of Genova
Via Montallegro, 1, 16145, Genova
Italy

8. PERFORMING ORGANIZATION REPORT NUMBER
10-2001 DISEG
ERO-4

9. SPONSORING / MONITORING AGENCY NAME(S) AND ADDRESS(ES)
European Research Office of the U.S. Army
223, Old Marylebone Road
London, NW1 5TH, England

10. SPONSORING / MONITORING AGENCY REPORT NUMBER

11. SUPPLEMENTARY NOTES

12a. DISTRIBUTION / AVAILABILITY STATEMENT
Approved for Public release; distribution unlimited.

12b. DISTRIBUTION CODE

13. ABSTRACT *(Maximum 200 Words)*

Through-thickness reinforcement (stitching, z-pins, weaving) is a promising technology to develop fail-safe load bearing components for aeronautical structures and lightweight armor and combat vehicles with superior capabilities. The through-thickness reinforcement enhances the performance of laminates against delamination failure, improving impact and damage tolerance and rendering stable or even suppressing crack propagation. The purpose of the work was to investigate basic aspects of the mechanics of through-thickness reinforced laminates. Focus has been on two problems. 1) The definition and validation of approximate mode I weight functions for orthotropic double cantilever beams. The weight functions allow the problem of large scale bridging delamination to be formulated as integral equations overcoming the limitations of beam theory approximations. 2) The formulation of a theoretical model to investigate the effectiveness of a through-thickness reinforcement in reducing the delamination-induced degradation of the dynamic properties of delaminated structures. The work performed under this contract has been published in [1-4].
KEYWORDS: through-thickness reinforcement; advanced composite laminates; delamination fracture; free vibrations; weight function methods; plate theories.

14. SUBJECT TERMS	15. NUMBER OF PAGES
	16. PRICE CODE

17. SECURITY CLASSIFICATION OF REPORT	18. SECURITY CLASSIFICATION OF THIS PAGE	19. SECURITY CLASSIFICATION OF ABSTRACT	20. LIMITATION OF ABSTRACT

NSN 7540-01-280-5500

Standard Form 298 (Rev. 2-89)
Prescribed by ANSI Std. Z39-18
298-102

ABSTRACT

Through-thickness reinforcement (stitching, z-pins) is a promising technology to develop fail-safe load bearing components for aeronautical structures and lightweight armor and combat vehicles with superior capabilities. The through-thickness reinforcement enhances the performance of laminates against delamination failure, improving impact and damage tolerance and rendering stable or even suppressing crack propagation. The through-thickness reinforcement creates large zones of bridging along the wake of the cracks developing tractions that reduce the crack driving force.

The purpose of the work was to investigate basic aspects of the mechanics of through-thickness reinforced laminates. Focus has been on two problems.

1) The definition and validation of approximate mode I weight functions for orthotropic double cantilever beams. The weight functions allow the problem of large scale bridging delamination of composite laminates to be formulated as integral equations overcoming the limitations imposed on accuracy by beam theory approximations. The weight functions have been deduced from the corresponding isotropic result using an orthotropy rescaling technique and have been applied to investigate the influence of the orthotropy on the fracture behavior of laminates in the presence of Dugdale's type crack bridging mechanisms.

2) The formulation of a theoretical model to investigate the effectiveness of a through-thickness reinforcement in reducing the delamination-induced degradation of the dynamic properties of delaminated structures. The model is based on the first order shear deformation plate theory and deals with plates with through-width delaminations. The bridging mechanisms are modeled as a uniform distribution of linear elastic springs that oppose the relative crack displacements. The model has been applied to predict the free vibrations of a delaminated cantilever beam. A variety of solutions and transitions in the dynamic response has been found on varying the stiffness of the ligaments. An application to a stitched carbon-epoxy laminate for the aeronautical industry shows that low area fractions of through-thickness reinforcement can substantially improve the dynamic response of delaminated structures and almost entirely restore their integrity.

KEYWORDS: through-thickness reinforcement; advanced composite laminates, delamination fracture; free vibrations; weight function methods; plate theories.

TABLE OF CONTENTS

	SECTION/PAGE NUMBER
Front Cover	1
Standard Form SF298	2
Abstract	3
Table of Contents	4
Technical Report	5
Literature Cited	7
Credit	7
Appendices	8

List Appendix Items:
Paper [1] prepared under this contract
Paper [2] prepared under this contract
Abstract [3] prepared under this contract
Paper [4] prepared under this contract

TECHNICAL REPORT

BACKGROUND AND STATEMENT OF THE PROBLEM

The purpose of the work was to investigate basic aspects of the mechanics of through-thickness reinforced laminates. Through-thickness reinforcement (stitching, z-pins) is a promising technology to develop fail-safe load bearing components for aeronautical structures and lightweight armor and combat vehicles with superior capabilities. A wide body of theoretical and experimental research has been produced over the last ten years that leaves no doubt that a through-thickness reinforcement substantially enhances the performance of laminates against delamination failure, improving impact and damage tolerance and rendering stable or even suppressing crack propagation (see references cited in [1-4]). The through-thickness reinforcement creates large zones of bridging along the wake of the cracks developing tractions that oppose the relative crack displacement and reduce the driving force for crack propagation.

In this project focus has been on two problems.

1) The definition and validation of approximate mode I weight functions for orthotropic double cantilever beams.

The weight functions allow the problem of large scale bridging delamination of composite laminates to be formulated as integral equations overcoming the limitations imposed on accuracy by beam theory approximations. Such an approach will permit the simulation of unusual phenomena of crack face closure and crack propagation in the presence of regions of contact that have been recently observed in tests performed on through-thickness reinforced laminates and that cannot be properly described by approximate theories.

2) The formulation of a theoretical model to investigate the effectiveness of a through-thickness reinforcement in reducing the delamination-induced degradation of the dynamic properties of delaminated structures.

It is expected that a through-thickness reinforcement would reduce the degradation of the dynamic properties of delaminated structures through the development of tractions acting along the surfaces of the delamination and opposing the relative crack displacements (opening and sliding). This problem has been investigated under this contract and the effects of a through-thickness reinforcement quantified through the proposed model.

APPROACH

1) The weight functions have been deduced from the corresponding isotropic result using an orthotropy rescaling technique and numerical results to match asymptotic solutions. The weight functions have been used in the formulation of a nonlinear fracture mechanics model where the problem has been posed as integral equations in terms of crack tip stress intensity factors. (see [1,3] for details)

2) A model based on the first order shear deformation plate theory has been formulated to analyze the dynamic response of plates in the presence of through-width delaminations. The bridging mechanisms are modeled as a uniform distribution of linear elastic springs that oppose the relative crack displacements and develop symmetric restoring forces during vibration. The model has been applied to predict the natural frequencies of vibration and modal shapes of a delaminated cantilever beam. The natural frequencies are defined through the solution of a boundary eigenvalue problem. An analytical solution has been found for the case of homogeneous material, negligible shear deformations, mid-plane delamination and *constrained model* assumption. A numerical procedure (based on a relaxation technique) has been formulated to solve general cases (see [2,4] for details).

RESULTS

During the course of the project three papers have been published (one in conference proceedings [4] and two in international journals [1,2]) where the results and conclusions of the work have been presented in great detail. A list of the main results obtained under this contract and future development of the work is given below:

1) Mode I weight functions for orthotropic double cantilever beams.

- Mode I weight functions have been derived and validated numerically that permit a single model to treat the progression from the initiation of a bridged crack to its propagation as a long crack with large scale bridging in orthotropic materials.

- A nonlinear fracture mechanics model has been formulated to analyze crack propagation under general large scale bridging conditions and results have been presented for the case of bridging mechanisms characterized by a Dugdale's type law.
- Based on the results obtained under this contract, work is currently in progress on the definition of mode II weight functions for orthotropic double cantilever beams. The weight functions will allow the analysis of crack propagation under mode I (double cantilever beams), mode II (end-notched flexural specimens) and mixed mode (mixed-mode bending specimen) conditions.
- The procedure proposed in [1] will be extended to define mode I weight functions for dynamic crack propagation.

2) *Dynamic response of delaminated beam-type structures in the presence of through-thickness reinforcement*

- A theoretical model has been formulated to analyze the free vibration response of composite laminate beam-type structures in the presence of linear-elastic crack bridging mechanisms acting along the crack surfaces.
- The model has been applied to the case of a cantilever beam and a variety of solutions and transitions in the dynamic response has been found on varying the stiffness of the ligaments.
- An application to a stitched carbon-epoxy laminate for the aeronautical industry has shown that low area fractions of through-thickness reinforcement can substantially improve the dynamic response of delaminated structures and almost entirely restore their integrity; in particular it has been observed that the *opening modes* are completely avoided in the presence of crack bridging mechanisms.
- Based on the results obtained under this contract, work is currently in progress to investigate and summarize the effectiveness of a through-thickness reinforcement for different boundary conditions, positions and lengths of the delamination in plates vibrating in cylindrical bending. This summary will be used to guide the optimal design of through-thickness reinforced structures. Future development will be in the investigation of the dynamic response of delaminated structures in the presence of nonlinear crack bridging mechanisms.

DIVULGATION OF THE RESULTS

Apart from being published in [1-4], the work completed during the project has been presented at three conferences:

- *10th Int. Congress of Fracture, ICF10*, December 2001, Honolulu, USA.
- *15th ASCE Engineering Mechanics Conference*, June 2002, New York, USA
- *14th US National Congress of Theoretical and Applied Mechanics*, July 2002, Blacksburg, VA, USA (special symposium on Impact of Composites).

LITERATURE CITED

[1] Massabò, R., Brandinelli, L., and Cox B.N. (2002), Mode I Weight Functions for an Orthotropic Double Cantilever Beam, *International Journal of Engineering Science,* in press. (*prepared under this contract and appended*)

[2] Brandinelli, L., Massabò, R., (2002), Free vibrations of delaminated beam-type structures with crack bridging, *Composite Structures* in press. (*prepared under this contract and appended*)

[3] Massabò, R., and Brandinelli, L., (2002), Delamination and dynamic response of through-thickness reinforced delaminated composites, book of abstracts, 14th US National Congress of Theoretical and Applied Mechanics, Blacksburg, June 2002. (*prepared under this contract and appended*)

[4] Brandinelli, L., and Massabò, R. (2002), Free vibrations of through-thickness reinforced delaminated beams, proceedings of the *15th ASCE Engineering Mechanics Conference*, June 2-5th, 2002, New York, USA, CDrom, ASCE. (*prepared under this contract and appended*)

The research reported in this document and published in [1-4] has been sponsored in part by the United States Army through its European Research Office.

APPENDIXES

- Paper [1] prepared under this contract
- Paper [2] prepared under this contract
- Abstract [3] prepared under this contract
- Paper [4] prepared under this contract

International Journal of Engineering Science, 2002, in press.

Mode I Weight Functions for an Orthotropic Double Cantilever Beam

R. Massabò [1*], L. Brandinelli [1], and B. N. Cox [2]
[1] Department of Structural and Geotechnical Engineering,
University of Genova, Genova, 16145, Italy
[2] Rockwell Scientific Co., Thousand Oaks, CA 91360, USA

Abstract

Approximate weight functions are proposed and validated numerically for an orthotropic double cantilever beam loaded in mode I. They define the stress intensity factor at the crack tip due to a pair of point forces acting on the crack surfaces and have been deduced from the corresponding isotropic result using an orthotropy rescaling technique. The weight functions allow mode I large scale bridging problems in beams and plates to be formulated as integral equations, in terms of stress intensity factors at the crack tip, without the limitations imposed on accuracy by beam theory approximations. The proposed functions are applied to investigate the influence of the orthotropy of the material on the fracture behavior of double cantilever beams in the presence of large scale bridging.

Keywords: Weight function, beam theory, double cantilever beam, orthotropy rescaling, bridging mechanisms.

1. Introduction

Over the last decade, an interesting class of fracture mechanics problems has arisen in laminated beams and plates, in which nonlinear crack bridging or cohesive mechanisms act over several scales. One archetypal material system of particular engineering interest is laminated polymer composite plies reinforced through the thickness by stitches, pins, or other means. Another generic problem that is important in electronics and packaging is the separation of elastic materials connected by layers of viscous fluids or visco-plastic media such as solder. In all these delamination problems, crack wake mechanisms may include near tip processes and distinct processes acting over the far crack wake. In the case of polymer composites containing through-thickness reinforcement, the near tip process could

* To whom correspondence should be addressed.
Current address: Civil and Environmental Engineering Department, Northwestern University, 2145 Sheridan Rd., Evanston, IL 60208, USA. Email: r-massabo@northwestern.edu ; Phone / fax: 1 847 467 4105 / 1 847 491 4011;

be the formation of a craze zone, which is usually confined to a domain ~ 1 mm or less; while the far-wake process could be the action of the through-thickness reinforcement, which can extend over many tens of mm. Since the far-wake process covers a domain that is often much larger than the laminate half-thickness, h, the fracture problem can be analysed accurately using an appropriate order of beam theory. But if the crack is short (of the same order as or less than h), then beam theory fails and a more accurate method is needed to calculate either the crack tip energy release rate or the crack tip stress intensity factors. Greater accuracy is also required when addressing a near-tip process such as a craze zone, where, even for a long crack, beam theory gives too limited a description of near-tip fields to account accurately for the effects of the zone on the fracture parameters.

The finite element method (FEM) offers a popular and convenient numerical alternative to beam theory. However, in the presence of plane stress or plane strain conditions, FEM involves the solution of fully two-dimensional problems; and can present some tiresome meshing challenges, especially when the boundaries of the bridging or cohesive zones move during crack evolution. Moreover, where the bridging tractions depend on the crack displacement, which is commonly the case, the nature of singularities in the near-tip crack displacement can be difficult to resolve properly via FEM. This has led in some instances to inaccurate results appearing in the literature.

Thus motivation exists for reducing the problem of a bridged crack and cohesive zone to a system of integral equations by means of weight functions. Weight functions, even when expressed as engineering approximations, can be assured to have the correct asymptotic forms and therefore offer the greatest control in numerical methods over singularities either at the crack tip or at discontinuities in the bridging mechanism in the crack wake. For special cases, the integral equation formulation leads to closed form solutions. Furthermore, the integral equation formulation reduces plane problems to one-dimensional problems, with distance from the crack tip the only spatial variable. This allows very rapid scanning of large quantities of parametric problems.

For mode I fracture problems, the required weight function expresses the mode I crack tip stress intensity factor generated by a pair of unit point forces acting normally to the fracture surfaces at any given distance from the crack tip. From this weight function, the net crack tip stress intensity factor due to the combined actions of an applied load and all bridging or cohesive mechanisms over all scales can be computed by simple superposition and the crack opening profile, by, for example, an application of Castigliano's theorem (e.g., [1,2]).

For special problems of cracks in infinite or semi-infinite bodies or cracks in long strips that are propagating across the strip, the definition of the mode I weight function is greatly simplified by the

observation, based on analytical results and fairly extensive numerical studies, that the weight function is independent or almost independent of the degree of anisotropy in an orthotropic body (provided the crack plane is aligned with a plane of elastic symmetry) ([3,4]. Thus weight functions evaluated for isotropic bodies can be used with good accuracy in more general cases. The only appearance of the degree of anisotropy is in the elastic constant that relates the crack tip stress intensity factor to the energy release rate.

In contrast, in plates or beams such as a double cantilever beam (DCB) specimen, a strong dependence on anisotropy does exist and, one suspects for this reason, no reasonably simple expression for the weight function for an orthotropic DCB has appeared in the literature. Since the degree of anisotropy in a common laminate material can be high, especially for a polymer composite but also for structural ceramic composites or layered systems in electronics, treating the effect of anisotropy on the weight function is essential to establishing an accurate integral equation formulation. This problem is taken up here. The required approximation to the weight function, which is canonical in the sense that it retains all the asymptotic features and the essential mathematical form of the exact solution, is derived from heuristic consideration of the weight function for an isotropic DCB specimen and the implications of orthotropy rescaling. An approximate weight function is also proposed and validated numerically for the special case of short cracks (much less than the laminate thickness) in isotropic and degenerate orthotropic DCB specimens. The last weight function will permit a single model to treat the progression from the initiation of a bridged crack to its propagation as a long crack with large scale bridging.

2. Mode I crack tip stress intensity factor in isotropic double cantilever beams

An exact solution for the stress intensity factor K_{IP} due to a pair of concentrated forces P applied per unit width onto the crack faces of a double cantilever beam at a distance d from the crack tip has been obtained by Foote and Buchwald (see Fig. 1.a) [5]. They solved the plane elasticity problem by applying the Wiener-Hopf technique to an isotropic infinite strip arbitrarily loaded by opening tractions acting along the crack surfaces and representing the concentrated loads in terms of the Dirac delta function. The strip and the applied loads were assumed to be symmetric about the mid-plane. A simple formula approximating the exact solution, which has an accuracy of 1.1% and can be applied to double cantilever beams with an uncracked ligament $c > 2h$ and containing a sufficiently long crack is also given in [5]:

$$\frac{K_{IP}h^{0.5}}{P}=\sqrt{12}\frac{d}{h}\left(1+0.673\frac{h}{d}\right)+\sqrt{\frac{2h}{\pi d}}-\left[0.815\left(\frac{d}{h}\right)^{0.619}+0.429\right]^{-1} \quad , \qquad (1)$$

where h is the half thickness of the specimen. For very small d/h the dimensionless K_{IP} of Eq. (1) approaches the exact solution of Irwin for a semi-infinite crack in an infinite sheet [6]:

$$\frac{K_I h^{0.5}}{P}=\sqrt{\frac{2h}{\pi d}} \quad . \qquad (2)$$

For very large d/h, Eq. (1) approaches the elementary beam theory solution for an Euler-Bernoulli double cantilever beam with built-in ends, $K_I h^{0.5}/P = \sqrt{12}\, d/h$ [6]. For $d/h \geq 0.3$ the exact K_{IP} is also well represented, with an error always lower than 4%, by Gross and Srawley's boundary collocation solution, $K_I h^{0.5}/P = \sqrt{12}\,(d/h+0.687)$, which is obviously numerically close to the first bracketed term on the right hand side of Eq. (1) [6]. The same limit solution is given by the "augmented beam model" of Kanninen [7], which accounts for the elasticity of the uncracked ligament ahead of the crack tip and removes the assumption of built-in ends. The dimensionless stress intensity factor of Eq. (1) is shown in the semi-logarithmic diagram of Fig. 1.b along with the two limiting solutions for small and large d/h.

The study in [5] and Eq. (1) refer only to an infinite strip or a double cantilever beam with an infinitely long crack (the crack length a does not appears in Eq. (1)). A lower limit for the normalized crack length a/h of the double cantilever beam specimen must be set for Eq. (1) to be valid for all d/h, with $0 < d/h \leq a/h$. The asymptotic limit of Eq. (1) for very small d/h, given by Eq. (2), is in fact correct only if $a >> d$, and should be replaced by Tada's solution [6] for a finite crack of length a in a semi-infinite sheet when a/h also becomes very small:

$$\frac{K_I h^{0.5}}{P}=\frac{2\sqrt{h}}{\sqrt{\pi d}}\frac{1}{\sqrt{1+x_1/a}}\left[1.3-0.3\left(\frac{x_1}{a}\right)^{5/4}\right] \quad , \qquad (3)$$

where $x_1 = a - d$ is the distance of the applied forces from the crack mouth. The value of K_I given in Eq. (3) ranges between the value given in Eq. (2), for $a >> d$, and 1.84 times the value of Eq. (2), for $a = d$.

A conservative lower limit for a/h for the applicability of Eq. (1) can be set as $a/h = 0.3$, so that when $d/h = a/h = 0.3$, Gross and Srawley's solution is already approached by the exact solution and the error is lower than 4%. This lower limit has been validated through finite element calculations which also

showed that the relative error between the predictions of Eq. (1) and the finite element results is within 1.5% for all normalized crack lengths $a/h \geq 0.35$ (see Appendix B).

3. Mode I crack tip stress intensity factor in orthotropic double cantilever beams

A double cantilever beam with a crack of length a loaded by a pair of opening forces P_i acting per unit width at the coordinate x_{1i} is shown in Fig. 2.a. Plane stress conditions are assumed in the plane x_1-x_3. The material is linearly elastic and orthotropic with principal material axes x_1 and x_3.

As shown in Appendix A, the response of the beam, and in particular the stress intensity factor at the crack tip K_{Ii}, is controlled by two dimensionless material parameters, λ and ρ, which depend on the four elastic constants of plane orthotropic elasticity. In terms of the engineering constants, λ and ρ take the form:

$$\lambda = \frac{E_3}{E_1}, \qquad \rho = \frac{\sqrt{E_1 E_3}}{2G_{13}} - \sqrt{\nu_{13}\nu_{31}}, \qquad n = \sqrt{\frac{1+\rho}{2}} \quad , \tag{4.a}$$

where E_1 and E_3 are the Young's moduli in the x_1 and x_3 directions, G_{13} is the shear modulus and ν_{13} and ν_{31} are Poisson's ratios in the plane x_1-x_3. The parameter n, which depends on ρ and will be used in the following, is also introduced in (4.a). To ensure the positive definiteness of the strain energy density function, the orthotropy ratios are such that $\lambda > 0$ and $\rho > -1$. In typical woods and composites ρ is in the range $0 < \rho < 5$ and λ in the range $0 < \lambda < 20$, with $\lambda < 1$ for fiber reinforced laminated composites.

For plane strain conditions, the parameters λ and ρ are again given by (4.a) but substituting the plane strain constants:

$$E_{1ps} = \frac{E_1}{(1-\nu_{12}\nu_{21})}, \quad E_{3ps} = \frac{E_3}{(1-\nu_{23}\nu_{32})}, \quad \nu_{13ps} = \frac{(\nu_{13}+\nu_{12}\nu_{23})}{(1-\nu_{12}\nu_{21})}, \quad \nu_{31ps} = \frac{(\nu_{31}+\nu_{32}\nu_{21})}{(1-\nu_{32}\nu_{23})}, \tag{4.b}$$

for E_1, E_3, ν_{13} and ν_{31}.

In the case of isotropy, $\lambda = \rho = 1$ and the stress intensity factor at the crack tip of the specimen of Fig. 2 is given by Eq. (1), with the substitutions $d = a - x_{1i}$ and $P = P_i$. The stress intensity factor for the case of orthotropy will be derived in the following.

3.1 Solution for orthotropic double cantilever beams with large notches

An expression for the strain energy release rate $\mathcal{G}_I$ in the orthotropic double cantilever beam specimen of Fig. 2.a has been obtained by Suo et al. [8] making use of the orthotropy rescaling technique and numerical calculations. The expression of $\mathcal{G}_I$ given in [8] depends on two terms: the first is the elementary beam theory result, which does not depend on the orthotropy and is an exact elasticity asymptote as $(a\text{-}x_{1i})/h \to \infty$; the second is a correction term which accounts for the influence of finite $(a\text{-}x_{1i})/h$. The expression proposed in [8] has an accuracy of 1% for all $(a\text{-}x_{1i})/h \geq 2\lambda^{-1/4}$ and $0 \leq \rho \leq 4$.

The stress intensity factor at the crack tip can be obtained from $\mathcal{G}_I$ of [8] using the orthotropic relationship between $\mathcal{G}_I$ and K_I:

$$K_I = \sqrt{\mathcal{G}_I E_1'} \quad , \tag{5.a}$$

where

$$E_1' = \frac{E_1 \lambda^{3/4}}{\sqrt{(1+\rho)/2}} = \frac{E_1 \lambda^{3/4}}{n} \quad . \tag{5.b}$$

In a dimensionless form, K_{Ii} is then given by:

$$\frac{K_{Ii} h^{0.5}}{P_i} = \frac{\lambda^{3/8}}{\sqrt{n}} \sqrt{12} \frac{a - x_{1i}}{h} \left(1 + Y_I(\rho)\, \lambda^{-1/4} \frac{h}{a - x_{1i}} \right) \quad , \tag{6}$$

where:

$$Y_I(\rho) = 0.677 + 0.146(\rho - 1) - 0.0178(\rho - 1)^2 + 0.00242(\rho - 1)^3 \quad , \tag{7}$$

is a correction term that accounts for the influence of ρ and has been obtained in [8] through finite element calculations. For an isotropic material, $\lambda = \rho = 1$, $Y_I(\rho) = 0.677$ and Eq. (6) coincides with Gross and Srawley's solution. The last term on the right hand side of Eq. (6) would not be present if the two delaminated beams were assumed to be Euler-Bernoulli beams built in at the crack tip. It describes the influence of the elasticity of the uncracked ligament ahead of the crack tip. It vanishes when the ratio $(a\text{-}x_{1i})/h$ becomes very large, because in this limit the condition of built-in ends becomes increasingly well satisfied.

Equations (5) and (6) correctly define the stress intensity factor and the strain energy release rate in conventional 2D laminates tested with typical notched specimens, for which $(a\text{-}x_{1i})/h \geq 2\lambda^{-1/4}$. On the other hand, Eq. (6) cannot be applied to investigate the influence of opening or closing forces acting very close to the crack tip such as those produced by the bridging mechanisms due to through-thickness reinforcement or crazing. To analyze these cases a solution for K_I valid over the whole range $(a\text{-}x_{1i})/h > 0$ is required.

3.2 Solution for degenerate orthotropic double cantilever beams

Consider the rescaled problem of Fig. 2.b where the x_1 axis of the problem of Fig. 2.a is rescaled as $\xi = \lambda^{1/4} x_1$. Following the orthotropy rescaling technique recalled in the Appendix A, the geometry and boundary conditions are rescaled in such a way that the crack length becomes $\lambda^{1/4}a$, the forces applied per unit width $\lambda^{-1/4}P_i$ and the stress intensity factor at the crack tip $\lambda^{-3/8}K_{Ii}$.

As shown in Appendix A, in a degenerate orthotropic solid characterized by $\rho = 1$, the rescaled problem in the plane ξ–x_3 is governed by the same equations of the original problem in an isotropic solid. Consequently, from Eq. (1), the rescaled stress intensity factor takes the form:

$$\lambda^{-3/8}K_{Ii} = \frac{\lambda^{-1/4}P_i}{h^{0.5}}\left\{\sqrt{12}\lambda^{1/4}\frac{(a-x_{1i})}{h}\left(1+\lambda^{-1/4}\frac{h}{(a-x_{1i})}0.677\right)+\right.$$
$$\left.+\sqrt{\frac{2h}{\pi\lambda^{1/4}(a-x_{1i})}}-\left[0.815\left[\lambda^{1/4}\frac{(a-x_{1i})}{h}\right]^{0.619}+\frac{1}{0.677\sqrt{12}}\right]^{-1}\right\}, \tag{8}$$

where the term 0.673 of Eq. (1) has been changed to 0.677 to satisfy Eqs. (6) and (7) for large $(a\text{-}x_{1i})/h$. In a dimensionless form, similar to that of Eq. (1), K_{Ii} becomes:

$$\frac{K_{Ii}h^{0.5}}{P_i} = \lambda^{3/8}\sqrt{12}\frac{a-x_{1i}}{h}\left(1+0.677\lambda^{-1/4}\frac{h}{a-x_{1i}}\right)+\sqrt{\frac{2h}{\pi(a-x_{1i})}}-$$
$$-\left[0.815\left(\lambda^{1/4}\frac{a-x_{1i}}{h}\right)^{0.619}\lambda^{-1/8}+\frac{0.4264}{\lambda^{1/8}}\right]^{-1} \tag{9}$$

Equation (9) is an exact extension of the isotropic result (1) to a degenerate orthotropic material. The equation has been validated through finite element calculations for λ varying in the range $0.025 \leq \lambda \leq 1.0$ and long enough cracks with error always within 2% (see Appendix B). The equation applies to beams with an uncracked ligament $c/h > 2\lambda^{-1/4}$.

Equation (9) includes the result expected for very small $(a\text{-}x_{1i})/h$, tending asymptotically to Irwin's solution of Eq. (2). In this limit, the stress intensity factor is not affected by the anisotropy of the material, as demonstrated by Sih et al. [3] for cracks in infinite sheets loaded by self-equilibrating loads acting on the crack surfaces. For large $(a\text{-}x_{1i})/h$, Eq. (9) approaches the solution of Suo et al., Eq. (6), with $\rho = n = 1$ and $Y_I(\rho) = 0.677$. Note that this upper limit as well as the connecting function given by the third term on the right hand side of Eq. (9) depend on the orthotropy of the material through λ. The dimensionless stress intensity factor of Eq. (9) is depicted in Fig. 3 for different values of λ. The dotted curves in the figure show the limiting solutions.

Equation (9) is correct for all $(a\text{-}x_{1i})/h$ provided the crack length a/h is higher than a limit value which the rules of orthotropy rescaling sets equal to $a/h = 0.35\lambda^{-1/4}$ for a 1.5% accuracy. Finite element calculations show that this is in fact a conservative limit for all cases with $\lambda < 1.0$ (see Appendix B).

3.3 Solution for orthotropic double cantilever beams

The stress intensity factor in generally orthotropic ($\lambda \neq 1$ and $\rho \neq 1$) double cantilever beams must approach the known asymptotic solutions for large and small $(a\text{-}x_{1i})/h$. For very small ratios $(a\text{-}x_{1i})/h$ the limit solution is given by Irwin's result for a semi-infinite crack in an infinite sheet, Eq. (2). As already noted, K_I in this limit does not depend on the elastic constants. For large $(a\text{-}x_{1i})/h$, the limit solution is given by Eq. (6). Solutions for intermediate values of $(a\text{-}x_{1i})/h$ require rigorous analyses of the problem which have been performed through finite element calculations. Only the effect of ρ needs to be calibrated numerically since the dependence of λ is known analytically and in materials with cubic symmetry, $\lambda = 1$, the plane elasticity problem is controlled by ρ alone (see Appendix A).

Based on these observations, the following expression is proposed as a canonical approximation to K_{Ii} for the degenerate orthotropic material, derived by modifying Eq. (9) to have the right asymptotic behavior and fit the finite element results:

$$\frac{K_{Ii}h^{0.5}}{P_i} = \frac{\lambda^{3/8}}{\sqrt{n}}\sqrt{12}\frac{a-x_{1i}}{h}\left(1+Y_I(\rho)\lambda^{-1/4}\frac{h}{a-x_{1i}}\right)+\sqrt{\frac{2h}{\pi(a-x_{1i})}} - \left[0.815\left(\frac{0.677}{Y_I(\rho)}\sqrt{n}\,\lambda^{1/4}\frac{a-x_{1i}}{h}\right)^{0.619}\lambda^{-1/8}+\frac{\sqrt{n}}{\sqrt{12}Y_I(\rho)\lambda^{1/8}}\right]^{-1} \quad (10)$$

The validity of Eq. (10) has been checked through finite element calculations for λ and ρ in the range $0.025 \leq \lambda \leq 1$ and $1 \leq \rho \leq 5$ with errors always less than 2%. Equation (9) is applicable for all ratios $(a\text{-}$

$x_{1i})/h$ provided the crack length a/h is higher than a limit value; the limit previously defined for the degenerate orthotropic materials, $a/h = 0.35\ \lambda^{-1/4}$, proves to be a conservative limit for all values of ρ (see Appendix B). As for the degenerate orthotropic material, Eq. (10) applies only to beams with uncracked ligaments $c/h > 2\lambda^{-1/4}$.

The dimensionless stress intensity factor of Eq. (10) is shown in Fig. 4 for $\lambda = 1$ and different values of the orthotropy parameter ρ to highlight the influence of ρ. For large ratios $(a-x_{1i})/h$, the effect of ρ becomes increasingly strong, as expected from Eq. (6), and the relative error between the exact solution and the solution for the degenerate orthotropic material becomes $(1-1/\sqrt{n})$. Thus only for rather small cracks, with $(a-x_{1i})/h < 0.7$, could the solution of Eq. (9) for the degenerate orthotropic solid ($\rho = 1$) be used for all values of ρ with acceptable error. For general cracks, Eq. (10) must be used. The dependence of the weight function on ρ for larger cracks is not shared by the strain energy release rate, $\mathcal{G}_I$, which becomes independent of ρ and λ when $(a-x_{1i})/h$ is large (see Eqs. (5-6)).

Figure 5 shows the dimensionless stress intensity factor of Eq. (10) for three pairs of λ and ρ representative of composites used in the aeronautical industry, $\lambda = 0.1$ and $\rho = 3$ (e.g. a quasi-isotropic carbon-epoxy laminate), $\lambda = 0.05$ and $\rho = 5$ (e.g. a unidirectional boron-epoxy laminate) and $\lambda = 1$ and $\rho = 1$ (an isotropic material).

4. Mode I crack tip stress intensity factor in double cantilever beams with short cracks

The stress intensity factors obtained in the previous sections refer to DCB specimens with normalized lengths of the crack higher than $a/h = 0.35\lambda^{-1/4}$. To the authors' knowledge there are no expressions available in the literature for cracks of lengths $a/h < 0.35\lambda^{-1/4}$, either for isotropic or orthotropic specimens. Knowing the expression of the stress intensity factors for cracks of any length can be useful in dealing with various mechanical problems, such as the problem of crack initiation.

In the case of isotropy, the problem is now controlled by two dimensionless variables, which define the normalized distance of the applied forces from the crack tip, $(a-x_{1i})/h$, and their relative position with respect to the crack length x_{1i}/a. This behavior can be observed in Eq. (3), which gives the asymptotic limit of the stress intensity factor for very small $(a-x_{1i})/h$. Equation (1) gives the exact stress intensity factor for very long cracks and it is therefore the asymptotic limit for $x_{1i}/a \rightarrow 1$ of the solution being sought. Equation (1) can then be modified as follows:

$$\frac{K_{Ii}h^{0.5}}{P}=\sqrt{12}\frac{a-x_{1i}}{h}\left(1+0.677\frac{h}{a-x_{1i}}\right)+\frac{2}{\sqrt{\pi}}\sqrt{\frac{h}{a-x_{1i}}}\left(1+\frac{x_{1i}}{a}\right)^{-1/2}\left[1.3-0.3\left(\frac{x_{1i}}{a}\right)^{5/4}\right]- \\ -\left[0.815\left(\frac{a-x_{1i}}{h}\right)^{0.619}f\left(\frac{x_{1i}}{a},\frac{a-x_{1i}}{h}\right)+0.4264\right]^{-1} \quad , \qquad (11)$$

where the second term on the right hand side has been changed from that given by Eq. (2) to that given by Eq. (3) and the multiplying function $f(x_{1i}/a, (a-x_{1i})/h)$ has been introduced in the third term. The function $f(x_{1i}/a, (a-x_{1i})/h)$ should be unity for $x_{1i}/a \rightarrow 1$, give the right asymptotic behaviors for large and small ratios $(a-x_{1i})/h$, and concur with numerical solutions for intermediate values of $(a-x_{1i})/h$ and $x_{1i}/a < 1$. The following is such a function:

$$f\left(\frac{x_{1i}}{a},\frac{a-x_{1i}}{h}\right)=g\left(\frac{x_{1i}}{a},\frac{a-x_{1i}}{h}\right)\left[1-\left(\frac{x_{1i}}{a}\right)^{6}\right]+\left(\frac{x_{1i}}{a}\right)^{6} \quad , \qquad (12.a)$$

with

$$g\left(\frac{x_{1i}}{a},\frac{a-x_{1i}}{h}\right)=\left(\frac{a-x_{1i}}{h}\right)^{-0.119}\left\{\left[A\exp\left[-B\ln\left(\frac{a-x_{1i}}{h}\right)\right]+C\right]^{-1}+D\right\} \quad , \qquad (12.b)$$

and

$$A=+2.9496\left(\frac{x_{1i}}{a}\right)^{3}-3.1554\left(\frac{x_{1i}}{a}\right)^{2}-0.5913\frac{x_{1i}}{a}+1.2101$$
$$B=-4.2955\left(\frac{x_{1i}}{a}\right)^{3}+6.6196\left(\frac{x_{1i}}{a}\right)^{2}-2.7173\frac{x_{1i}}{a}+1.4264$$
$$C=-2.3278\left(\frac{x_{1i}}{a}\right)^{3}+3.5239\left(\frac{x_{1i}}{a}\right)^{2}-1.6963\frac{x_{1i}}{a}+1.2934 \qquad (12.c)$$
$$D=-0.1127\left(1-\frac{x_{1i}}{a}\right)$$

The particular shape of the function $f(x_{1i}/a, (a-x_{1i})/h)$ has been chosen so that f is almost equivalent to g over most of the range $0 \le x_{1i}/a < 1$; and only for $x_{1i}/a \rightarrow 1$ becomes equal to 1. Equation (11) has an accuracy better than 2% for $x_{1i}/a \le 1$ and $(a-x_{1i})/h > 0$. It applies to beams with an uncracked ligament $c/h > 2$.

Figure 6 shows the dimensionless stress intensity factor of Eq. (11) as a function of the normalized distance of the applied forces from the crack tip, $(a-x_{1i})/h$, on varying x_{1i}/a. The figure highlights the expected variations in K_{Ii} with respect to the solution of Eq. (1), shown in the diagram as the curve marked $x_{1i}/a = 1$.

Following the procedure of Section 3.2, Eqs. (11)-(12) can be rescaled to define the mode I crack tip stress intensity factor in degenerate orthotropic DCB specimens:

$$\frac{K_{1i}h^{0.5}}{P}=\lambda^{3/8}\sqrt{12}\frac{a-x_{1i}}{h}\left(1+0.677\lambda^{-1/4}\frac{h}{a-x_{1i}}\right)+\frac{2}{\sqrt{\pi}}\sqrt{\frac{h}{a-x_{1i}}}\left(1+\frac{x_{1i}}{a}\right)^{-1/2}\left[1.3-0.3\left(\frac{x_{1i}}{a}\right)^{5/4}\right]- \\ -\left[0.815\lambda^{-1/8}\left(\lambda^{1/4}\frac{a-x_{1i}}{h}\right)^{0.619}f\left(\frac{x_{1i}}{a},\frac{a-x_{1i}}{h},\lambda\right)+\frac{0.4264}{\lambda^{1/8}}\right]^{-1} \quad (13)$$

with:

$$f\left(\frac{x_{1i}}{a},\frac{a-x_{1i}}{h},\lambda\right)=g\left(\frac{x_{1i}}{a},\frac{a-x_{1i}}{h},\lambda\right)\left[1-\left(\frac{x_{1i}}{a}\right)^{6}\right]+\left(\frac{x_{1i}}{a}\right)^{6}$$

$$g\left(\frac{x_{1i}}{a},\frac{a-x_{1i}}{h},\lambda\right)=\left(\lambda^{1/4}\frac{a-x_{1i}}{h}\right)^{-0.119}\left\{\left[A\exp\left[-B\ln\left(\lambda^{1/4}\frac{a-x_{1i}}{h}\right)\right]+C\right]^{-1}+D\right\} \quad (14)$$

Equation (13) has been validated through finite element calculations for λ varying in the range $0.025 \le \lambda \le 1.0$ with error always less than 2%. It applies to beams with an uncracked ligament $c/h > 2\lambda^{-1/4}$. The influence of λ on the solution is similar to that already observed in Figure 3. The extension of Eq. (13) to a generally orthotropic material is more complicated.

5. Summary of mode I weight functions for orthotropic double cantilever beams

The stress intensity factors calculated in the previous section define the mode I weight functions for double cantilever beams with a mid-plane crack of length a, $h_I(x_{1i},a,h,\rho,\lambda) = K_{Ii} / P_i$, where K_{Ii} is given by Eq. (1) and Eq. (11) for isotropic materials, by Eq. (9) and Eq. (13) for degenerate orthotropic and by Eq. (10) for generally orthotropic materials. The results are summarized in a dimensionless form in Table 1 and Table 2.

The weight functions allow the definition of the stress intensity factor, K_{Ip}, at the tip of the crack in double cantilever beams subject to general distributions of tractions, $p(x_1)$, acting along the crack faces:

$$K_{Ip} = \int_{a_0}^{x_{1f}} h_I(x_1, a, h, \rho, \lambda) p(x_1)\, dx_1 \quad , \tag{15}$$

where a_0 and x_{1f} are the limits of the loaded region. In large scale bridging problems a_0 typically represents the length of a notch or a region of the laminate where there are no active bridging mechanisms and x_{1f} is the tip of the crack (Fig. 7).

6. Fracture behavior of orthotropic double cantilever beams in the presence of large scale bridging

The weight functions derived above are applied in this Section to analyze crack growth in an orthotropic double cantilever beam with bridging mechanisms acting along the crack. The stress intensity factor at the crack tip of the beam when loaded by a pair of opening forces P, acting at the coordinate $x_1 = 0$, and by closing tractions p, acting along a-a_0 as shown in Fig. 7, is given by:

$$K_I = K_{IP} + K_{Ip} = K_{IP} - \int_{a_0/h}^{a/h} h_I(x_1/h, a/h, \rho, \lambda) h^{0.5} p(x_1)\, d(\frac{x_1}{h}) \quad , \tag{16}$$

where K_{IP} is given by Eq. (10) for $x_{1i} = 0$, and K_{Ip} is the stress intensity factor due to opening tractions p.

If the tractions p are created by through-thickness reinforcement or other bridging mechanisms acting along the crack surfaces, they depend on the crack opening displacement, u_3, and are a priori unknown. In particular, if $u_3(x_1) > 0$, then $p[u_3(x_1)] = p_3[u_3(x_1)]$ are closing tractions depicting the bridging mechanisms. The value of p_3 as a function of u_3 is defined through the bridging traction law, $p_3(u_3)$, which is deducible from micromechanical or macromechanical models and experiments (see [9] for the case of stitched laminates). If $u_3(x_1) = 0$, then $p[u_3(x_1)] = - p_c[(x_1)]$ are opening tractions depicting the effect of contact pressure arising along the crack.[1] The contact pressure and the size of the regions of contact or bridging are unknown a priori and can be determined through a compatibility condition for the crack opening displacement.

At the onset of crack propagation, K_I of Eq. (17) is equal to the intrinsic fracture toughness, $K_I = K_{Ic}$, and the dimensionless critical load for crack propagation takes the form:

[1] The existence of regions of contact along the surfaces of the crack in double cantilever beams in large scale bridging conditions has been observed experimentally in [10,11] and explained theoretically in [12].

$$\frac{P_{cr}}{K_{Ic}h^{0.5}} = \frac{1}{h_I(0,a/h,\rho,\lambda)h^{0.5}}\left\{1+\frac{p_{30}h^{0.5}}{K_{Ic}}\int_{a_0/h}^{a/h}\left[h_I(x_1/h,a/h,\rho,\lambda)h^{0.5}\,\frac{p[u_3(x_1/h)]}{p_{30}}\mathrm{d}(\frac{x_1}{h})\right]\right\}, \qquad (18)$$

where p_{30} is a normalizing value of the crack face tractions, p_3, given for instance by their maximum value. Recalling the expression for $E_1^{'}$ and that $K_{Ic} = \sqrt{\mathcal{G}_{Ic}E_1^{'}}$, Eq. (18) can be modified to facilitate direct comparison between isotropic and orthotropic cases:

$$\frac{P_{cr}}{\sqrt{\mathcal{G}_{Ic}E_1h}} = \frac{1}{h_I(0,a/h,\rho,\lambda)h^{0.5}}\left\{\frac{\lambda^{3/8}}{\sqrt{n}}+\frac{p_{30}h^{0.5}}{\sqrt{\mathcal{G}_{Ic}E_1}}\int_{a_0/h}^{a/h}\left[h_I(x_1/h,a/h,\rho,\lambda)h^{0.5}\,\frac{p[u_3(x_1/h)]}{p_{30}}\mathrm{d}(\frac{x_1}{h})\right]\right\}. \qquad (19)$$

As we will see later, the dimensionless number appearing within the right hand side of Eq. (18) and (19), $p_{30}h^{0.5}/\sqrt{\mathcal{G}_{Ic}E_1}$ or $p_{30}h^{0.5}\lambda^{3/8}/(K_{Ic}\sqrt{n})$, is a measure of the brittleness of the structure [13].

The crack opening displacement at the generic coordinate x_{1i} is defined as a function of the crack tip stress intensity factor and the elastic constants of the material through the following relationship:

$$u_3(x_{1i}) = u_3(x_{1i})_P + u_3(x_{1i})_p = \lambda_{iP}P - \int_{a_0}^{a}\lambda_{ij}p[u_3(x_{1j})]\,\mathrm{d}x_{1j} \qquad (20)$$

where λ_{ij} is the localized compliance, which defines the crack opening displacement at x_{1i} due to a pair of unit opening forces acting at x_{1j}. The localized compliance can be defined through an energy balance or Castigliano's theorem and is given by:

$$\lambda_{ij} = \frac{2}{E_1^{'}}\int_0^a h_I(x_{1i}/h,a'/h,\rho,\lambda)\;h_I(x_{1j}/h,a'/h,\rho,\lambda)\,\mathrm{d}a' \qquad (21)$$

where $E_1^{'}$ is the orthotropy constant of Eq. (5.b).

Once the crack opening displacement is known, the statically indeterminate problem defined by the nonlinear integral equations (19), (20) and (21) is solved for general bridging laws, $p_3(u_3)$, through a discretization. A self-consistent solution for the crack profile is obtained iteratively through a numerical procedure [1,2].

In the special case of bridging mechanisms described by a Dugdale type bridging law, $p_3 = p_{30}$, the bridging tractions do not depend on u_3 and Eq. (19) alone gives the dimensionless critical load for

crack propagation. The model predicts the absence of regions of contact for this case confirming the beam theory predictions of [12].

Figures 8.a, 8.b and 8.c show dimensionless diagrams of the critical load for crack propagation as a function of the normalized crack length in double cantilever beams with $a_0 = 0$. Three different values of the dimensionless parameter $p_{30}h^{0.5}/\sqrt{\mathcal{G}_{Ic}E_1}$ are considered, as marked. The curves (*a*), (*b*) and (*c*) in each diagram describe the response of an isotropic material, an orthotropic material with $\lambda = 0.1$ and $\rho = 3$ and an orthotropic material with $\lambda = 0.05$ and $\rho = 5$, respectively. The elementary beam theory curves, obtained in [12] assuming the two delaminated beams to be built in at the crack tip and neglecting shear deformations ($\gamma = 0$), are also shown in the diagrams. The influence of shear deformations ($\gamma \neq 0$) on the beam theory results is shown in Figure 8.b.

The response of the double cantilever beam is controlled by the dimensionless parameter $p_{30}h^{0.5}/\sqrt{\mathcal{G}_{Ic}E_1}$ and the two orthotropy ratios, λ and ρ. The three diagrams highlight a scaling transition in the macrostructural response of the beam which is typical of brittle matrix composites with Dugdale-type reinforcement [13]: the behavior changes from strain softening to strain-hardening on increasing the dimensionless group $p_{30}h^{0.5}/\sqrt{\mathcal{G}_{Ic}E_1}$. Moreover, if p_{30}, h and $\sqrt{\mathcal{G}_{Ic}E_1}$ are changed so as to keep the dimensionless group constant, the beams will experience the same type of response. As for the influence of λ and ρ, an increase in the degree of anisotropy leads to more ductile response (Fig. 8.a) and facilitates strain hardening behavior (Fig. 8.b-c).

The anisotropy of the material affects the response especially for relatively small values of *a/h*. In the case of large-scale bridging (Figs. 8.b-c), two different regimes of behavior are delineated by a transition value of $a/h = 1/(1.73p_{30}h^{0.5}/\sqrt{\mathcal{G}_{Ic}E_1})^{0.5}$, corresponding to the point where all curves cross each other. If *a/h* is smaller than the transition value, the anisotropy of the material strongly affects the response, and the elementary beam theory solution does not describe the actual behavior even qualitatively. For *a/h* larger than the transition value, all curves tend to become parallel, with a common slope given by $p_{30}h^{0.5}/(2\sqrt{\mathcal{G}_{Ic}E_1})$, and the deviation between the elementary beam theory solution and the correct solution becomes independent of the crack length and given by $1/2Y_I(\rho)\lambda^{-1/4}$ $p_{30}h^{0.5}/\sqrt{\mathcal{G}_{Ic}E_1}$. The fractional error is $Y_I(\rho)\lambda^{-1/4}/(a/h)$, which is independent of the intrinsic fracture toughness of the laminate, $\mathcal{G}_{Ic}$, and the magnitude of the bridging tractions and coincides with the analogous fractional error of the case with no bridging [8]. It depends only on the crack length and the degree of anisotropy. This error could be removed through the use of modified beam theories accounting for the influence of the elastic material ahead of the crack tip [7].

7. Conclusions

Canonical expressions for the mode I weight function for an orthotropic DCB specimen have been derived and validated by finite element methods. By combining results for short and long cracks, a set of expressions has been assembled that are collectively accurate to within 2% over a wide range of degrees of anisotropy. The canonical expressions retain the correct asymptotic limits for small and large cracks and special cases of elastic symmetry. Thus expedient and accurate study of singularities and other special characteristics of bridged crack problems can be based on their use.

The weight functions are the essential prerequisite for integral equation formulations of fracture problems in which bridging or cohesive mechanisms are present on small and large scales. The weight functions will allow equally accurate and convenient solution of crack initiation problems, in which the crack length remains smaller than or comparable to the laminate half-width; and large-scale bridging problems, in which bridging effects may extend over zones many tens of times the laminate half-width.

ACKNOWLEDGMENTS: RM and LB were supported by the European Research Office of the US Army, Contract number N68171-01-M-5909, and by the Italian Department for the University and for Scientific and Technological Research. BNC was supported by the U.S. Army Research Office, Contract Number DAAD19-99-C-0042 which also facilitated the international collaboration.

REFERENCES

1. Cox, B.N., and Marshall, D.B. (1991) Stable and unstable solutions for bridged cracks in various specimens. *Acta Metall. Mater.* **39**, 579-89.
2. Carpinteri, A., and Massabò, R. (1996) Bridged versus cohesive crack in the flexural behavior of brittle matrix composites, *Int. Journal of Fracture,* **81**, 125-145.
3. Sih, G.C., Paris, P.C., and Irwin, G.R., (1965), On cracks in rectilinear anisotropic bodies, *Int. J. of Fracture*, 1, 189-203.
4. H. A. Luo and R. Ballarini, (1994), The Effects of Anisotropy on the Nonlinear Behavior of Bridged Cracks in Long Strips, *J. Mech. Phys. Solids*, 42(2), 141-157.
5. Foote, R. M. L., and Buchwald, V.T., (1985), An exact solution for the stress intensity factor for a double cantilever beam, *Int. J. of Fracture*, 29, 125-134.
6. Tada, H., Paris, P.C. and Irwin, G.R. (1985) *The Stress Analysis of Cracks Handbook.* Paris Productions Inc., St. Louis, Missouri.

7. Kanninen, M.F. (1973), An augmented doucle cantilever beam model for studying crack propagation and arrest, *Int. Journal Fracture*, 9, 83-92.
8. Suo, Z., Bao, G., Fan, B., and Wang, T.C., (1991), Orthotropy rescaling and implications for fracture in composites, *Int. J. Solids Structures*, **28**(2), 235-248.
9. R. Massabò, D. R. Mumm, and B. N. Cox, "Characterizing Mode II Delamination Cracks in Stitched Composites," *Int. J. Fracture*, **92**, 1-38 (1998).
10. D.D.R. Cartié and I.K. Partridge, (1999), Delamination Behaviour of z-Pinned Laminates, *Proc. ICCM12*, Paris, July, 1999, ed., T. Massard, Woodhead Publishing Limited, Melbourne.
11. Rugg, K.L., Cox, B.N. and Massabò, R. (2001), Mixed mode delamination of polymer composite laminates reinforced through the thickness by z-fibers, *Composites, part A*, **33**/2, 177-190.
12. Massabò R. and B.N. Cox (2001), Unusual characteristics of mixed mode delamination fracture in the presence of large scale bridging, *Mech. Comp. Mater. Structures,* 8(1), 61-80.
13. Carpinteri, A., and Massabò, R. (1997) Continuous versus discontinuous bridged crack model for fiber-reinforced materials in flexure, *Int. Journal of Solids and Structures,* **34**(18), 2321-2338.
14. Suo, Z., (1990), Delamination specimens for orthotropic materials, *Journal of Applied Mechanics,* 57, 627-634.
15. ANSYS, release 5.5.3, Ansys Inc., Canonsburg, PA, U.S.A..
16. Shih, C.F., De Lorenzi, H.G. and German, M.D., (1976), Crack extension modelling with singular quadratic isoparametric elements, *Int. J. Fracture*, 12, 647-651.
17. Barsoum, R.S., Tringular Quarter-point elements as elastic and perfectly-plastic crack tip elements, *Int. J. Numerical Methods in Engineering,* 11, 85-98.
18. Sauma, V.E. and Sikiotis, E. S. (1986), Stress intensity factors in anisotropic bodied using singular isoparametris elements, *Engineering Fracture Mechanics*, 25(1), 115-121.
19. J.R. Rice, (1968), A path independent integral and the approximate analysis of strain concentration by notches and cracks, *Journal of Applied Mechanics,* 35, 379-386.

Appendix A – Orthotropy rescaling

An orthotropy rescaling technique has been proposed by Suo [14] to reduce plane elasticity problems for orthotropic materials to equivalent problems for materials with cubic symmetry.

For plane stress problems in the plane x_1–x_3, with x_1 and x_3 principal material axes and assuming negligible body forces, compatibility implies:

$$\frac{\partial^4 U}{\partial x_1^4} + 2\lambda^{1/2}\rho\frac{\partial^4 U}{\partial x_1^2 \partial x_3^2} + \lambda\frac{\partial^4 U}{\partial x_3^4} = 0 \tag{A.1}$$

where $U(x_1, x_3)$ is the Airy stress function, related to the in-plane stresses by:

$$\sigma_1 = \frac{\partial^2 U}{\partial x_3^2}, \quad \sigma_3 = \frac{\partial^2 U}{\partial x_1^2}, \quad \sigma_{13} = -\frac{\partial^2 U}{\partial x_1 \partial x_3}. \tag{A.2}$$

The dimensionless parameters λ and ρ in Eq. (A.1) depend on the elastic constants of the material and have been defined in the body of the text, Eq. (4.a).

Equation (A.1) shows that in orthotropic simply-connected sheets with tractions prescribed on the boundary, stresses depend on only two materials parameters, λ and ρ. Moreover, if the x_1 axis is rescaled as $\xi = \lambda^{1/4} x_1$, Eq. (A.1) shows dependency on ρ only:

$$\frac{\partial^4 U}{\partial \xi^4} + 2\rho\frac{\partial^4 U}{\partial \xi^2 \partial x_3^2} + \frac{\partial^4 U}{\partial x_3^4} = 0 \tag{A.3}$$

The boundary conditions for U can be rescaled accordingly to yield:

$$\sigma_1 = \frac{\partial^2 U}{\partial x_3^2}, \quad \lambda^{-1/2}\sigma_3 = \frac{\partial^2 U}{\partial \xi^2}, \quad \lambda^{-1/4}\sigma_{13} = -\frac{\partial^2 U}{\partial \xi \partial x_3} \tag{A.4}$$

Equations (A.1), (A.3) and (A.4) show that the orthotropic problem in the rescaled plane ξ–x_3 is reduced to the equivalent problem for a material with cubic symmetry, namely with $\lambda = 1$. Moreover, the special case of a degenerate orthotropic material, a material with $\rho = 1$, is governed in the rescaled plane by the same equation which governs the isotropic problem. Consequently, solutions for degenerate orthotropic materials can be readily constructed from the isotropic results.

Equations (A.3) and (A.4) also show that the stress intensity factors for a crack in the x_1 direction, K_I and K_{II}, being given by the limits for $x_1 \to 0$ of $(2\pi x_1)^{1/2}\sigma_3(x_1,0)$ and $(2\pi x_1)^{1/2}\sigma_{13}(x_1,0)$, respectively, rescale as $\lambda^{-3/8}K_I$ and $\lambda^{-1/8}K_{II}$. Moreover, the component of the resultant force on an arc T_3 rescale as $\lambda^{-1/4}T_3$ while the component T_1 remains unchanged.

Appendix B – Finite element validation

Finite element calculations were performed using ANSYS5.5 [15] in order to validate the proposed weight functions and their limit of applicability. The stress intensity factor generated by a pair of point forces acting along the crack surfaces has been calculated using two different techniques, the displacement correlation technique and the J-integral. The finite element meshes were composed of quadratic elements with a rosette of quarter-point elements at the crack tip that embody the linear elastic fracture mechanics square root singularity. Convergence studies were carried out for each loading configuration to define the necessary degree of refinement of the meshes.

The displacement correlation technique used here has been proposed by Shih et al. [16] on the basis of Barsoum's demonstration that quarter-point elements show the square root singularity of elastic fracture mechanics [17]. The technique has then been extended to anisotropic problems by Sauma and Sikiotis [18]. It allows the calculation of stress intensity factors performing simple post-processor operations on 4 nodal displacements of the quarter-point elements along the crack faces. The J-integral calculations [19] were performed following the procedure implemented in ANSYS5.5. The stress intensity factor was then extracted from $J = \mathcal{G}_I$ using the relationship (5.a). Due to the very fine meshes used in the analyses the two calculations yielded virtually identical results.

Validation of Eqs. (9) and (10) for large cracks

Table I shows normalized stress intensity factors and relative errors between FE calculations and Eq. (9) for a degenerate orthotropic material ($\rho = 1$) with different values of λ in the range $0.025 \le \lambda \le 1.0$ on varying $(a\text{-}x_{1i})/h$ in the range 0.01 – 5.0.

TABLE I

$\rho = 1$	$(a\text{-}x_{1i})/h$	5.0	2.0	1.0	0.5	0.3	0.1	0.05	0.01
$\lambda = 1$	FEM	19.666	9.273	5.793	4.112	3.564	3.605	4.314	8.303
	Eq. (9)	19.643	9.242	5.801	4.161	3.611	3.608	4.300	8.247
	Error (%)	0.116	0.342	-0.153	-1.168	-1.318	-0.085	0.309	0.682
$\lambda = 0.25$	FEM	12.271	6.092	4.019	3.103	2.879	3.278	4.090	8.208
	Eq. (9)	12.243	6.070	4.054	3.146	2.908	3.263	4.055	8.161
	Error (%)	0.197	0.348	-0.871	-1.384	-1.009	0.481	0.868	0.572
$\lambda = 0.025$	FEM	5.822	3.216	2.382	2.152	2.214	2.939	3.859	8.107
	Eq. (9)	5.802	3.224	2.434	2.173	2.218	2.915	3.825	8.074
	Error (%)	0.343	-0.247	-2.151	-0.977	-0.179	0.819	0.858	0.399

Table II shows normalized stress intensity factors and relative errors between FE calculations and Eq. (10) for a material with cubic symmetry ($\lambda = 1$) with different values of ρ in the range $1 \le \rho \le 5$ on varying $(a\text{-}x_{1i})/h$ in the range 0.01 – 5.0.

TABLE II

$\lambda = 1$	$(a\text{-}x_{1i})/h$	5.0	2.0	1.0	0.5	0.3	0.1	0.05	0.01
$\rho = 1$	See Table I								
$\rho = 3$	FEM	17.237	8.498	5.590	4.145	3.635	3.661	4.348	8.319
	Eq. (10)	17.178	8.408	5.494	4.099	3.634	3.685	4.353	8.286
	Error (%)	0.337	1.057	1.704	1.118	0.009	-0.629	-0.100	0.394
$\rho = 5$	FEM	16.138	8.241	5.566	4.247	3.750	3.736	4.400	8.341
	Eq. (10)	16.048	8.099	5.445	4.162	3.730	3.784	4.435	8.327
	Error (%)	0.555	1.725	2.172	2.00	0.517	-1.261	-0.788	0.170

Finally, Table III shows normalized stress intensity factors and relative errors between FE calculations and Eq. (10) for a generally orthotropic material with different values of λ and ρ in the range $0.025 \leq \lambda \leq 1.0$ and $1 \leq \rho \leq 5$ on varying $(a\text{-}x_{1i})/h$ in the range 0.01 – 5.0.

TABLE III

	$(a\text{-}x_{1i})/h$	5.0/6.0	2.0	1.0	0.5	0.3	0.1	0.05	0.01
$\lambda = 0.1$ $\rho = 3$	FEM	8.145	4.460	3.220	2.695	2.608	3.146	4.001	8.169
	Eq. (10)	8.086	4.390	3.197	2.700	2.627	3.152	3.991	8.142
	Error (%)	0.734	1.564	0.71	-0.186	-0.724	-0.206	0.235	0.332
$\lambda = 0.05$ $\rho = 5$	FEM	6.327	3.725	2.841	2.490	2.472	3.077	3.954	8.147
	Eq. (10)	6.235	3.646	2.817	2.501	2.500	3.101	3.961	8.132
	Error (%)	1.447	2.124	0.825	-0.454	-1.163	-0.781	-0.177	0.190
$\lambda = 0.025$ $\rho = 5$	FEM	5.165/5.837	3.132	2.477	2.254	2.299	2.984	3.891	8.118
	Eq. (10)	5.087/5.753	3.095	2.475	2.275	2.330	3.005	3.895	8.106
	Error (%)	1.508/1.433	1.202	0.0892	-0.942	-1.306	-0.705	-0.095	0.151

Validation of Eqs. (1), (9) and (10) for short cracks

To validate Eqs. (1), (9) and (10) for very short cracks and define the minimum crack length required for their applicability, the problem of a double cantilever beam loaded by a pair of concentrated forces acting at the coordinate $x_{1i} = 0$ has been considered and analyzed by the finite element method on varying the orthotropy ratios in the ranges $0.025 \leq \lambda \leq 1.0$ and $1 \leq \rho \leq 5$.

For an isotropic material, Eq. (1) proves to have an accuracy higher than 1.5% for all crack lengths higher than $a/h = 0.35$. For a degenerate orthotropic material, Eq. (9) proves to have an accuracy higher than 2% for all crack lengths higher than $a/h = 0.35\lambda^{-1/4}$. The same limit is also a conservative limit for generally orthotropic materials.

TABLE CAPTIONS

Table 1: Dimensionless mode I weight functions for isotropic, degenerate orthotropic and generally orthotropic double cantilever beams. Accuracy better than 2% for crack lengths $a/h \geq 0.35\lambda^{-1/4}$.

Table 2: Dimensionless mode I weight functions for isotropic and degenerate orthotropic double cantilever beams. Accuracy better than 2% for all crack lengths.

FIGURE CAPTIONS

Figure 1.a: Schematic of an infinitely long strip [5].

Figure 1.b: Solid curve: dimensionless stress intensity factor in the isotropic strip of Fig. 1.a (Foote and Buchwald and Eq. (1)). Dashed curves: limiting solutions for very small *d/h* (Irwin) and large *d/h* (Gross and Srawley).

Figure 2: a) Schematic of a double cantilever beam loaded by a pair of point forces P_i. b) Orthotropy rescaling: the geometry and boundary conditions are rescaled from the original problem a).

Figure 3: Dimensionless stress intensity factor in the degenerate orthotropic ($\rho = 1$) beam of Fig. 2.a , Eq. (9).

Figure 4: Dimensionless stress intensity factor in the orthotropic beam of Fig. 2.a with cubic symmetry ($\lambda = 1$), Eq. (10).

Figure 5: Dimensionless stress intensity factor in the orthotropic beam of Fig. 2.a, Eq. (10).

Figure 6: Dimensionless stress intensity factor in the isotropic beam of Fig. 2.a on varying x_{1i}/a, Eq. (11).

Figure 7: Schematic of a double cantilever beam in the presence of bridging mechanisms.

Figure 8: Dimensionless critical load versus normalized crack length in orthotropic DCB specimens: a) No bridging mechanisms, $p_{30}h^{0.5}/\sqrt{\mathcal{G}_{Ic}E_1} = 0.0$; b) $p_{30}h^{0.5}/\sqrt{\mathcal{G}_{Ic}E_1} = 0.1$; c) $p_{30}h^{0.5}/\sqrt{\mathcal{G}_{Ic}E_1} = 0.3$. (curves (a): $\lambda = 1$ and $\rho = 1$; curves (b) $\lambda = 0.1$ and $\rho = 3$; curves (c) $\lambda = 0.05$ and $\rho = 5$).

TABLE 1

Material:	Dimensionless Weight Function: $h_1(\frac{x_{1i}}{h},\frac{a}{h},\rho,\lambda)\,h^{0.5}$	Accuracy:
Isotropic [5]	$\sqrt{12}\frac{a-x_{1i}}{h}\left(1+0.677\frac{h}{a-x_{1i}}\right)+\sqrt{\frac{2h}{\pi(a-x_{1i})}}-\left[0.815\left(\frac{a-x_{1i}}{h}\right)^{0.619}+0.4264\right]^{-1}$	better than 1.5% for $a/h \geq 0.35$, $c/h \geq 2$.
Degenerate Orthotropic ($\rho=1$)	$\lambda^{3/8}\sqrt{12}\frac{a-x_{1i}}{h}\left(1+0.677\lambda^{-1/4}\frac{h}{a-x_{1i}}\right)+\sqrt{\frac{2h}{\pi(a-x_{1i})}}-\left[0.815\left(\lambda^{1/4}\frac{a-x_{1i}}{h}\right)^{0.619}\lambda^{-1/8}+\frac{0.4264}{\lambda^{1/8}}\right]^{-1}$	better than 2% for $0.025 \leq \lambda \leq 1$, $a/h \geq 0.35\lambda^{-1/4}$, $c/h \geq 2\lambda^{-1/4}$.
Orthotropic	$\frac{\lambda^{3/8}}{\sqrt{n}}\sqrt{12}\frac{a-x_{1i}}{h}\left(1+Y_1(\rho)\lambda^{-1/4}\frac{h}{a-x_{1i}}\right)+\sqrt{\frac{2h}{\pi(a-x_{1i})}}-\left[0.815\left(\frac{0.677}{Y_1(\rho)}\sqrt{n}\lambda^{1/4}\frac{a-x_{1i}}{h}\right)^{0.619}\lambda^{-1/8}+\frac{\sqrt{n}}{\lambda^{1/8}\sqrt{12}Y_1(\rho)}\right]^{-1}$	better than 2% for $0.025 \leq \lambda \leq 1$, $1 \leq \rho \leq 5$, $a/h \geq 0.35\lambda^{-1/4}$, $c/h \geq 2\lambda^{-1/4}$.

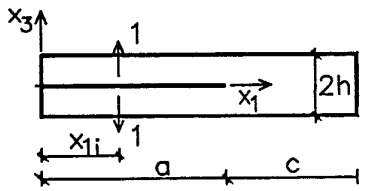

x_1 and x_3 = principal material axes

Notation:

$$Y_1(\rho) = 0.677 + 0.146(\rho-1) - 0.0178(\rho-1)^2 + 0.00242(\rho-1)^3$$

$$\lambda = \frac{E_3}{E_1}, \quad \rho = \frac{\sqrt{E_1 E_3}}{2G_{13}} - \sqrt{\nu_{13}\nu_{31}}, \quad n = \sqrt{\frac{1+\rho}{2}}$$

Plane Stress: E_1 and E_3 Young's moduli in x_1 and x_3 directions

G_{13} shear modulus in plane x_1-x_3, ν_{13} and ν_{31} Poisson's ratios in plane x_1-x_3

Plane Strain: substitute:

$$E_{1ps} = \frac{E_1}{(1-\nu_{12}\nu_{21})}, \quad E_{3ps} = \frac{E_3}{(1-\nu_{23}\nu_{32})}, \quad \nu_{13ps} = \frac{(\nu_{13}+\nu_{12}\nu_{23})}{(1-\nu_{12}\nu_{21})}, \quad \nu_{31ps} = \frac{(\nu_{31}+\nu_{32}\nu_{21})}{(1-\nu_{32}\nu_{23})}$$

for E_1, E_3, ν_{13} and ν_{31}.

TABLE 2

Material:	Dimensionless Weight Function: $h_1(\frac{x_{1i}}{h},\frac{a}{h},\rho,\lambda)\,h^{0.5}$	Accuracy:
Isotropic	$\sqrt{12}\,\frac{a-x_{1i}}{h}\left(1+0.677\,\frac{h}{a-x_{1i}}\right)+\frac{2}{\sqrt{\pi}}\sqrt{\frac{h}{a-x_{1i}}}\left(1+\frac{x_{1i}}{a}\right)^{-1/2}\left[1.3-0.3\left(\frac{x_{1i}}{a}\right)^{5/4}\right]-\left[0.815\left(\frac{a-x_{1i}}{h}\right)^{0.619}f\left(\frac{x_{1i}}{a},\frac{a-x_{1i}}{h}\right)+0.4264\right]^{-1}$ where: $f\left(\frac{x_{1i}}{a},\frac{a-x_{1i}}{h}\right)=g\left(\frac{x_{1i}}{a},\frac{a-x_{1i}}{h}\right)\left[1-\left(\frac{x_{1i}}{a}\right)^6\right]+\left(\frac{x_{1i}}{a}\right)^6$; $g\left(\frac{x_{1i}}{a},\frac{a-x_{1i}}{h}\right)=\left(\frac{a-x_{1i}}{h}\right)^{-0.119}\left\{\left[A\exp\left[-B\ln\left(\frac{a-x_{1i}}{h}\right)\right]+C\right]^{-1}+D\right\}$	better than 2% for $c/h \geq 2$.
Degenerate Orthotropic ($\rho=1$)	$\lambda^{3/8}\sqrt{12}\,\frac{a-x_{1i}}{h}\left(1+0.677\lambda^{-1/4}\,\frac{h}{a-x_{1i}}\right)+\frac{2}{\sqrt{\pi}}\sqrt{\frac{h}{a-x_{1i}}}\left(1+\frac{x_{1i}}{a}\right)^{-1/2}\left[1.3-0.3\left(\frac{x_{1i}}{a}\right)^{5/4}\right]-\lambda^{1/8}\left[0.815\left(\lambda^{1/4}\,\frac{a-x_{1i}}{h}\right)^{0.619}f\left(\frac{x_{1i}}{a},\frac{a-x_{1i}}{h},\lambda\right)+0.4264\right]^{-1}$ where: $f\left(\frac{x_{1i}}{a},\frac{a-x_{1i}}{h},\lambda\right)=g\left(\frac{x_{1i}}{a},\frac{a-x_{1i}}{h},\lambda\right)\left[1-\left(\frac{x_{1i}}{a}\right)^6\right]+\left(\frac{x_{1i}}{a}\right)^6$; $g\left(\frac{x_{1i}}{a},\frac{a-x_{1i}}{h},\lambda\right)=\left(\lambda^{1/4}\,\frac{a-x_{1i}}{h}\right)^{-0.119}\left\{\left[A\exp\left[-B\ln\left(\lambda^{1/4}\,\frac{a-x_{1i}}{h}\right)\right]+C\right]^{-1}+D\right\}$	better than 2% for $0.025 \leq \lambda \leq 1$, $c/h \geq 2\lambda^{-1/4}$.

and:

$A = 2.9496(x_{1i}/a)^3 - 3.1554(x_{1i}/a)^2 - 0.5913(x_{1i}/a) + 1.2101$; $B = -4.2955(x_{1i}/a)^3 + 6.6196(x_{1i}/a)^2 - 2.7173(x_{1i}/a) + 1.4264$;

$C = -2.3278(x_{1i}/a)^3 + 3.5239(x_{1i}/a)^2 - 1.6963(x_{1i}/a) + 1.2934$; $D = -0.1127(1 - x_{1i}/a)$

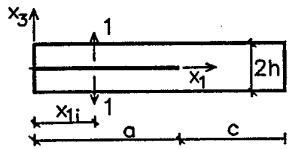

Notation: $\lambda = E_3 / E_1$ Plane Stress: E_1 and E_3 Young's moduli in x_1 and x_3 directions, G_{13} shear modulus in plane x_1-x_3, ν_{13} and ν_{31} Poisson's ratios in plane x_1-x_3. Plane Strain: substitute for E_1, E_3, ν_{13} and ν_{31} :

$E_{1ps} = \frac{E_1}{(1-\nu_{12}\nu_{21})}$, $E_{3ps} = \frac{E_3}{(1-\nu_{23}\nu_{32})}$, $\nu_{13ps} = \frac{(\nu_{13}+\nu_{12}\nu_{23})}{(1-\nu_{12}\nu_{21})}$, $\nu_{31ps} = \frac{(\nu_{31}+\nu_{32}\nu_{21})}{(1-\nu_{32}\nu_{23})}$

x_1 and x_3 = principal material axes

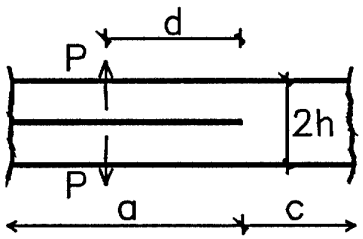

Figure 1.a: Schematic of an infinitely long strip [5].

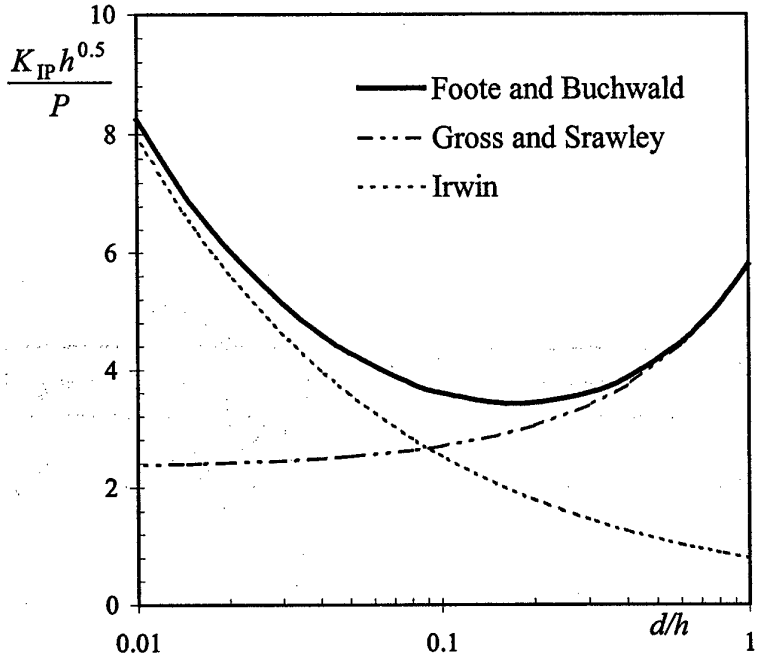

Figure 1.b: Solid curve: dimensionless stress intensity factor in the isotropic strip of Fig. 1.a (Foote and Buchwald and Eq. (1)). Dashed curves: limiting solutions for very small *d/h* (Irwin) and large *d/h* (Gross and Srawley).

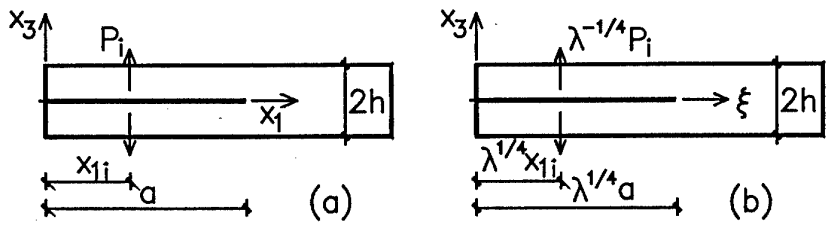

Figure 2: a) Schematic of a double cantilever beam loaded by a pair of opening forces P_i.
b) Orthotropy rescaling: the geometry and boundary conditions are rescaled
from the original problem.

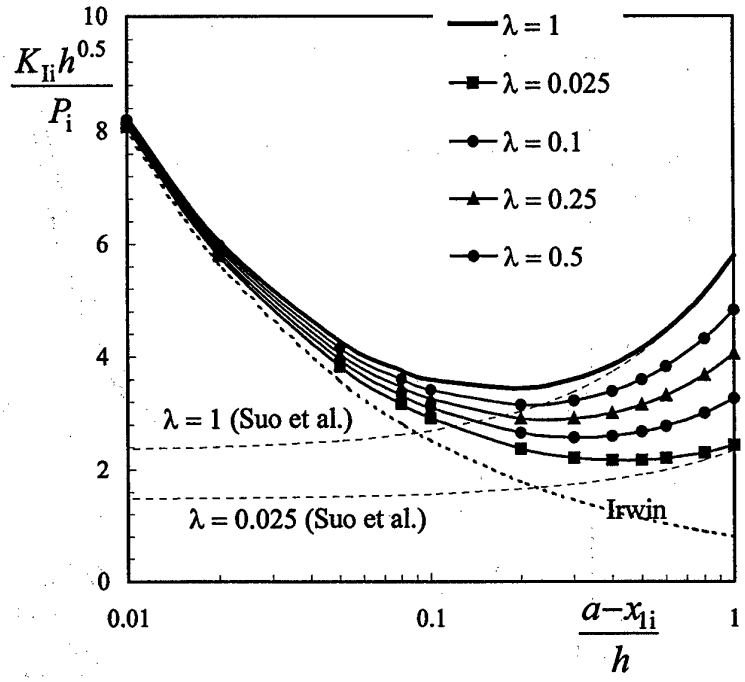

Figure 3: Dimensionless stress intensity factor in the degenerate orthotropic ($\rho = 1$) beam of Fig. 2.a , Eq. (9).

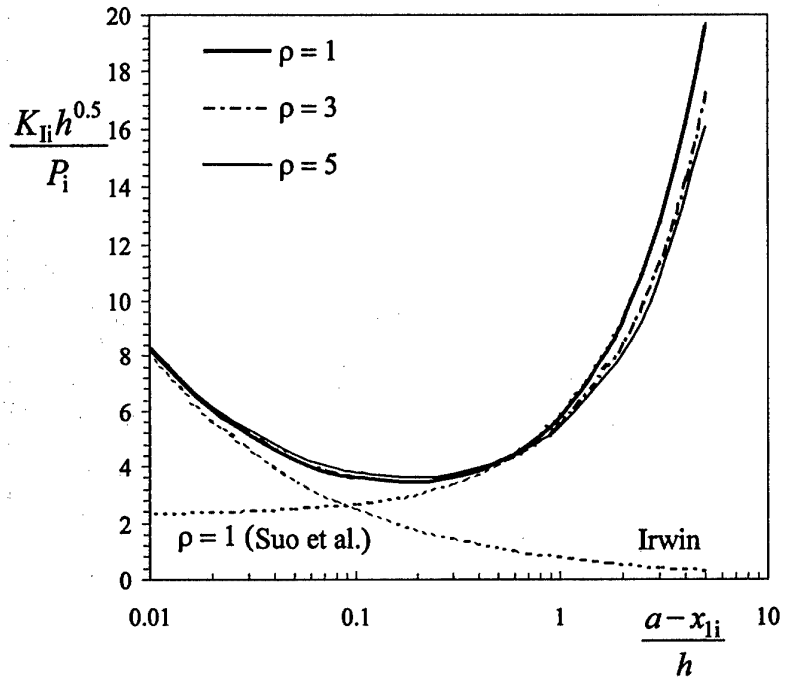

Figure 4: Dimensionless stress intensity factor in the orthotropic beam of Fig. 2.a with cubic symmetry ($\lambda = 1$), Eq. (10).

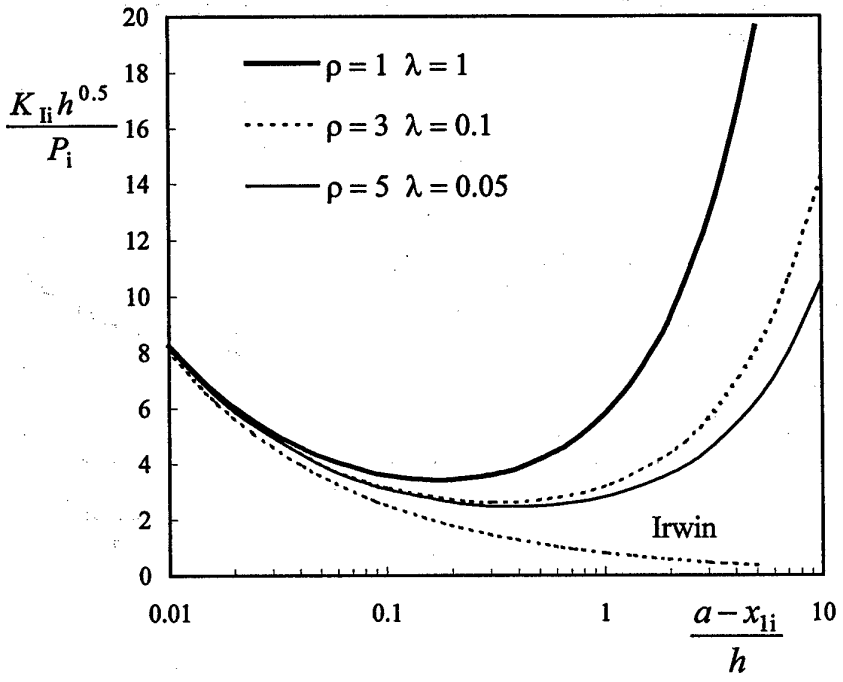

Figure 5: Dimensionless stress intensity factor in the orthotropic beam of Fig. 2.a, Eq. (10).

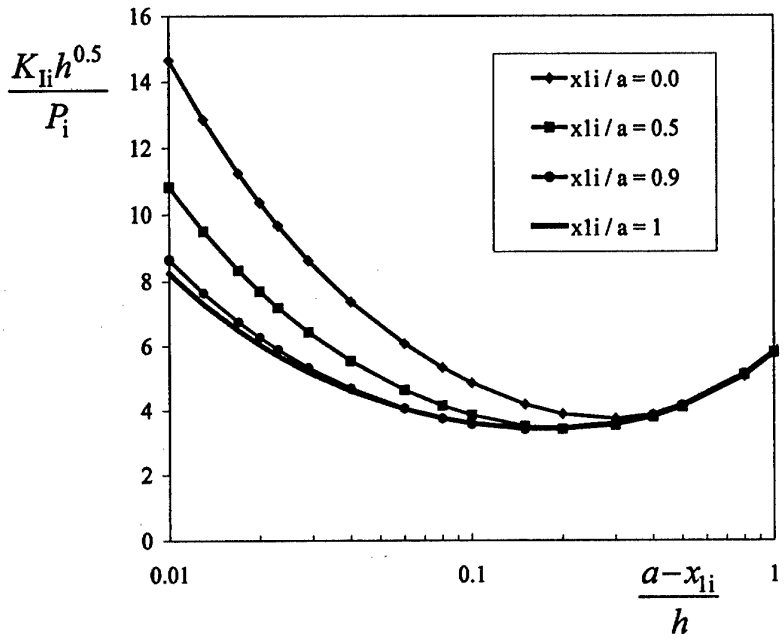

Figure 6: Dimensionless stress intensity factor in the isotropic beam of Fig. 2.a on varying x_{1i} / a, Eq. (11).

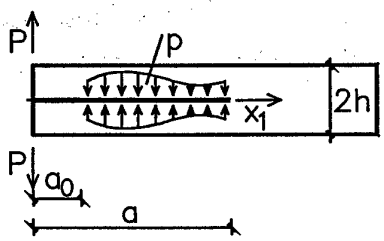

Figure 7: Schematic of a double cantilever beam in the presence of bridging mechanisms.

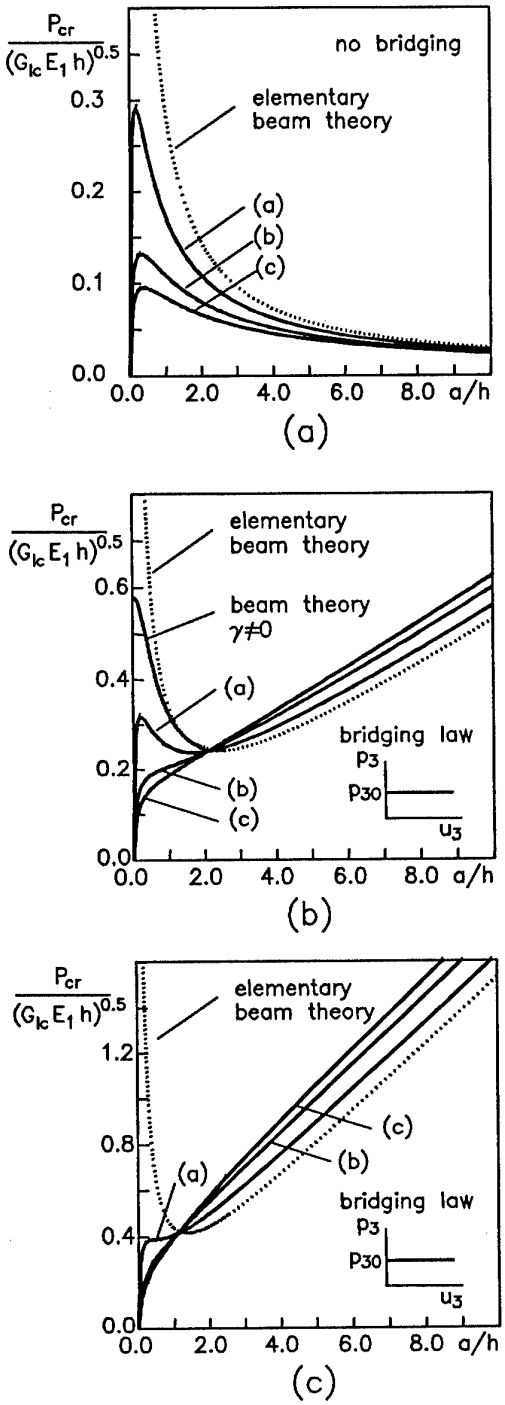

Figure 8: Dimensionless critical load versus normalized crack length in orthotropic DCB specimens: a) No bridging mechanisms, $p_{30}h^{0.5}/\sqrt{\mathcal{G}_{Ic}E_1} = 0.0$; b) $p_{30}h^{0.5}/\sqrt{\mathcal{G}_{Ic}E_1} = 0.1$; c) $p_{30}h^{0.5}/\sqrt{\mathcal{G}_{Ic}E_1} = 0.3$. (curves (a): $\lambda = 1$ and $\rho = 1$; curves (b) $\lambda = 0.1$ and $\rho = 3$; curves (c) $\lambda = 0.05$ and $\rho = 5$)

Submitted to Composite Structures, October 2002. Accepted, December 2002.

FREE VIBRATIONS OF DELAMINATED BEAM-TYPE STRUCTURES WITH CRACK BRIDGING

Luigi Brandinelli[1] and Roberta Massabò[2,*]

[1] Department of Structural and Geotechnical Engineering, University of Genoa, Italy.
[2] Department of Civil and Environmental Engineering, Northwestern University, Evanston, USA.

ABSTRACT

The dynamic response of laminated beam-type structures presenting delaminations is characterized by stiffness degradation, natural frequency shifts and, in special cases, the occurrence of opening modes during vibration. The paper investigates how bridging mechanisms acting between the surfaces of the delaminations may affect these behaviors. Such mechanisms could be developed by a through-thickness reinforcement (stitching, z-pins) applied to the laminate in order to improve its resistance and tolerance against delamination fracture. A model based on the theory of bending of laminated plates is formulated where the bridging mechanisms are modeled as a uniform distribution of linear elastic springs that oppose longitudinal and transversal relative displacements between the surfaces of the delamination. The model is applied to predict natural frequencies and modal shapes of a delaminated cantilever beam with a rectangular cross section. A variety of solutions and transitions in the dynamic response is found on varying the stiffness of the ligaments. A transition from damaged (unbridged) to intact beam values is predicted upon increasing the stiffness of both longitudinal and transversal springs. An application of the model to a stitched carbon-epoxy laminate for the aeronautical industry shows that low percentages of through-thickness reinforcement can substantially improve the dynamic response of delaminated structures.

Keywords: Delamination, dynamics, natural frequencies of vibration, beam theory, composite laminates, through-thickness reinforcement.

1. INTRODUCTION

Fiber reinforced polymer matrix laminates are characterized by high strength and stiffness to weight ratios that make them particularly suited to develop load-bearing components for a variety of applications of the aerospace, naval and aeronautical industries. The utilization of these materials,

* Corresponding author. Address: 2145 Sheridan Road, Evanston, IL 60208, USA. Phone/fax: (847) 467 4105 / (847) 491 4011.
E-mail: r-massabo@northwestern.edu

however, has been limited by their high sensitivity to interlaminar flaws that, in the presence of interlaminar stresses, can easily propagate and lead to catastrophic failures or unacceptable loss of stiffness. Interlaminar flaws may originate during fabrication, mainly due to air trapped in the resin and also to imperfect bonding, matrix cracks or broken fibers; they may also be service-induced, as because of impact with foreign objects and fatigue loading.

Besides being a major cause of stiffness and strength degradation, delamination also causes changes in the dynamic response of composite laminates. Extensive experimental and theoretical investigations have shown that delaminations cause shifts of the natural frequencies of vibration along with changes in the modal shapes. Openings of the delaminated surfaces during vibration, the so-called "opening modes", have also been experimentally detected and theoretically reproduced [1-3].

In this paper, a model based on a particularization of the first order shear deformation theory for anisotropic laminated plates in cylindrical bending [4-6] has been formulated in order to study the dynamic response of delaminated composite plates in the presence of bridging mechanisms acting between the crack surfaces. Following the approach described in [3], a through-width delaminated plate has been modeled by using four elementary plates connected at the delamination edges. The bridging mechanisms are represented by a uniform distribution of springs that oppose longitudinal and transversal relative crack displacements [7]. In this paper only linear elastic springs, exerting symmetric restoring forces during vibration, have been considered. This assumption leads to analytical or semi-analytical solutions of the problem allowing a complete description of the variety of modal shapes and associated natural frequencies that arise due to the presence of bridging ligaments of different stiffness. Nonlinear bridging mechanisms and the problem of nonlinear contact during vibration will be studied elsewhere.

Bridging mechanisms acting between the crack surfaces could represent the action developed by a through-thickness reinforcement, such as stitching or z-pins. The efficacy of the technology of through-thickness reinforcement in enhancing delamination resistance and damage and impact tolerance of composite laminates has been abundantly documented in the last twenty years [8-11]. The through-thickness reinforcements create large zone of bridging along the wake of the delamination that shield the crack tip from the applied loads thus reducing the driving force for crack propagation or even suppressing crack growth [7,12-15]. A through-thickness reinforcement can reduce the loss of stiffness due to delamination, modify modes of failure and prevent catastrophic collapses of the structural components.

It is expected that a through-thickness reinforcement will also reduce the delamination-induced degradation of the dynamic properties of composite structures by opposing the relative displacements between the delamination surfaces during vibration. This behavior will be investigated using the proposed theoretical model.

The analysis of the degradation of the dynamic properties of delaminated beam-type structures in

the presence of a through-thickness reinforcement has special relevance. It is well known that the influence of short delaminations on the first natural frequencies of vibration is limited and that only considerably long delaminations degrade the first frequencies to a certain extent [1-3]. Such long delaminations, however, would not be acceptable in traditional laminate structures. Through-thickness reinforced laminates, on the other hand, can be used within a damage tolerant design of composite structures. These damage tolerant structures would be able to tolerate delaminations of considerable length due to the action developed by the through thickness reinforcement. It is then important to understand and quantify the effects these long delaminations might have on the dynamic response and investigate the influence of the through-thickness reinforcement.

2. MODELING AND TESTING OF DELAMINATED BEAMS

Free vibrations of delaminated composite beams were first studied by Ramkumar et al. in 1979 [16]. Their analytical model, based on four Timoshenko's beams connected at the delamination edges (Fig. 1), neglected the coupling between flexural and axial vibrations and therefore led to an overestimation of the drop in the natural frequencies caused by delamination and observed in experimental tests. Wang et al. [1] improved the analytical model by including the coupling effect and obtained a better agreement with experimental frequency measurements. In these first models, also known as *free models*, the two sub-laminates above and below the delamination plane were allowed to vibrate independently. For special geometrical configurations (very long cracks close to the surface of the beam) this assumption could lead to overlapping of the sublaminates during portions of the vibration cycle.

To avoid the overmentioned incompatibility, Mujumdar and Suryanarayan [17] imposed the two delaminated parts to have the same transversal displacement during vibration. This so-called *constrained model* was later adopted by Tracy and Pardoen [18] to study the free vibrations of simply supported isotropic beams and showed good agreement with finite element results and experimental frequency measurements.

The problem of the interaction between sublaminates during free and forced vibrations of composite beams in the presence of one or more delamination cracks has been investigated in [3,19-23]. Luo and Hanagud [3] studied the problem of a beam with a single delamination applying Timoshenko beam theory. They modelled the contact forces that arise during the compression cycles using a uniform distribution of transversal springs. A piece-wise linear spring stiffness was defined to allow transversal relative displacements up to a pre-set amount and simulate the transversal elasticity of the two sublaminates. Further overlap was impeded by an infinite spring stiffness. The springs opposed no resistance to opening displacements. Different frequencies and modal shapes were then defined corresponding to the different spring stiffness and the results combined in the solution of a forced

vibration problem. Lee in [22] applied a higher-order plate theory within a layerwise approach [24,25,26] to numerically investigate the free vibrations of delaminated plates.

Other recent studies have dealt with the problem of free vibrations with respect to post-buckled states [27-29], and the problem of the influence of delamination cracks on the flutter characteristics of laminated plates [30]. Flutter is a self-excited oscillation caused by the aerodynamic forces generated by the motion of a structure immersed in a wind flow – once a critical velocity has been reached, the structure starts to vibrate violently. In [30] the presence of delaminations has been shown to alter the conditions characterizing the onset of flutter in composite plates and reduce the flutter boundary.

3. ASSUMPTIONS AND BASIC FORMULATION OF THE MODEL

Figure 1 shows a laminated plate of length L, thickness t and width w (w>>t) with a through-width delamination of length L_{del} parallel to the x-y plane, with x the longitudinal geometrical axis of the plate. The delamination identifies four plates, for $i = 1, \ldots 4$, of length L_i, thickness t_i, cross sectional area S_i and central moment of inertia I_i. The distance of the plate centroidal axes from the delamination plane is indicated with h_i. The position of the mid-point of the delamination in the plane x-z is identified by $L_c = L_1 + L_{del}/2$ and t_3.

The laminate consists of n linearly elastic and transversally isotropic laminae with material density ρ. The principal material axes of the laminae are arbitrarily oriented and the layup is such to ensure plain strain conditions parallel to the plane x-z. Only small deformations and small displacements are considered. Based on these assumptions, the plate vibrates in cylindrical bending and the governing equations coincide with those of a beam characterized by a reduced flexural stiffness. In the following, the terms beam and plate will be used interchangeably.

Linear bridging mechanisms acting along the surfaces of the delamination are represented in the model by means of uniformly distributed linear elastic springs that exert symmetric restoring forces to both transversal and longitudinal relative displacements between the delamination surfaces. The stiffness in the transverse and longitudinal directions are indicated with k_v and k_t, respectively.

The generalized displacements of the axis of ith beam are the transverse displacement, w_i, the axial displacement, u_i, and the bending rotation, φ_i; the shear deformation γ_i is related to w_i and φ_i, through the compatibility relation:

$$\gamma_i = \varphi_i + \frac{\partial w_i}{\partial x} \quad . \tag{1}$$

The stress resultants per unit width are the normal force, N_i, shear force, Q_i, and bending moment, M_i, for $i = 1,.., 4$ (Fig.1).

The constitutive equations for the ith beam are:

$$N_{\mathrm{i}} = A_{\mathrm{i}}\varepsilon_{\mathrm{xi}} + B_{\mathrm{i}}\kappa_{\mathrm{xi}} \quad , \tag{2}$$

$$M_i = B_{\mathrm{i}}\varepsilon_{\mathrm{xi}} + D_{\mathrm{i}}\kappa_{\mathrm{xi}} \quad , \tag{3}$$

$$Q_{\mathrm{i}} = G_{\mathrm{i}}\gamma_{\mathrm{i}} \quad , \tag{4}$$

where $\varepsilon_{\mathrm{xi}} = u_{i,x}$ and $\kappa_{\mathrm{xi}} = \varphi_{i,x}$ are the axial deformation and bending curvature and the comma indicates partial differentiation; the laminate stiffness coefficients A_{i}, B_{i}, D_{i} and $\mathrm{G_i}$ are defined using lamination theory and the assumptions in [6].

The equations of motion for the intact parts of the beam are:

$$\begin{aligned} N_{\mathrm{i},\mathrm{x}} &= \rho S_{\mathrm{i}} u_{\mathrm{i},\mathrm{tt}} \quad , \\ Q_{\mathrm{i},\mathrm{x}} &= \rho S_{\mathrm{i}} w_{\mathrm{i},\mathrm{tt}} \quad , \qquad \mathrm{i} = 1, 4 \\ M_{\mathrm{i},\mathrm{x}} - Q_{\mathrm{i}} &= \rho I_{\mathrm{i}} \varphi_{\mathrm{i},\mathrm{tt}} \quad , \end{aligned} \tag{5a,b,c}$$

where the terms on the right hand side account for the inertia of the plate and the symbol t has been used for the time variable. For the upper and lower sublaminates, the equations of motion are:

$$\begin{aligned} N_{2,\mathrm{x}} + k_t(u_3 - u_2 - \varphi_2 h_2 - \varphi_3 h_3) &= \rho S_2 u_{2,\mathrm{tt}} \quad , \\ Q_{2,\mathrm{x}} + k_v(w_3 - w_2) &= \rho S_2 w_{2,\mathrm{tt}} \quad , \\ M_{2,\mathrm{x}} - Q_2 + k_t h_2(u_3 - u_2 - \varphi_2 h_2 - \varphi_3 h_3) &= \rho I_2 \varphi_{2,\mathrm{tt}} \quad , \end{aligned} \tag{6a,b,c}$$

$$\begin{aligned} N_{3,\mathrm{x}} - k_t(u_3 - u_2 - \varphi_2 h_2 - \varphi_3 h_3) &= \rho S_3 u_{3,\mathrm{tt}} \quad , \\ Q_{3,\mathrm{x}} - k_v(w_3 - w_2) &= \rho S_3 w_{3,\mathrm{tt}} \quad , \\ M_{3,\mathrm{x}} - Q_3 + k_t h_3(u_3 - u_2 - \varphi_2 h_2 - \varphi_3 h_3) &= \rho I_3 \varphi_{3,\mathrm{tt}} \quad . \end{aligned} \tag{7a,b,c}$$

Equations (5-7) can be expressed in terms of displacement components by exploiting equations (2-4) and the compatibility relations.

A harmonic type solution is assumed for the free vibration problem. The solution is characterized by a single angular frequency ω and the displacement field assumes the following form:

$$u_i(x,t)=u_i(x)e^{j\omega t} \qquad w_i(x,t)=w_i(x)e^{j\omega t} \qquad \varphi_i(x,t)=\varphi_i(x)e^{j\omega t} \qquad i=1,..4\ . \qquad (8a,b,c)$$

Substitution of Eqs. (8a,b,c) into the equations of motion leads to a system of twelve ordinary differential equations. To determine the twelve displacement amplitudes, $u_i(x)$, $w_i(x)$, $\varphi_i(x)$, and the angular frequency, ω, the eigenvalue boundary value problem is completed by continuity and boundary conditions. Such equations will be explicitly stated in a dimensionless form in the following section.

4. DIMENSIONLESS FORMULATION

The thickness of the intact beam, t, its extensional stiffness coefficient, A_1, and the material density, ρ, are chosen as fundamental quantities to define the following dimensionless groups for the geometric variables, the generalized displacements and the elastic stiffness coefficients:

$$\xi=\frac{x}{t},\quad \hat{L}=\frac{L}{t}\ ,\quad \hat{L}_c=\frac{L_c}{t}\ ,\quad \hat{L}_{del}=\frac{L_{del}}{t}\ ,\quad \hat{t}_3=\frac{t_{del}}{t}\ ,\quad \hat{t}_2=1-\hat{t}_3\ ,\quad \hat{h}_i=\frac{h_i}{t},$$
$$\hat{u}_i=\frac{u_i}{t}\ ,\quad \hat{w}_i=\frac{w_i}{t}\ , \qquad (9a,b,c)$$
$$\hat{A}_i=\frac{A_i}{A_1}\ ,\quad \hat{B}_i=\frac{B_i}{A_1 t}\ ,\quad \hat{D}_i=\frac{D_i}{A_1 t^2}\ ,\quad \hat{G}_i=\frac{G_i}{A_1}\ ,$$

with i = 1, ...4. The dimensionless stiffness parameters for the transversal and longitudinal springs are:

$$\alpha=\frac{k_v t^2}{A_1} \quad \text{and} \quad \beta=\frac{k_t t^2}{A_1}\ , \qquad (9d,e)$$

and the dimensionless eigenvalue is:

$$\psi=\frac{\rho\omega^2 t^3}{A_1}\ . \qquad (9f)$$

The twelve governing equations in the thirteen unknowns $\hat{u}_i, \hat{w}_i, \varphi_i$ (i = 1,...4) and ψ are expressed in a dimensionless form as follows:

$$\hat{u}_{i,\xi\xi}+\psi\hat{u}_i-\hat{B}_i\hat{w}_{i,\xi\xi\xi}-\psi\frac{\hat{B}_i}{\hat{G}_i}\hat{w}_{i,\xi}=0 \qquad i=1,4\ , \qquad (10a,b)$$

$$\hat{w}_{\mathrm{i},\xi\xi\xi\xi}+\psi\left(\frac{1}{\hat{G}_i}+\frac{1}{12\hat{D}_i}\right)\hat{w}_{\mathrm{i},\xi\xi}+\frac{\psi}{\hat{D}_i}\left(\frac{\psi}{12\hat{G}_i}-1\right)\hat{w}_i-\frac{\hat{B}_i}{\hat{D}_i}\hat{u}_{\mathrm{i},\xi\xi\xi}=0 \qquad \mathrm{i}=1,4\ , \tag{11a,b}$$

$$\varphi_{\mathrm{i},\xi}=-\frac{\psi}{\hat{G}_i}\hat{w}_{\mathrm{i}}-\hat{w}_{\mathrm{i},\xi\xi} \qquad \mathrm{i}=1,4\ , \tag{12a,b}$$

$$\begin{aligned}&\hat{u}_{2,\xi\xi\xi}+\psi\frac{\hat{t}_2}{\hat{A}_2}\hat{u}_{2,\xi}-\frac{\hat{B}_2}{\hat{A}_2}\hat{w}_{2,\xi\xi\xi\xi}-\psi\frac{\hat{B}_2\hat{t}_2}{\hat{A}_2\hat{G}_2}\hat{w}_{2,\xi\xi}-\alpha\frac{\hat{B}_2}{\hat{A}_2\hat{G}_2}\left(\hat{w}_{3,\xi\xi}-\hat{w}_{2,\xi\xi}\right)+\\&\frac{\beta}{\hat{A}_2}\left[\hat{u}_{3,\xi}-\hat{u}_{2,\xi}+\psi\frac{\hat{h}_2\hat{t}_2}{\hat{G}_2}\hat{w}_2+\hat{h}_2\hat{w}_{2,\xi\xi}+\psi\frac{\hat{h}_3\hat{t}_3}{\hat{G}_3}\hat{w}_3+\hat{h}_3\hat{w}_{3,\xi\xi}+\alpha\left(\frac{\hat{h}_2}{\hat{G}_2}-\frac{\hat{h}_3}{\hat{G}_3}\right)\left(\hat{w}_3-\hat{w}_2\right)\right]=0\end{aligned}\ , \tag{13}$$

$$\begin{aligned}&\hat{w}_{2,\xi\xi\xi\xi}+\psi\hat{t}_2\left(\frac{1}{\hat{G}_2}+\frac{\hat{t}_2^2}{12\hat{D}_2}\right)\hat{w}_{2,\xi\xi}+\psi\frac{\hat{t}_2}{\hat{D}_2}\left(\frac{\hat{t}_2^3\psi}{12\hat{G}_2}-1\right)\hat{w}_2+\frac{\alpha}{\hat{G}_2}\left(\hat{w}_{3,\xi\xi}-\hat{w}_{2,\xi\xi}\right)+\frac{\alpha}{\hat{D}_2}\left(\frac{\hat{t}_2^3\psi}{12\hat{G}_2}-1\right)\left(\hat{w}_3-\hat{w}_2\right)-\\&\frac{\beta\hat{h}_2}{\hat{D}_2}\left[\hat{u}_{3,\xi}-\hat{u}_{2,\xi}+\psi\frac{\hat{h}_2\hat{t}_2}{\hat{G}_2}\hat{w}_2+\hat{h}_2\hat{w}_{2,\xi\xi}+\psi\frac{\hat{h}_3\hat{t}_3}{\hat{G}_3}\hat{w}_3+\hat{h}_3\hat{w}_{3,\xi\xi}+\alpha\left(\frac{\hat{h}_2}{\hat{G}_2}-\frac{\hat{h}_3}{\hat{G}_3}\right)\left(\hat{w}_3-\hat{w}_2\right)\right]=0\end{aligned}\ , \tag{14}$$

$$\varphi_{2,\xi}=-\frac{\psi}{\hat{G}_2}\hat{w}_2-\frac{\alpha}{\hat{G}_2}\left(\hat{w}_3-\hat{w}_2\right)-\hat{w}_{2,\xi\xi}\ , \tag{15}$$

$$\begin{aligned}&\hat{u}_{3,\xi\xi\xi}+\psi\frac{\hat{t}_3}{\hat{A}_3}\hat{u}_{3,\xi}-\frac{\hat{B}_3}{\hat{A}_3}\hat{w}_{3,\xi\xi\xi\xi}-\psi\frac{\hat{B}_3\hat{t}_3}{\hat{A}_3\hat{G}_3}\hat{w}_{3,\xi\xi}+\alpha\frac{\hat{B}_3}{\hat{A}_3\hat{G}_3}\left(\hat{w}_{3,\xi\xi}-\hat{w}_{2,\xi\xi}\right)-\\&\frac{\beta}{\hat{A}_3}\left[\hat{u}_{3,\xi}-\hat{u}_{2,\xi}+\psi\frac{\hat{h}_2\hat{t}_2}{\hat{G}_2}\hat{w}_2+\hat{h}_2\hat{w}_{2,\xi\xi}+\psi\frac{\hat{h}_3\hat{t}_3}{\hat{G}_3}\hat{w}_3+\hat{h}_3\hat{w}_{3,\xi\xi}+\alpha\left(\frac{\hat{h}_2}{\hat{G}_2}-\frac{\hat{h}_3}{\hat{G}_3}\right)\left(\hat{w}_3-\hat{w}_2\right)\right]=0\end{aligned}\ , \tag{16}$$

$$\begin{aligned}&\hat{w}_{3,\xi\xi\xi\xi}+\psi\hat{t}_3\left(\frac{1}{\hat{G}_3}+\frac{\hat{t}_3^2}{12\hat{D}_3}\right)\hat{w}_{3,\xi\xi}+\psi\frac{\hat{t}_3}{\hat{D}_3}\left(\frac{\hat{t}_3^3\psi}{12\hat{G}_3}-1\right)\hat{w}_3-\frac{\alpha}{\hat{G}_3}\left(\hat{w}_{3,\xi\xi}-\hat{w}_{2,\xi\xi}\right)-\frac{\alpha}{\hat{D}_3}\left(\frac{\hat{t}_3^3\psi}{12\hat{G}_3}-1\right)\left(\hat{w}_3-\hat{w}_2\right)-\\&\frac{\beta\hat{h}_3}{\hat{D}_3}\left[\hat{u}_{3,\xi}-\hat{u}_{2,\xi}+\psi\frac{\hat{h}_2\hat{t}_2}{\hat{G}_2}\hat{w}_2+\hat{h}_2\hat{w}_{2,\xi\xi}+\psi\frac{\hat{h}_3\hat{t}_3}{\hat{G}_3}\hat{w}_3+\hat{h}_3\hat{w}_{3,\xi\xi}+\alpha\left(\frac{\hat{h}_2}{\hat{G}_2}-\frac{\hat{h}_3}{\hat{G}_3}\right)\left(\hat{w}_3-\hat{w}_2\right)\right]=0\end{aligned}\ , \tag{17}$$

$$\varphi_{3,\xi}=-\frac{\psi}{\hat{G}_3}\hat{w}_3+\frac{\alpha}{\hat{G}_3}\left(\hat{w}_3-\hat{w}_2\right)-\hat{w}_{3,\xi\xi}\ . \tag{18}$$

The kinematic and static continuity conditions at the delamination edge $\xi_1=L_1/t$ are:

$$\hat{w}_1 = \hat{w}_2, \qquad \hat{w}_1 = \hat{w}_3, \tag{19a,b}$$

$$\varphi_1 = \varphi_2, \qquad \varphi_1 = \varphi_3 , \tag{20a,b}$$

$$\hat{u}_2 = \hat{u}_1 + \left(\hat{h}_1 - \hat{h}_2\right)\varphi_1, \qquad \hat{u}_3 = \hat{u}_1 + \left(\hat{h}_1 + \hat{h}_3\right)\varphi_1, \tag{21a,b}$$

$$M_1 = M_2 + M_3 - (h_2 - h_1)N_2 + (h_3 + h_1)N_3, \quad Q_1 = Q_2 + Q_3, \quad N_1 = N_2 + N_3 \ . \tag{22a,b,c}$$

Analogous relations are written for the other delamination edge at $\xi = \left(L_1 + L_{\text{del}}\right)/t$. Equations (21a,b and 22a) refer to all cases where the centroidal axis of the beam 1 is above the plane of the delamination. Cases where the centroidal axis of the beam 1 is below the delamination plane are described by the same equation substituting $\hat{h}_1$ (or h_1) with $-\hat{h}_1$ (or $-h_1$).

For a cantilever beam clampled at $\xi = 0$ the boundary conditions in the absence of applied forces are:

$$\hat{u}_1 = 0, \qquad \hat{w}_1 = 0, \qquad \varphi_1 = 0 \ , \qquad \text{at } \xi = 0 \ , \tag{23a,b,c}$$

$$N_4 = 0, \qquad M_4 = 0 \ , \qquad Q_4 = 0 \ , \qquad \text{at } \xi = \hat{L} \ . \tag{24a,b,c}$$

The system of equations (10-18) and the continuity and boundary conditions (19-24) constitute a two-point boundary eigenvalue problem with internal conditions in terms of the generalized displacements $\hat{u}_i, \hat{w}_i, \varphi_i$ and the eigenvalue ψ. The problem generally requires a numerical integration such as that presented in Appendix I.

The proposed model has been validated by referring to the asymptotic frequency values obtained by letting the spring stiffness vanish (thus simulating the absence of reinforcement) and indefinitely grow (absence of delamination). For a vanishing spring stiffness, the experimental tests of Shen and Grady [2], on delaminated cantilever beams, have been reproduced [31,32]. Luo and Hanagud [3] used the same tests to validate their beam model. For very high spring stiffness, the frequency values predicted by the model approach the values corresponding to an intact beam [33].

5. ANALYTICAL SOLUTION

A closed-form solution of the boundary eigenvalue problem presented in the previous section is obtained under the following additional assumptions:

a) mid-plane delamination: $t_2 = t_3 = t/2$;

b) *constrained model*: $w_2 = w_3 = w$;

c) homogeneous material;

d) negligible shear deformations: $\gamma_i = 0$ for i = 1,...4.

As it will be shown later, the assumption (b) is satisfied in all cases but for very long delaminations close to the surface of the beam when opening modes may develop [1-3]. In all other cases the transversal springs are not activated during vibration and the solution therefore does not depend on the normalized stiffness coefficient α (Eq. 9d). The assumption (c) is satisfied by all isotropic and orthotropic homogeneous materials and by unidirectional lay-ups made of the same orthotropic laminae. Furthermore, laminates with many layers and no bending/extensional coupling, such as quasi-isotropic laminates typically used for aeronautical applications and cross-plies $[0/90]_n$, belong to this category. The assumption leads to $B_i = 0$ (i = 1,...4) and $A_1 = E_1 t$, with E_1 the reduced longitudinal Young's modulus.

The problem reduces to the determination, besides the eigenvalue ψ, of the seven functions $\hat{u}_i(\xi)$, $\hat{w}_1(\xi)$, $\hat{w}_4(\xi)$ and $\hat{w}(\xi)$, for i = 1,...4, representing the dimensionless displacement amplitudes. Equations (10,11,13,16) simplify as follows:

$$\hat{u}_{i,\xi\xi} + \psi \hat{u}_i = 0 \quad , \qquad i = 1,4 \quad , \tag{25a,b}$$

$$\hat{w}_{i,\xi\xi\xi\xi} + \psi \hat{w}_{i,\xi\xi} - 12\psi \hat{w}_i = 0 \quad , \qquad i = 1,4 \quad , \tag{26a,b}$$

$$\hat{u}_{2,\xi\xi} + \psi \hat{u}_{2,\xi} + 2\beta \left(\hat{u}_3 - \hat{u}_2 + \frac{\hat{w}_{,\xi}}{2} \right) = 0 \quad , \tag{27}$$

$$\hat{u}_{3,\xi\xi} + \psi \hat{u}_{3,\xi} - 2\beta \left(\hat{u}_3 - \hat{u}_2 + \frac{\hat{w}_{,\xi}}{2} \right) = 0 \quad . \tag{28}$$

Moreover, by introducing the relative longitudinal displacement $\hat{u}_r = \hat{u}_3 - \hat{u}_2$, the last two equations can be combined to give:

$$\hat{u}_{r,\xi\xi} + (\psi - 4\beta)\hat{u}_r + 2\beta \hat{w}_{,\xi} = 0 \quad . \tag{29}$$

Finally, Eqs. (14) and (17) reduce to the following expression:

$$\hat{w}_{,\xi\xi\xi\xi} - (12\beta - \psi)\hat{w}_{,\xi\xi} - 48\psi \hat{w} = 24\beta \hat{u}_{r,\xi} \quad . \tag{30}$$

Equations (25, 26, 29 and 30) constitute a system of six ordinary differential equations in the unknowns

ψ, $\hat{u}_1(\xi)$, $\hat{u}_4(\xi)$, $\hat{w}_1(\xi)$, $\hat{w}_4(\xi)$, $\hat{u}_r(\xi)$ and $\hat{w}(\xi)$. The kinematic continuity conditions (19-20) at the first delamination edge ξ_1 become:

$$\hat{w}_1 = \hat{w}, \quad \hat{w}_{1,\xi} = \hat{w}_{,\xi}, \quad \hat{u}_2 = \hat{u}_1 + \frac{\hat{w}_{1,\xi}}{4}, \quad \hat{u}_3 = \hat{u}_1 - \frac{\hat{w}_{1,\xi}}{4}. \tag{31}$$

Similar conditions are posed at the other delamination edge. The static continuity conditions (22a,b,c) and boundary conditions (23) and (24) remain unchanged.

The solution procedure of the system of equations is outlined in the Appendix II. The general solution is:

$$\hat{u}_1(\xi) = C_1 \sin(\delta_1 \xi), \tag{32}$$

$$\hat{u}_4(\xi) = C_2 \cos[\delta_1(\xi - \xi_L)], \tag{33}$$

$$\hat{w}_1(\xi) = C_3 \sin(\eta_1 \xi) + C_4 \cos(\eta_1 \xi) + C_5 \sinh(\theta_1 \xi) + C_6 \cosh(\theta_1 \xi), \tag{34}$$

$$\hat{w}_4(\xi) = C_7 \sin(\eta_1 \xi) + C_8 \cos(\eta_1 \xi) + C_9 \sinh(\theta_1 \xi) + C_{10} \cosh(\theta_1 \xi), \tag{35}$$

$$\begin{aligned}\hat{u}_r(\xi) = {} & C_{11} f_1 \sin(\alpha_1 \xi) - C_{12} f_1 \cos(\alpha_1 \xi) + C_{13} g_2 \cosh(\alpha_2 \xi) - C_{14} g_2 \sinh(\alpha_2 \xi) + \\ & + C_{15} g_3 \cosh(\alpha_3 \xi) + C_{16} g_3 \sinh(\alpha_3 \xi)\end{aligned}, \tag{36}$$

$$\begin{aligned}\hat{w}(\xi) = {} & C_{11} \cos(\alpha_1 \xi) + C_{12} \sin(\alpha_1 \xi) + C_{13} \cosh(\alpha_2 \xi) + C_{14} \sinh(\alpha_2 \xi) + \\ & + C_{15} \cosh(\alpha_3 \xi) + C_{16} \sinh(\alpha_3 \xi)\end{aligned}, \tag{37}$$

$$\begin{aligned}u_2(\xi) = {} & C_{11} p_1 \sin(\alpha_1 \xi) - C_{12} q_1 \cos(\alpha_1 \xi) + C_{13} p_2 \cos(\alpha_2 \xi) - C_{14} q_2 \sin(\alpha_2 \xi) + \\ & + C_{15} p_3 \cosh(\alpha_3 \xi) + C_{16} q_3 \sinh(\alpha_3 \xi) + C_{17} \cos(\psi \xi) + C_{18} \sin(\psi \xi)\end{aligned}. \tag{38}$$

where the parameters $\delta_i, \eta_i, \vartheta_i, \alpha_i, f_i, p_i, q_i$ and ζ are defined in the Appendix II. They depend on geometrical parameters, material properties and the natural angular frequency ω. The continuity and boundary conditions (22-24,31) define a system of eighteen algebraic equations in the eighteen integration constants C_i, i = 1, ..18.

The natural frequencies and corresponding modal shapes are then calculated by imposing the vanishing of the determinant of the system coefficients. It is worth noting that for very low and very large values of the normalized longitudinal stiffness of the ligaments, β, a high precision is required in the numerical solution.

6. NUMERICAL SOLUTION: *CONSTRAINED MODEL*

If any of the assumptions stated at the beginning of the previous section are removed, a closed form solution of the two-point boundary eigenvalue problem is no longer attainable. It is still possible however to proceed with a numerical integration using the method outlined in the Appendix I, which is based on a relaxation technique [34].

The model described in Sections 3 and 4 has been used to investigate the role played by the bridging mechanisms in reducing the delamination-induced degradation of the dynamic properties of delaminated cantilever beams. In this section, results obtained under the assumptions of *constrained model*, $w_2 = w_3 = w$, homogeneous material and negligible shear deformations, will be presented in order to investigate the influence of the longitudinal springs. In the next section, a special geometry leading to opening modes will be examined to investigate the influence of the transversal springs.

The results are presented in terms of normalized natural frequency of vibration f/f_0, with f_0 the natural frequency of the corresponding intact beam, dimensionless longitudinal stiffness of the ligaments $\beta = k_t t / E_1$, normalized length of the delamination, L_{del}/L, normalized length of the beam, L/t, and normalized position of the mid-point of the delamination, L_c/t. The parameter β has been varied between 10^{-7} to 1.0.

It is well known that the first natural frequency of vibration is degraded only by very long delaminations. The diagram of Fig. 2, which refers to $L_{del}/L = 0.50$, $L/t = 50$ and $L_c/L = 0.5$ and shows the first natural frequency versus the dimensionless stiffness β for different thicknesswise positions of the delamination, confirms this result. For very small values of β all curves tend to the normalized frequencies of the delaminated beam in the absence of through-thickness reinforcement [3]. As expected, the curves show a transition from damaged and unbridged values to the values corresponding to an intact beam ($f = f_0$) upon increasing the elastic spring stiffness β. The maximum degradation caused by the delamination corresponds to the case $t_2/t = 0.5$ – for higher values of t_2/t the dynamic properties of the delaminated beam are progressively more affected by the behavior of the thicker sublaminate.

The chart in Fig. 3 illustrates how the f/f_0 ratio corresponding to the first natural frequency varies as a function of β for different delamination locations along the beam length. The chart refers to $L_{del}/L = 0.50$, $t_2/t = 0.5$ and $L/t = 50$ (low values of L_c/L indicate delaminations close to the clamped end). The frequency reduction is stronger for delaminations close to the clamped end.

Figure 4 refers to the first three natural frequency ratios plotted as a function of β for a beam with $L/t = 50$, $L_c/L = 0.5$, $L_{del}/L = 0.25$ and $t_2/t = 0.5$. It can be noted that the reduction of the third natural frequency is considerably higher than those corresponding to the first two modes. Likewise, the effectiveness of the through-thickness reinforcements is correspondingly more evident, taking the value of the third natural frequency from $0.843 f_0$ to f_0 on increasing β.

It is important to note that for all results presented in this section, apart from the curve of Fig. 2 corresponding to $t_2/t = 0.9$ (see next section), the approximation of *constrained model* coincides with the rigorous solution and the sublaminates above and below the delamination plane vibrate with the same transversal displacement.

7. NUMERICAL SOLUTION: GENERAL CASE

In the results presented in this section the assumption of *constrained model* has been relaxed allowing the two sublaminates above and below the delamination plane to vibrate independently. The dimensionless transversal spring stiffness α has been varied between two limit values, α_s and α_c. The two values have been chosen so that when α tends to α_s the frequency ratio approaches the value corresponding to $\alpha = 0$, a condition referred to as *shear-bridged model* that coincides with the *free model* in the special case $\beta = 0$; when α tends to α_c the frequency ratio approaches the value obtained through the *constrained model* and further increases in the value of α do not modify the solution.

Following the experimental and theoretical observations in [2,3], a slender beam, $L/t = 150$, with a long delamination, $L_{del}/L = 0.5$, close to the surface, $t_2/t = 0.9$, has been examined in order to be able to observe the phenomenon of crack opening during vibration. The delamination is centrally located, $L_c/L = 0.5$. As in the previous section, results are presented for a homogeneous material and negligible shear deformations.

In the presence of opening modes, the closure forces exerted by the transversal springs when the delamination opens represent the action of the bridging mechanisms, whereas the opening forces of the same springs simulate the elastic contact forces due to the closure of the delamination. Therefore, allowing relative transversal displacements of the sublaminates causing springs compression does not necessarily imply overlapping of the sublaminates axes, as already observed in Mujumdar et al. [16], as long as the vibration amplitudes remain sufficiently small. In this paper the spring stiffness has been assumed constant in the tensile and compressive regimes. This assumption simplifies the solution of the problem and is not expected to substantially affect the conclusions.

The influence of the spring stiffness parameters on frequency ratios and modal shapes of a cantilever beam are described in Sections 7.1 and 7.2, respectively. Due to the slenderness of the beam, the solutions presented in this section will be quantitatively correct only in a regime of vibration characterized by small amplitudes.

7.1 Influence of spring stiffness parameters on frequency ratios

The frequency ratio f/f_0 corresponding to the first natural frequency of vibration is plotted in Fig. 5 versus the longitudinal stiffness β for $\alpha_s = 10^{-10}$, $\alpha_c = 10^{-8}$ (corresponding to the *shear-bridged* and

constrained models, respectively) and an intermediate value $\alpha = 10^{-9}$. It can be noted that the solution is only slightly affected by α and the intact beam frequency ratio is always approached by adequately increasing β. The negligible influence of α can be explained by noting that, even in the absence of bridging mechanisms, the first modal shape of the delaminated beam is characterized by a small opening of the delamination, thus slightly differing from the *constrained model* condition (see Fig. 11).

For the second natural vibration mode, the frequency reduction induced by the delamination on the cantilever beam in the absence of bridging mechanisms is 59.2% and the limits on α are $\alpha_s = 10^{-11}$ and $\alpha_c = 10^{-7}$. Figure 6 shows a plot of the frequency ratio versus β for $\alpha = \alpha_s$, $\alpha = \alpha_c$ and three intermediate values. In this case the intact beam frequency ratio is approached only for $\alpha \gtrsim \alpha_c$. As it will be shown in Section 7.2 (Fig. 12), the modal shape of the delaminated beam in the absence of bridging mechanisms strongly differs from the *constrained model* approximation, being characterized by a delamination opening whose amplitude is considerably higher than that defining the vibrational motion of the rest of the beam; therefore, for $\alpha < \alpha_c$ the condition $f/f_0 = 1$ cannot be approached.

The trend described for the second natural frequency occurs for the third natural mode as well. In this case, the frequency reduction induced by the delamination on the beam in the absence of bridging mechanisms amounts to 63.4% and the limits on α are $\alpha_s = 10^{-9}$ and $\alpha_c = 10^{-6}$. The plot of the frequency ratio versus β for $\alpha = \alpha_s$, $\alpha = \alpha_c$ and three intermediate values is shown in Fig. 7. In this case the frequency ratio of an intact beam is no longer approached by simply raising α even for $\alpha \gtrsim \alpha_c$. The chart also highlights a limited effect of β in all cases where $\alpha < \alpha_c$.

Figures 8-10 show the dependence of the frequency ratio on the transversal spring stiffness parameter α. The curves in Fig. 8 confirm the negligible influence of α on the first frequency ratio. The chart of Fig. 9, referring to the second natural frequency, clearly shows that the frequency reduction induced by the delamination is completely recovered only if $\alpha \gtrsim \alpha_c = 10^{-7}$. For decreasing values of α, the curves show a growing spread in the vertical direction, which confirms the higher effectiveness of the longitudinal springs. Similarly, the curves in Fig. 10 show that, for the third natural frequency, the degradation induced by the delamination is almost recovered if $\alpha \gtrsim \alpha_c = 10^{-6}$ and $\beta \gtrsim 10^{-4}$. In this case, however, the curves are practically unaffected by β for low values of α.

7.2 Influence of spring stiffness parameters on modal shapes

The two charts in Figure 11 show the first modal shape of the cantilever delaminated beam corresponding to the two limiting solutions of *constrained model* with $\beta = 0$ and *free model* ($\alpha = 0$ and $\beta = 0$). In these graphs and those that follow, the modal shapes have been normalized assuming a unit deflection at the free end. The horizontal and vertical axes define the normalized position along the beam, ξ=x/t, and the normalized deflection, $\overline{w} = w(x)/w(L)$. For $\alpha = 10^{-10}$ the presence of the delamination causes an almost undetectable opening mode that disappears, as expected, for $\alpha = \alpha_c = 10^{-8}$. However, since $\beta = 0$, the normalized frequency of vibration remains lower than one.

Increasing the value of β from 0 to 1 leads to the vanishing of the opening mode and a frequency ratio approaching unity.

The sequence of six charts of Figure 12 describes the evolution of the second modal shape on varying α between α_s and α_c with $\beta = 0$. For the *free model* condition, corresponding to $\alpha = 10^{-10}$, the thinner sublaminate shows a modal shape that is almost symmetric with respect to the center of the delamination, whereas the rest of the beam vibrates according to the first modal shape of an intact cantilever beam. By raising α, the amplitude of the opening mode progressively decreases and the rest of the beam assumes a modal shape corresponding to the second natural frequency of an intact beam. The effect of letting β vary from zero to unit, for each value of α, is that of reducing the amplitude of the opening mode without introducing major alterations in the modal shape.

The evolution of the third modal shape of the delaminated beam for increasing values of α and for $\beta = 0$ is shown in the nine charts of Figure 13. Up to $\alpha \approx 2.0 \cdot 10^{-8}$, the thinner sublaminate vibrates according to the first modal shape of an intact beam clamped at both ends and is out of phase with the rest of the beam that vibrates according to the second modal shape of an intact cantilever beam. The amplitude of the opening mode progressively increases on raising α and this phenomenon has to be thought of as the beginning part of a more complex modification of the modal shape. For α higher then $3.5 \cdot 10^{-8}$, the amplitude of the opening mode decreases, and two interesting modifications appear in the modal shape of the beam: a) the deflected shape of thinner sublaminate crosses the delamination at an intermediate point along the delamination; b) the modal shape of the rest of the beam tends toward that corresponding to the third natural mode of an intact beam. By further increasing α, the thinner sublaminate progressively assumes an anti-symmetric modal shape across the delamination, resembling that corresponding to the second natural mode of an intact beam clamped at both ends. Finally, for $\alpha = \alpha_c \approx 10^{-6}$, the opening mode disappears and the beam vibrates according to a typical third modal shape of an intact beam.

The effect of β on the third modal shape depends on the value assumed for α. For $\alpha \lesssim 2.0 \cdot 10^{-8}$, the effect of raising β is that of increasing the amplitude of the opening mode without altering the modal shape shown by the first four charts of Figure 13. On the other hand, for $\alpha \gtrsim 3.5 \cdot 10^{-8}$, the higher the value of β, the smaller the amplitude of the opening mode, even though the constrained model condition can be reached only for $\alpha \gtrsim \alpha_c = 10^{-6}$. At $\alpha \approx 3.5 \cdot 10^{-8}$, the effect of raising β is illustrated in the three charts of Fig. 14: the thinner sublaminate vibrates with increasing amplitude whereas the rest of the beam is progressively constrained to modify its modal shape from that corresponding to the third natural mode of an intact beam (for $\beta = 0$) back to the second natural mode of an intact beam (for $\beta = 1$).

8. DISCUSSION

In order to understand the variety of results and transitions in the dynamic response observed in Sections 6 and 7, a differentiation must be made between configurations characterized by the absence of opening modes and configurations characterized by the presence of opening modes. For the first the rigorous solution of the problem coincides with the *constrained model* approximation.

Absence of opening modes

When the delamination is not very long and close to the surface of the beam or when the stiffness of the transversal springs is higher than α_c (i.e., $\alpha > 10^{-8} \div 10^{-6}$), the two sub-laminates above and below the delamination plane vibrate with the same transversal displacement. In all these cases, however, the presence of the delamination leads to relative sliding displacements between the crack faces that, in the absence of longitudinal crack bridging mechanisms, reduce both the flexural stiffness of the member and the natural frequencies of vibrations.

The different effect the delamination has on the first, second and third natural frequencies (see Fig. 5) is explained by the different sliding displacements arising during vibration in the corresponding modal shapes. The first and second modal shapes (see for instance last charts of Fig. 11 and 12) are such that very small crack sliding arises during vibration and the beam behaves almost like an intact beam. On the other hand, the third modal shape is such that large sliding displacements arise during vibration and consequently the effect of the delamination on the frequency reduction is much stronger (see for instance last chart of Fig. 13).

The above observations have been confirmed by numerical calculations. The diagram of Fig. 15 has been obtained for the special geometry of Section 7 ($L_{del}/L = 0.5$, $L_c/L = 0.5$, $L/t = 150$ and $t_2/t = 0.9$) and assuming $\beta = 0$ in order to describe how the sliding displacement between the crack surfaces is controlled by the stiffness of the transversal springs. A parameter λ has been introduced as a measure of the total sliding displacement:

$$\lambda = \frac{1}{t}\int_0^{L_{del}} |u_2 - u_3 + \varphi_2 h_2 + \varphi_3 h_3| dx . \tag{39}$$

where the integrand defines the crack sliding at the coordinate x along the delamination. The parameter λ has been calculated numerically and diagrammed as a function of α for the first three modal shapes. In the diagram, the absence of opening modes corresponds to values of α higher than $\alpha_c = 10^{-8} \div 10^{-6}$. The diagram shows that, for such values of α, λ corresponding to the first and second modes of vibration is virtually zero while large values of λ characterize the third mode.

In all configurations characterized by the absence of opening modes, the effect of the longitudinal springs is always that of restoring the conditions of an intact beam (see Figs. 2-4).

Presence of opening modes

In the configurations characterized by opening modes during vibration substantial reductions of all natural frequencies are typically observed. This happens both when crack sliding displacements are allowed, i.e. when $\beta = 0$ (see first charts of Fig. 12-14), and when they are impeded by stiff londitudinal springs (see last chart of Fig. 14).

The longitudinal springs have different influence on the first, second and third natural frequencies of vibration. For the second mode of vibration large crack sliding displacements are observed in the absence of bridging mechanisms, for $\alpha = 0$ and $\beta = 0$ (Fig. 15 and first chart of Fig. 12). Consequently, when present, the longitudinal springs will be significantly engaged and their influence on the frequency ratio will be strong (Fig. 6). For the third mode of vibration, on the other hand, negligible crack sliding displacements are observed in the absence of crack bridging mechanisms (Fig. 15 and first chart of Fig. 13) and consequently the longitudinal springs will not have a strong influence on the frequency ratios unless the stiffness of the transversal springs is simultaneously increased to prevent the opening (Fig. 7). In this case the beam then behaves as explained above for the *constrained mode* case.

9. APPLICATION TO A STITCHED QUASI-ISOTROPIC LAMINATE

The model formulated in the previous sections has been applied to investigate if a through-thickness reinforcement could contrast the degradation of the dynamic properties of delaminated beams. To this purpose, a 48-ply carbon/epoxy quasi-isotropic laminate, of thickness 7.2 mm, stitched with glass fiber tows and tested in [35-36] has been considered. The laminate had a reduced longitudinal Young's modulus of 49 GPa and a shear modulus of 2.6 GPa. The stitches were spaced according to a square array of side 3.2 mm, with a resulting stitch area fraction of 0.062.

Experimental shear tests have been performed in [35] in order to define the constitutive relationship, shear load versus crack sliding displacement, of a single stitch. The tests were carried out loading in shear small notched cubes containing just one or two stitches. Experimental curves representing the shear force applied to the stitch versus the relative sliding displacement are shown in Fig. 16. The experimental data show a linearly increasing branch followed by a nonlinearly decreasing one at a large value of the sliding displacement corresponding to the failure of the stitch. The results presented in Fig. 16 have been used to define the constitutive law of the longitudinal springs of the theoretical model by assuming an equivalent uniform distribution of reinforcements (see right ordinate axis of the diagram of Fig. 16). The approximation of discrete stitches as uniformly distributed springs is correct provided the stitch density is high enough and the length of the delamination is sufficiently long. For relatively small values of the sliding displacement the experimental data can then be

approximated by a linear bridging law describing the first branch of the experimental curve. The equivalent normalized stiffness of the uniformly distributed springs of the theoretical model is $\beta = 0.01$.

Cuboidal specimens similar to those tested in shear were also tested in axial tension in [36] and the stitches showed an axial stiffness much greater than the shear stiffness. This implies that the value of the normalized stiffness of the transversal springs, α, is much higher than all values of α_c presented in Section 7 so that the *constrained model* assumption is always satisfied.

Circles have been used to highlight the solutions corresponding to $\beta = 0.01$ in Figs. 2-4. The data in Fig. 2 show that for a mid-plane delamination, $t_2/t = 0.5$, the reinforcements are able to raise the f/f_0 ratio from 0.926 to 0.992. Figure 3 shows that, for the particular geometry considered, $\beta = 0.01$ ensures that no reduction is observed in the first natural frequency regardless of the location of the delamination along the beam. Finally, the chart of Fig. 4 indicates that the third natural frequency mostly benefits of the reinforcements: the f/f_0 ratio is brought from 84.4 % to 94.7% of its intact value. The recovery is even greater for longer delaminations. Results corresponding to the material tested in [35] can be observed in the diagrams of Figs. 5-10 for $\beta = 0.01$ and α corresponding to the constrained model (c.m.).

10. CONCLUSIONS

A theoretical model has been formulated to investigate how linear elastic bridging mechanisms can reduce the degrading effects of delaminations on the dynamic response of beam-type structures. The model is based on the first order shear deformation theory for laminated plates and includes the effect of the rotational inertia. The bridging mechanisms are represented by uniformly distributed springs that oppose transversal and longitudinal relative displacements between the surfaces of the delamination.

Assuming no extensional/bending coupling in the beam constitutive equations, negligible shear deformations and the absence of opening modes, the model has been applied to analyze cantilever beams with rectangular cross sections and delaminations differently located in the longitudinal and transversal directions. The effectiveness of the longitudinal springs on reducing the natural frequency shifts has been demonstrated through the transition from damaged to intact beam values upon increasing the stiffness of the springs.

The model has then been applied to a geometrical configuration of the delaminated beam in which, in the absence of bridging mechanisms, opening modes would occur. The influence of both longitudinal and transversal spring stiffness on the first natural frequencies and corresponding modal shapes has been assessed. It has been shown that, by increasing the transversal longitudinal spring stiffness from zero to relatively high values, the modal shape of the delaminated beam undergoes a transition during which the opening mode progressively disappears. Simultaneously, the global mode of vibration of the beam changes: from a first to a second mode of vibration for the second modal

shape and from a second to a third mode of vibration for the third modal shape.

The model has been formulated for composite laminates characterized by extensional/bending constitutive coupling. Results have been presented only for a homogeneous material and assuming negligible shear deformations. It is expected that the quantitative results will be modified if the lay-up of the laminate is not symmetric about the mid-planes of the beams. However, the general conclusions drawn on the dynamic response of delaminated beams, the transitions observed on varying the stiffness of the springs and the influence of a through-thickness reinforcement are expected to hold true.

The application of the model to a laminate composite reinforced through the thickness by stitching and previously tested in [35], has shown that low percentages of through-thickness reinforcements can substantially improve the dynamic response of delaminated beams and restore the conditions of an intact beam. In particular, low area fractions of through-thickness reinforcement can ensure the absence of opening modes during vibration also for geometries characterized by very long delamination cracks close to the surface of the beam.

ACKNOWLEDGMENTS

The authors would like to acknowledge support from the European Research Office of the U.S. Army, contract number N68171-01-M-5909 to the University of Genoa, from the Italian Department for the University and for Scientific and Technological Research and from Northwestern University.

REFERENCES

1. Wang JTS, Liu YY, Gibby JA. Vibration of split beams. *Journal of Sound and Vibration* 1982; 84 (4): 491-502.
2. Shen M, Grady JE. Free vibrations of delaminated beams. *AIAA Journal* 1992; 30 (5), 1361-1370.
3. Luo H, Hanagud S. Dynamics of delaminated beams. *International Journal of Solids and Structures* 2000; 37: 1501-1519.
4. Yang PC, Norris CH, Stavsky Y. Elastic wave propagation in heterogeneous plates. International *Journal of Solids and Structures* 1966; 2: 665-684.
5. Whitney JM, Leissa AW. Analysis of heterogeneous anisotropic plates. *Journal of Applied Mechanics* 1969; 36(2): 261-266.
6. Whitney JM, Pagano NJ. Shear deformation in heterogeneous anisotropic plates. *Journal of Applied Mechanics* 1970; 37: 1031-1036.
7. Massabò R, Cox BN. Concepts for bridged mode II delamination cracks. *J. Mech. Phys. Solids* 1999; 47 (6):, 1265-1300.

8. Mouritz AP, Bannister MK, Falzon PJ, Leong KH. Review of Applications for Advanced Three-Dimensional Fibre Textile Composites. *Composite A.* 1999; 30 (12): 1445-1461.
9. Freitas G, Magee C, Dardzinski P, Fusco T. Fiber Insertion Process for Improved Damage Tolerance in Aircraft Laminates. *Journal of Advanced Materials* 1994; 25(4): 36-43.
10. Dransfield, K, Baillie C, Mai YW. Improving the Delamination Resistance of CFRP by Stitching – a Review. *Composite Science and Technology* 1994; 50: 305-317.
11. Dexter HB, Funk JG. Impact Resistance and Interlaminar Fracture Toughness of Through-the-thickness Reinforced Graphite/Epoxy. *AIAA Journal* 1986; 86-CP: 700-709.
12. Jain LK, Mai YW. Analysis of stitched laminated ENF specimens for interlaminar mode-II fracture toughness. *Int. Journal of Fracture* 1994; 68 (3): 219-244.
13. Jain LK, Mai YW. Determination of mode II delamination toughness of stitched laminated composites. *Composite Science and Technology* 1995; 55: 241-253.
14. Massabò R, Mumm D, Cox BN. Characterizing mode II delamination cracks in stiched composites. *Int. Journal of Fracture* 1998; 92 (1): 1-38.
15. Massabò, R., and Cox, B.N., Unusual characteristics of mixed mode delamination fracture in the presence of large scale bridging, *Mechanics of Composite Materials and Structures*, 2001, 8(1), 61-80.
16. Ramkumar RL, Kulkarni SV, Pipes RB. Free vibration frequencies of a delaminated beam. In: Reinforced Plastics/Composites Institute, 34th Annual Technical Conference, 1979. The Society of the Plastics Industry Inc. 22-E, 1-5.
17. Mujumdar PM, Suryanarayan S. Flexural vibration of beams with delaminations. Journal of Sound and Vibrations 1988; 125 (3): 441-461.
18. Tracy JL, Pardoen GC. Effect of delamination on the natural frequencies of composite laminates. *Journal of Composite Materials* 1989; 23: 1201-1215.
19. Ju F, Lee HP, Lee KH. Dynamic response of delaminated composite beams with intermittent contact in delaminated segments. *Composite Engineering* 1994; 4 (12): 1211-1224.
20. Kwon YW, Aygunes H. Dynamic finite element analysis of laminated beams with delamination cracks using contac-impact conditions. *Computer & Structures* 1994; 58 (6): 1161-1169.
21. Lu X, Lestari W., Hanagud S. Nonlinear vibrations of a delaminated beam. *Journal of Vibration and Control* 2001; 7: 803-831.
22. Lee J. Free Vibration analysis of delaminated composite beams. *Computers and Structures* 2000; 74, 121-129.
23. Tenek HT, Henneke EG, Gunzburger MD. Vibration of delaminated composite plate and some applications to non-destructive testing. *Composite Structures* 1993; 23(3); 253-262.
24. Nosier A., Reddy, J.N.. On vibration and buckling of symmetric laminated plates according to shear deformation theory. *Acta Mechanica*, Part I 1992; 94: 123-144.

25. Nosier A., Reddy, J.N.. On vibration and buckling of symmetric laminated plates according to shear deformation theory. *Acta Mechanica*, Part II 1992; 94: 145-169.
26. Nosier A., Kapania R.K., Reddy, J.N.. Free-vibration analysis of laminated plates using a layerwise theory. *AIAA Journal.* 1993; 31(12): 2335-2346.
27. Yin WL, Jane KC. Vibration of delaminated beam-plate relative to buckled states. *Journal of Sound and Vibration* 1992; 156(1): 125-140.
28. Jane KC, Chen CC. Postbuckling deformation and vibration of a delaminated beam-plate with arbitrary delamination location. *Mechanics Research Communications* 1998; 25(3): 337-351.
29. Chang TP, Liang JY. Vibration of postbuckled delaminated beam-plates. *Int. J. Solids Structures* 1998; 35(12): 1199-1217.
30. Shiau L. Delamination effect on flutter of homogeneous laminated plates. *Journal of Aerospace Engineering* 1992; 6 (3): 284-298.
31. Brandinelli L, Massabò R. Dynamic response of delaminated beams in the presence of through-thickness reinforcements (in Italian). In: Proc. of the 15th AIMETA Conference of the Italian Association of Theoretical and Applied Mechanics, Taormina, Italy, 2001, ISSN 1592-8950.
32. Brandinelli L., Delamination fracture and dynamics of advanced composite structures, Thesis for Ph. D. Degree, Department of Structural and Geothecnical Engineering, University of Genova, Genova Italy, in preparation, 2003.
33. Meirovitch L. Methods of Analytical Dynamics. New York, NY: McGraw-Hill, 1967.
34. Keller, HB Numerical methods for two-point boundary value problems. Waltham, MA: Blaisdell, 1968.
35. Cox, B.N., Massabò, R., Mumm, D., Turrettini, A. and Kedward, K. (1997), Delamination fracture in the presence of through-thickness reinforcement, proc. of the ICCM-11 *International Conference on Composite Materials*, Venue, Gold Coast, Australia, M.L. Scott (ed.), Woohhead Publishing, Melbourne, vol.1, 159-177.
36. Turrettini, A., Thesis for Masters Degree, Department of Mechanical Engineering, University of California, Santa Barbara, 1996.
37. Press W.P, Teukolsky, S.A., Vetterling, W.T. and Flannery, B.P., Numerical recipes in fortran, Cambridge University Press, 2nd edition, UK, 1992.

APPENDIX I: NUMERICAL SOLUTION OF THE BOUNDARY EIGENVALUE PROBLEM

For the numerical solution of the boundary eigenvalue problem formulated in Section 4 the governing equations (10-18) are first transformed into an equivalent sets of first order ordinary differential equations. To this purpose, the following notation is introduced:

$$\hat{u}_{i_j} = \frac{\partial \hat{u}_{i_{j-1}}}{\partial \xi}, \qquad \hat{w}_{i_j} = \frac{\partial \hat{w}_{i_{j-1}}}{\partial \xi}, \qquad \varphi_{i_j} = \frac{\partial \varphi_{i_{j-1}}}{\partial \xi}, \tag{A1.1}$$

where it is understood that:

$$\hat{u}_{i_0} = \hat{u}_i, \qquad \hat{w}_{i_0} = \hat{w}_i, \qquad \varphi_{i_0} = \varphi_i. \tag{A1.2}$$

The unknowns quantities of the problem are the 32 displacements introduced in (A1.1, A1.2) and the eigenvalue ψ. The system is completed by the boundary and continuity conditions (19-24) and by artificially adding the equation

$$\psi_{,\xi} = 0 \tag{A1.3}$$

,

which merely states that the eigenvalue is independent from the dimensionless abscissa ξ [37].

The system of governing equations and related boundary and continuity conditions define a two-point boundary value problem with internal boundary conditions which are solved numerically using a relaxation technique [34,37]. The dependent variables are arbitrarily numbered in order to define the unknown vector $\vec{y} = \{y_1, y_2 \cdots y_N\}$. The first order ordinary differential equations (ODEs) are then replaced by approximate finite difference equations (FDEs) on a grid of points that spans the interval of interest. The present problem involves $N = 33$ coupled first-order ODEs approximated by just as many FDEs on a mesh of M points, leading to a total of N x M unknowns.

The relaxation method provides the solution by starting with an initial guess that is improved iteratively. As for the iteration scheme, the multidimensional Newton's method provides a simple algebraic matrix equation to be solved for the N corrections Δy_i at the M grid points. Following the procedure described in [37] for two-boundary value problems and adapting it to deal with the presence of the internal conditions, the matrix of the algebraic system takes a special "block diagonal" form that allows efficient inversion. More details on the numerical solution can be found in [33].

APPENDIX II: DERIVATION OF THE GENERAL SOLUTION

The general integrals (32-35) of Eqs. (25a,b) and (26a,b) are straightforward. The following parameters have been introduced in (32-35) with $i = 1$ and 4:

$$\delta_i = \sqrt{\psi}, \quad \eta_i = \sqrt{\frac{\psi}{2}\left(\sqrt{1+\frac{48}{\psi}}+1\right)}, \quad \vartheta_i = \sqrt{\frac{\psi}{2}\left(\sqrt{1+\frac{48}{\psi}}-1\right)}, \tag{A2.1}$$

In order to determine Eqs. (36,37), Eq. (30) has to be solved with respect to $\hat{u}_{r,\xi}$. Substituting the result into Eq. (29), after differentiation with respect to ξ, provides the following ordinary differential equation in the unknown $\hat{w}$:

$$\hat{w}_{,\xi\xi\xi\xi\xi\xi} + \chi\hat{w}_{,\xi\xi\xi\xi} + \delta\hat{w}_{,\xi\xi} + \phi\hat{w} = 0 \quad , \tag{A2.2}$$

where the quantities χ, δ and ϕ are functions of the eigenvalue ψ and the stiffness parameter β:

$$\chi = 2(\psi - 8\beta), \qquad \delta = \psi(\psi - 16\beta - 48), \qquad \phi = 48\psi(4\beta - \psi) \quad . \tag{A2.3}$$

The general solution of Eq. (A2.2) corresponds to Eq. (37), where the quantities α_i are the solutions of the cubic characteristic equation associated to the differential equation (A2.2).

Differentiating Eq. (30) with respect to ξ and substituting the result into Eq. (29) provides:

$$\hat{u}_r = \frac{1}{\tau}\left[-\hat{w}_{,\xi\xi\xi\xi\xi} + \mu\hat{w}_{,\xi\xi\xi} + \nu\hat{w}_{,\xi}\right] \quad , \tag{A2.4}$$

where τ, μ and ν are given by:

$$\tau = 24\beta(\psi - 4\beta), \qquad \mu = 12\beta - \psi, \qquad \nu = 48(\psi - \beta) \quad . \tag{A2.5}$$

Substituting Eq. (37) into Eq. (A2.5) provides the general integral (36), where the quantities f_i and g_i take the following form:

$$f_i = \frac{\alpha_i}{\psi}\left(\frac{\alpha_i^4}{\tau} + \frac{\lambda\alpha_i^2}{\tau} - 48\frac{\psi}{\tau} + 2\beta\right), \qquad g_i = -\frac{\alpha_i}{\psi}\left(\frac{\alpha_i^4}{\tau} - \frac{\lambda\alpha_i^2}{\tau} - 48\frac{\psi}{\tau} - 2\beta\right) \quad . \tag{A2.6}$$

Finally, rewriting Eq. (27) as:

$$\hat{u}_{2,\xi\xi} + \psi\hat{u}_{2,\xi} = -2\beta\left(\hat{u}_r + \frac{\hat{w}_{,\xi}}{2}\right) \quad , \tag{A2.7}$$

and substituting Eqs. (36,37), leads to the general integral (38), with p_i and q_i given by:

$$p_i = -2\beta\left(f_i - \frac{\alpha_i}{2}\right), \qquad q_i = -2\beta\left(f_i + \frac{\alpha_i}{2}\right) \quad . \tag{A2.8}$$

FIGURE CAPTIONS

Figure 1: a) Schematic of the four-beam model for a delaminated beam; b) Stress resultants and displacements.

Figure 2: Normalized first natural frequency of vibration as a function of the normalized stiffness β for different transversal locations of the delamination ***(constrained model).***

Figure 3: Normalized first natural frequency of vibration as a function of the normalized stiffness β for different longitudinal locations of the delamination ***(constrained model).***

Figure 4: Normalized first, second and third natural frequencies of vibration as a function of the normalized stiffness β for a mid-plane delamination centrally located ***(constrained model).***

Figure 5: Dependance of the frequency ratio on the normalized stiffness β for the first natural frequency (s.m.: shear-bridged model; c.m.: constrained model).

Figure 6: Dependance of the frequency ratio on normalized stiffness β for the second natural frequency (s.m.: shear-bridged model; c.m.: constrained model).

Figure 7: Dependance of the frequency ratio on the normalized stiffness β for the third natural frequency (s.m.: shear-bridged model; c.m.: constrained model).

Figure 8: Dependance of the frequency ratio on the normalized stiffness α for the first natural frequency (s.m.: shear-bridged model; c.m.: constrained model).

Figure 9: Dependance of the frequency ratio on the normalized stiffness α for the second natural frequency (s.m.: shear-bridged model; c.m.: constrained model).

Figure 10: Dependance of the frequency ratio on the normalized stiffness α for the third natural frequency (s.m.: shear-bridged model; c.m.: constrained model).

Figure 11: Evolution of the first modal shape versus the normalized stiffness α, assuming $\beta = 0$.

Figure 12: Evolution of the second modal shape versus the normalized stiffness α, assuming $\beta = 0$.

Figure 13: Evolution of the third modal shape versus the normalized stiffness α, assuming $\beta = 0$.

Figure 14: Evolution of the third modal shape versus the normalized stiffness β, assuming $\alpha = 3.5*10^{-8}$.

Figure 15: Dependence of the parameter λ on the transversal spring stiffness α, assuming $\beta = 0$.

Figure 16: Shear load versus sliding displacement from cuboidal specimens of a stitched quasi-isotropic laminate containing one S-2 glass fiber tow (after [35]).

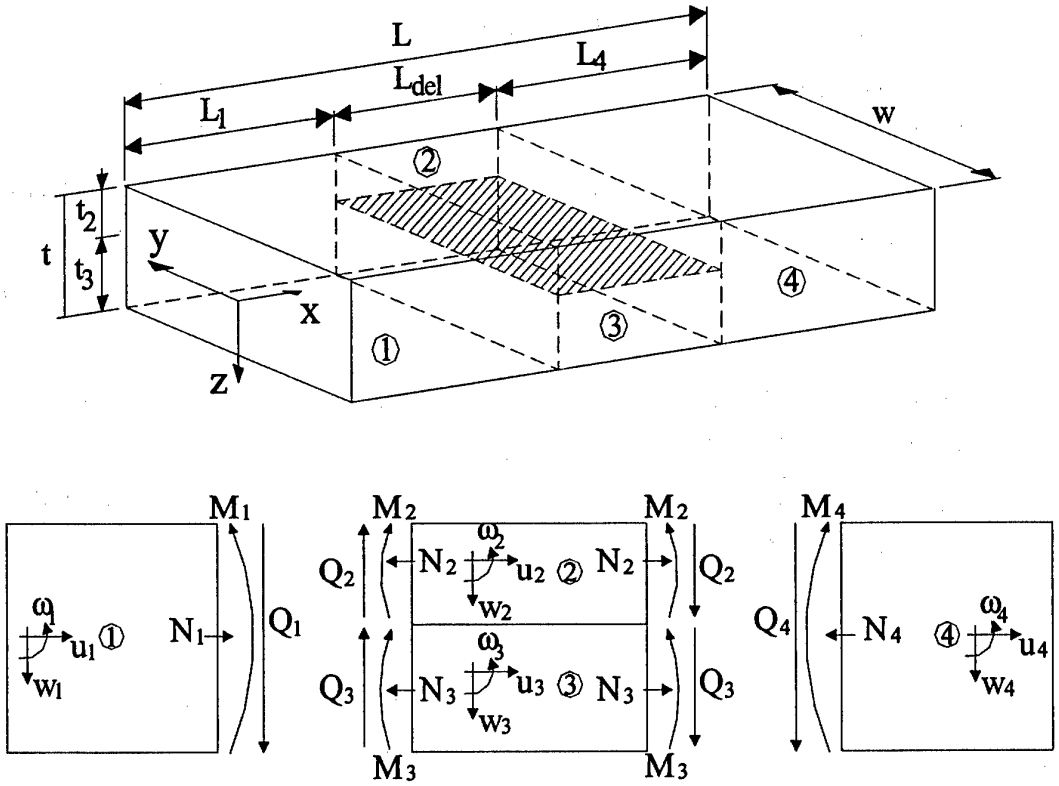
L
L_del
L_4
L_1
w
t
t_2
t_3
y
x
z
①
②
③
④
M_1
N_1
Q_1
ω_1
u_1
w_1
M_2
Q_2
N_2
ω_2
u_2
w_2
Q_3
N_3
ω_3
u_3
w_3
M_3
M_4
Q_4
N_4
ω_4
u_4
w_4

FIGURE 1

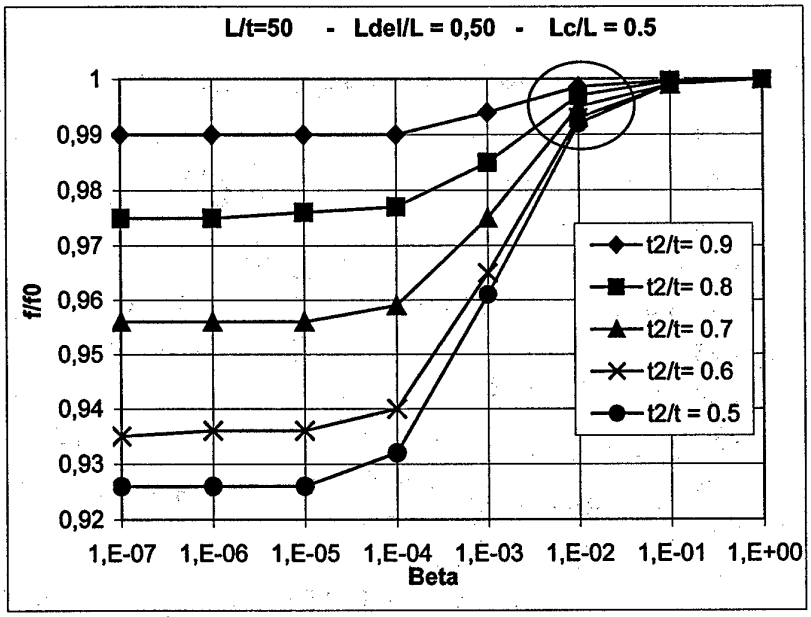
L/t=50 - Ldel/L = 0,50 - Lc/L = 0.5
f/f0
1
0,99
0,98
0,97
0,96
0,95
0,94
0,93
0,92
1,E-07
1,E-06
1,E-05
1,E-04
1,E-03
1,E-02
1,E-01
1,E+00
Beta
t2/t= 0.9
t2/t= 0.8
t2/t= 0.7
t2/t= 0.6
t2/t = 0.5

FIGURE 2

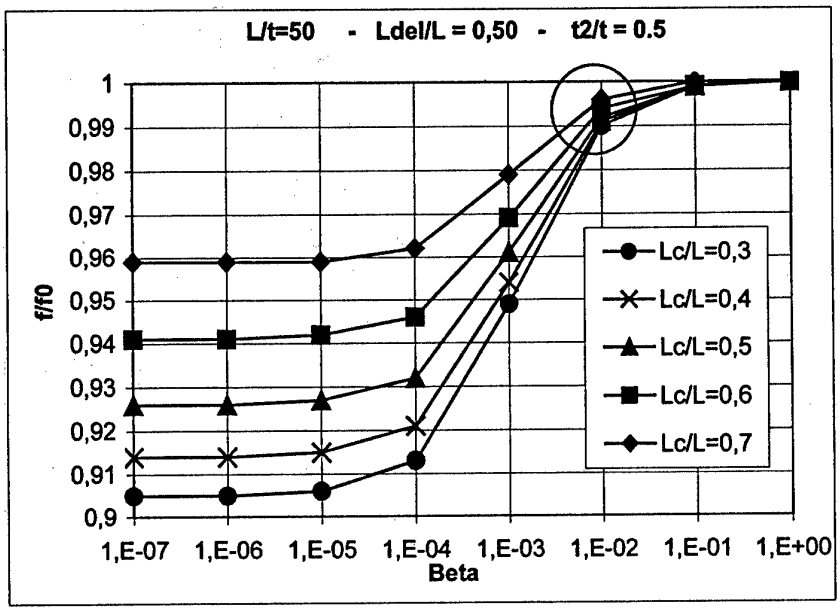
L/t=50 - Ldel/L = 0,50 - t2/t = 0.5
f/f0
1
0,99
0,98
0,97
0,96
0,95
0,94
0,93
0,92
0,91
0,9
1,E-07
1,E-06
1,E-05
1,E-04
1,E-03
1,E-02
1,E-01
1,E+00
Beta
Lc/L=0,3
Lc/L=0,4
Lc/L=0,5
Lc/L=0,6
Lc/L=0,7

FIGURE 3

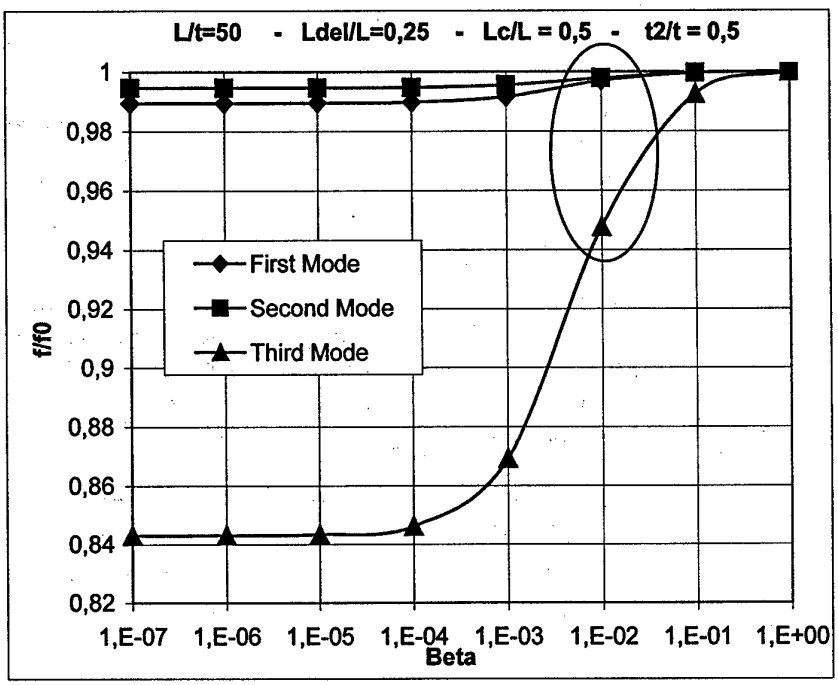
L/t=50 - Ldel/L=0,25 - Lc/L = 0,5 - t2/t = 0,5
1
0,98
0,96
0,94
0,92
0,9
0,88
0,86
0,84
0,82
f/f0
First Mode
Second Mode
Third Mode
1,E-07
1,E-06
1,E-05
1,E-04
1,E-03
1,E-02
1,E-01
1,E+00
Beta

FIGURE 4

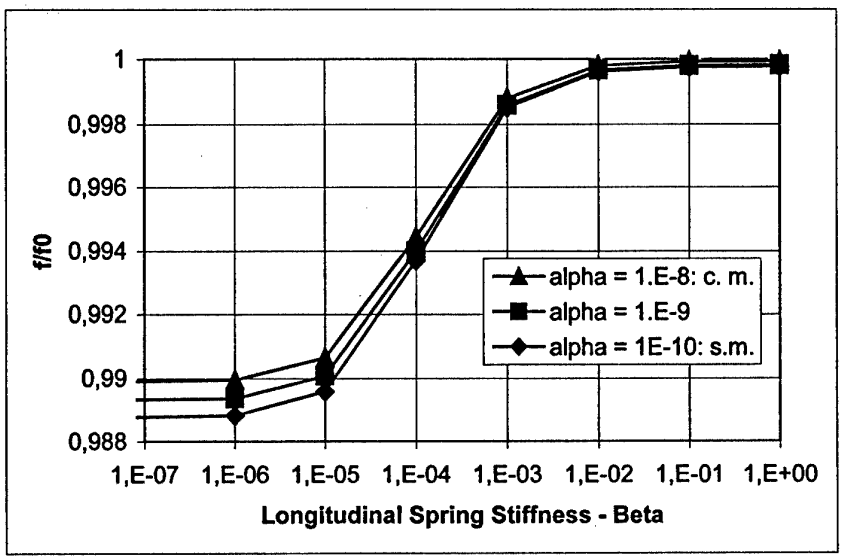
1
0,998
0,996
0,994
0,992
0,99
0,988
f/f0
1,E-07
1,E-06
1,E-05
1,E-04
1,E-03
1,E-02
1,E-01
1,E+00
Longitudinal Spring Stiffness - Beta
alpha = 1.E-8: c. m.
alpha = 1.E-9
alpha = 1E-10: s.m.

FIGURE 5

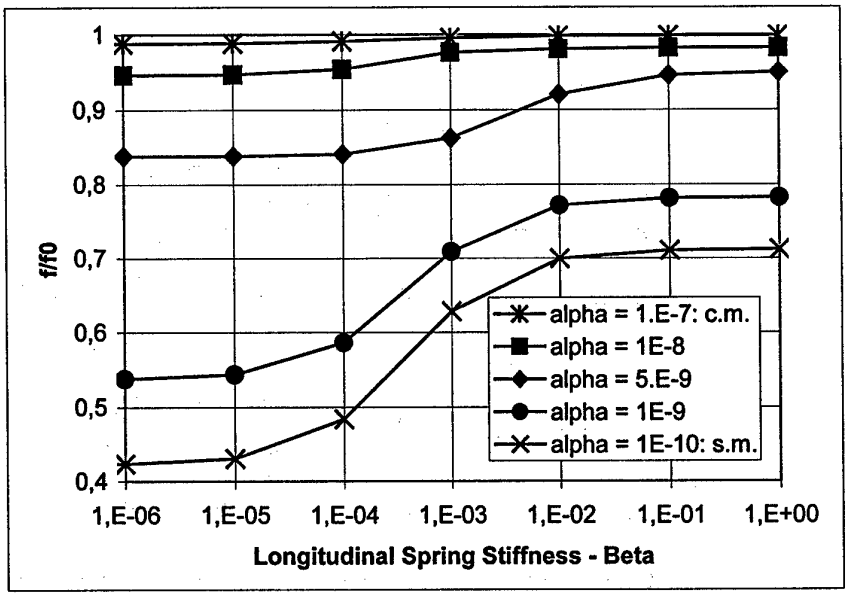
1
0,9
0,8
0,7
0,6
0,5
0,4
f/f0
1,E-06
1,E-05
1,E-04
1,E-03
1,E-02
1,E-01
1,E+00
Longitudinal Spring Stiffness - Beta
alpha = 1.E-7: c.m.
alpha = 1E-8
alpha = 5.E-9
alpha = 1E-9
alpha = 1E-10: s.m.

FIGURE 6

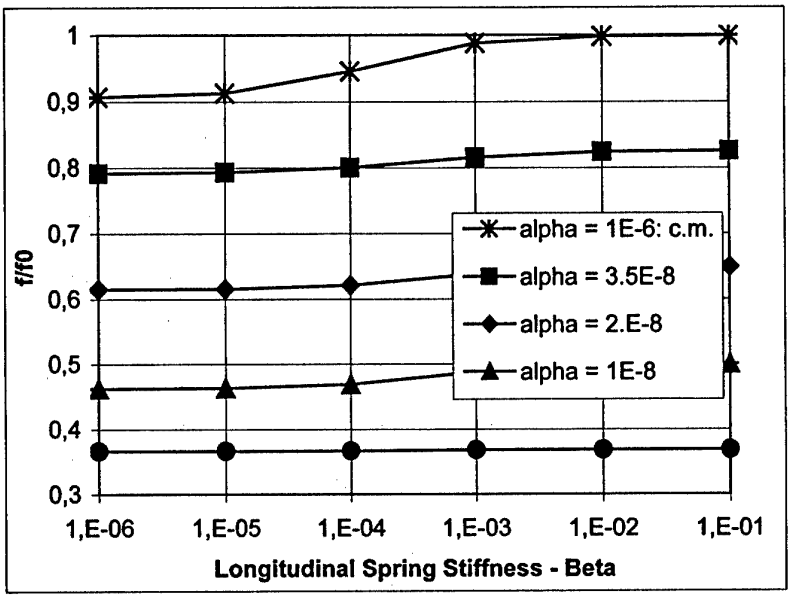
1
0,9
0,8
0,7
0,6
0,5
0,4
0,3
f/f0
1,E-06
1,E-05
1,E-04
1,E-03
1,E-02
1,E-01
Longitudinal Spring Stiffness - Beta
alpha = 1E-6: c.m.
alpha = 3.5E-8
alpha = 2.E-8
alpha = 1E-8

FIGURE 7

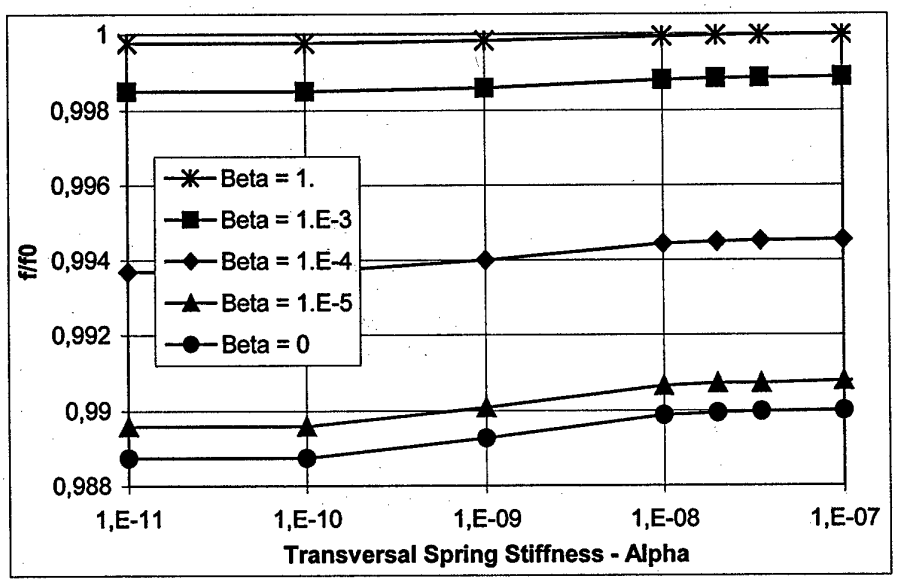
1
0,998
0,996
0,994
0,992
0,99
0,988
f/f0
Beta = 1.
Beta = 1.E-3
Beta = 1.E-4
Beta = 1.E-5
Beta = 0
1,E-11
1,E-10
1,E-09
1,E-08
1,E-07
Transversal Spring Stiffness - Alpha

FIGURE 8

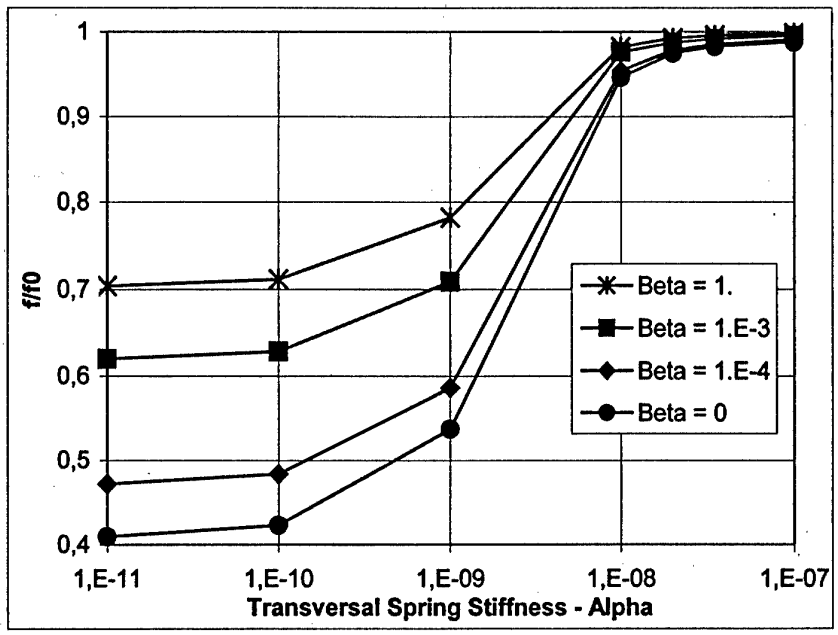
1
0,9
0,8
0,7
0,6
0,5
0,4
f/f0
1,E-11
1,E-10
1,E-09
1,E-08
1,E-07
Transversal Spring Stiffness - Alpha
Beta = 1.
Beta = 1.E-3
Beta = 1.E-4
Beta = 0

FIGURE 9

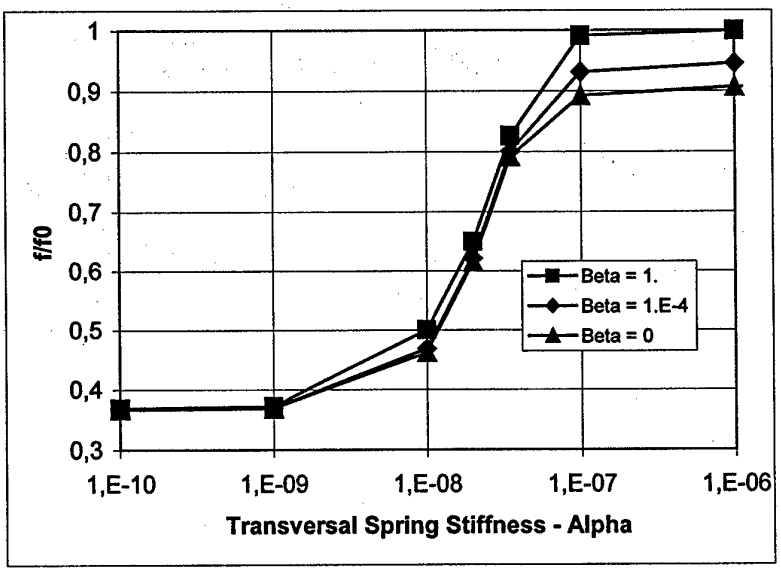
1
0,9
0,8
0,7
0,6
0,5
0,4
0,3
f/f0
1,E-10
1,E-09
1,E-08
1,E-07
1,E-06
Transversal Spring Stiffness - Alpha
Beta = 1.
Beta = 1.E-4
Beta = 0

FIGURE 10

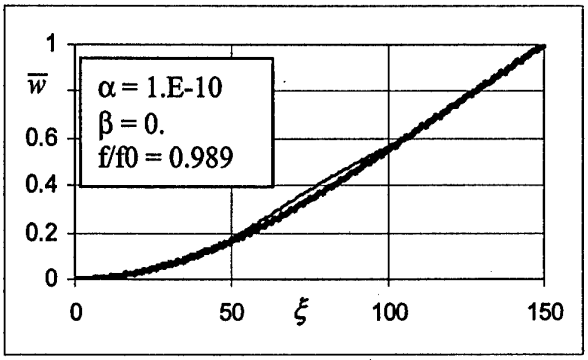
1
$\overline{w}$
0.6
0.4
0.2
0
α = 1.E-10
β = 0.
f/f0 = 0.989
0
50
ξ
100
150

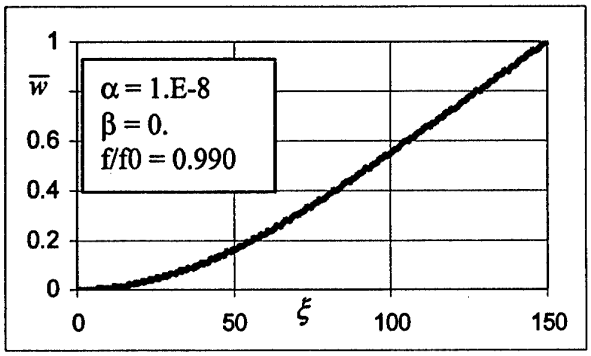
1
$\overline{w}$
0.6
0.4
0.2
0
α = 1.E-8
β = 0.
f/f0 = 0.990
0
50
ξ
100
150

FIGURE 11

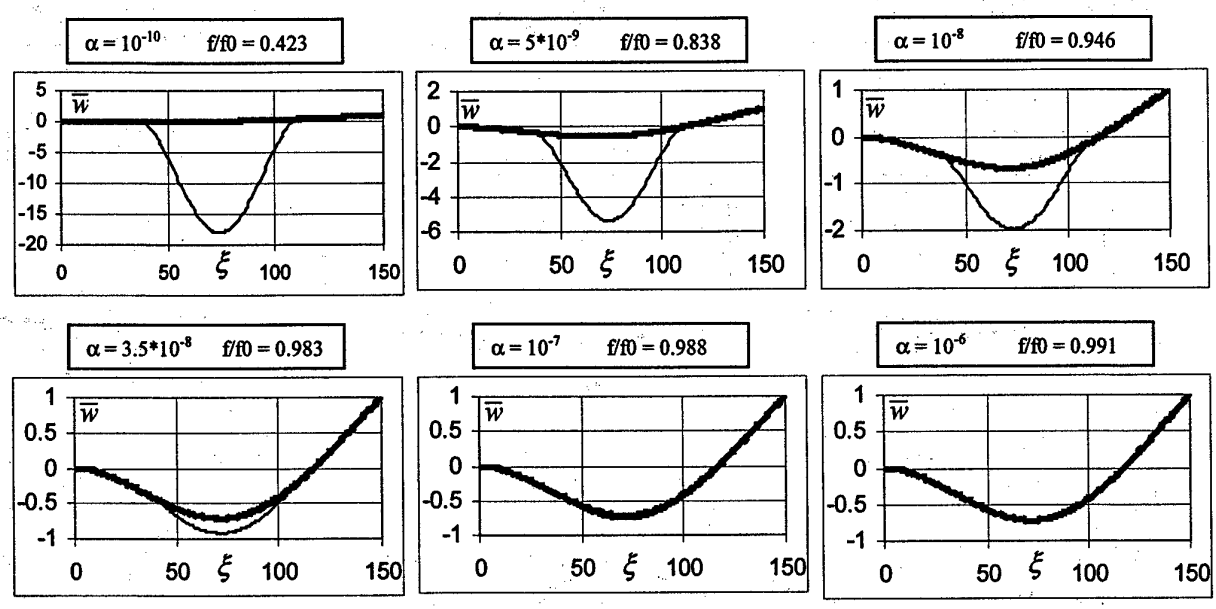
α = 10^-10 f/f0 = 0.423
α = 5*10^-9 f/f0 = 0.838
α = 10^-8 f/f0 = 0.946
α = 3.5*10^-8 f/f0 = 0.983
α = 10^-7 f/f0 = 0.988
α = 10^-6 f/f0 = 0.991
w̄
ξ
0
50
100
150

FIGURE 12

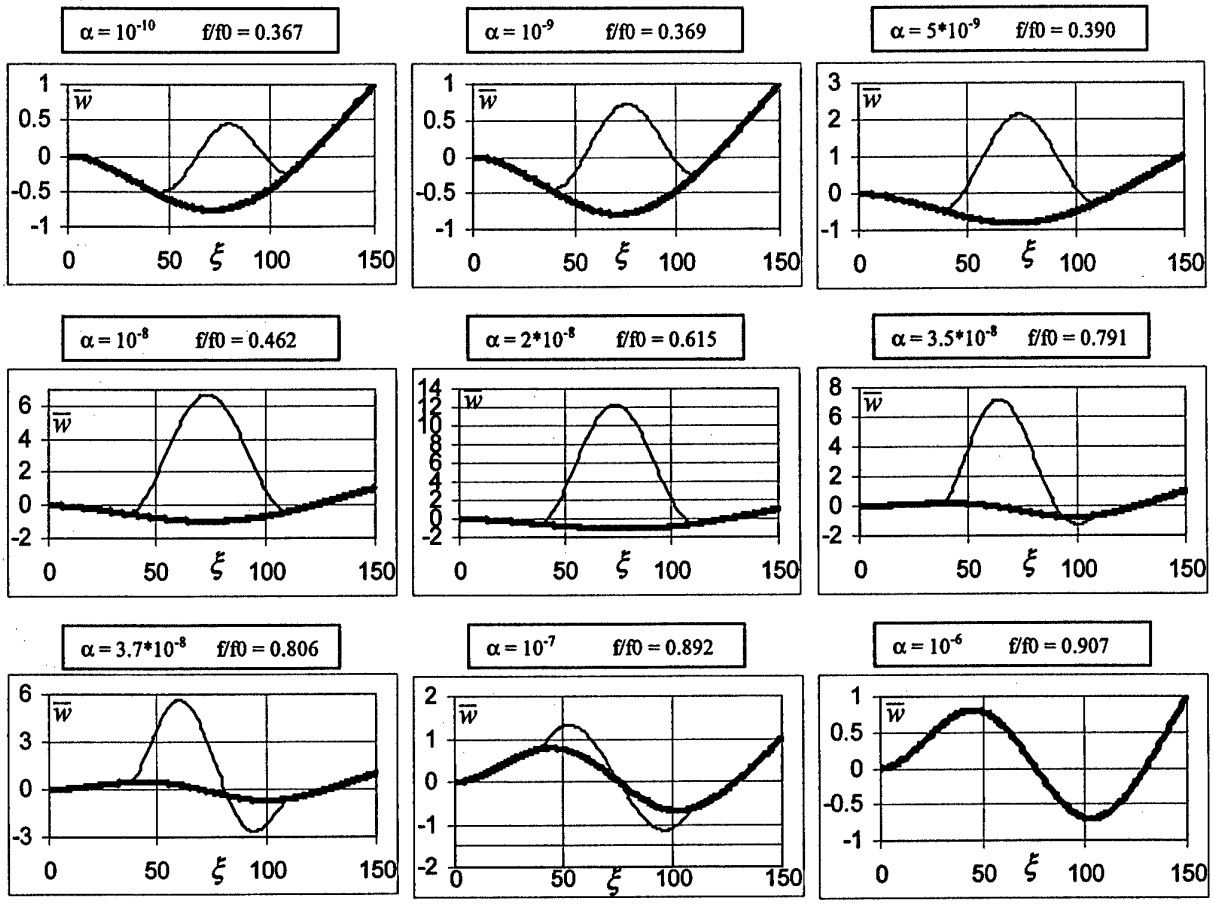
α = 10^-10 f/f0 = 0.367
α = 10^-9 f/f0 = 0.369
α = 5*10^-9 f/f0 = 0.390
α = 10^-8 f/f0 = 0.462
α = 2*10^-8 f/f0 = 0.615
α = 3.5*10^-8 f/f0 = 0.791
α = 3.7*10^-8 f/f0 = 0.806
α = 10^-7 f/f0 = 0.892
α = 10^-6 f/f0 = 0.907
w
ξ
0
50
100
150

FIGURE 13

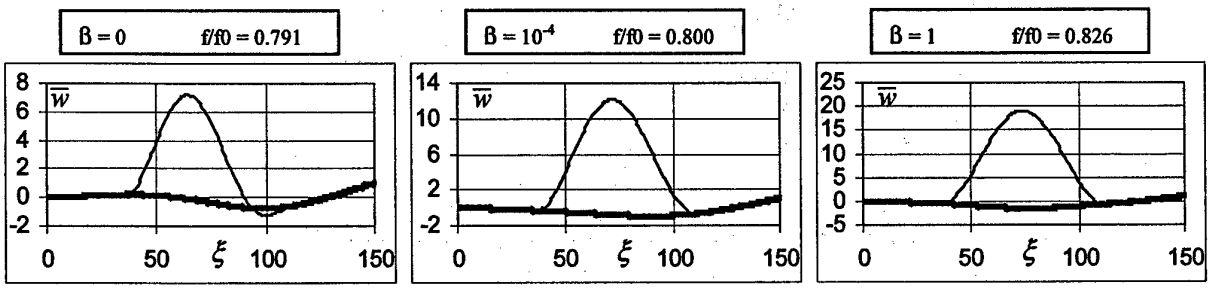
β = 0 f/f0 = 0.791
β = 10⁻⁴ f/f0 = 0.800
β = 1 f/f0 = 0.826
w̄
ξ
8
6
4
2
0
-2
14
10
6
2
-2
25
20
15
10
5
0
-5
0
50
100
150

FIGURE 14

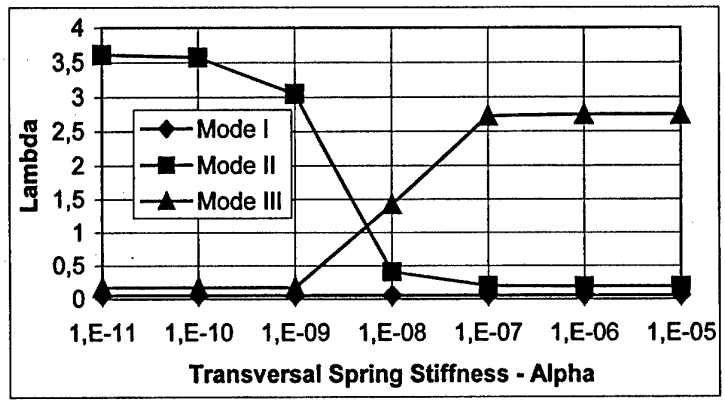
4
3,5
3
2,5
2
1,5
1
0,5
0
Lambda
Mode I
Mode II
Mode III
1,E-11
1,E-10
1,E-09
1,E-08
1,E-07
1,E-06
1,E-05
Transversal Spring Stiffness - Alpha

FIGURE 15

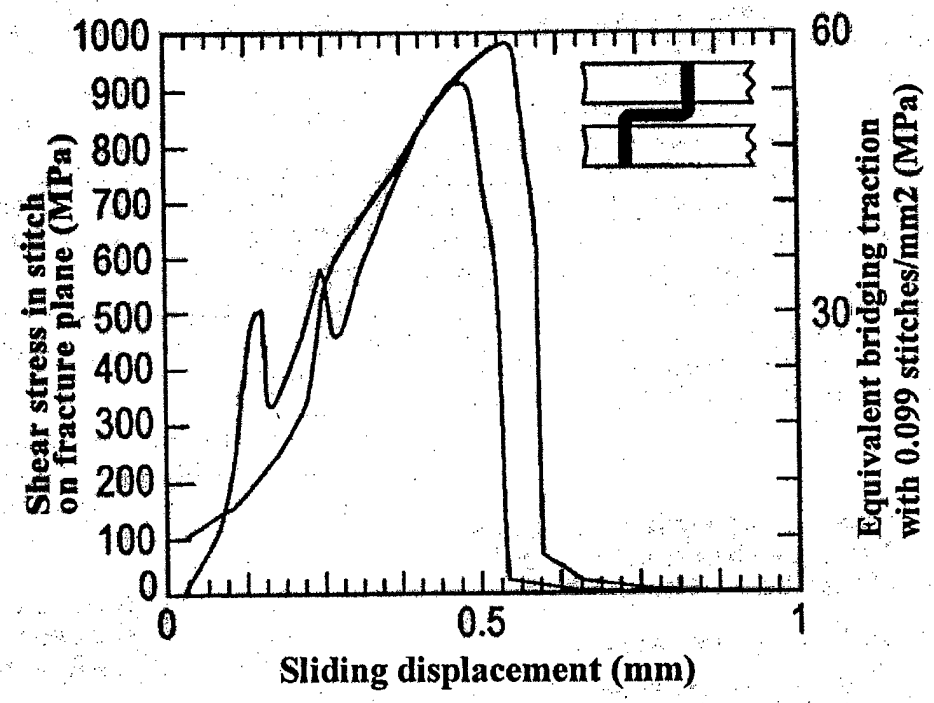
1000
900
800
700
600
500
400
300
200
100
0
Shear stress in stitch on fracture plane (MPa)
60
30
Equivalent bridging traction with 0.099 stitches/mm2 (MPa)
0
0.5
1
Sliding displacement (mm)

FIGURE 16

reinforcement percentage and fiber orientation for the different layers. This type of structure should allow for a significant weight reduction in comparison with similar metallic shields, while the overall energy absorption is expected to satisfy the application requirements that, taking into account the train mass, are very severe.

The first phase of the research activity has been devoted to the experimental characterization of the proposed material, with particular attention to the interface between the composite layer and the foam. To this aim a number of quasi-static and impact tests have been run both on tensile and bending specimens of the composite laminates and on square plates of the whole sandwich.

The second phase of the research activity has been devoted to the finite element modeling of the characterization tests run in the first phase. The purpose of this second phase was to assess the capability of the FE code material model to simulate the experimental tests and to define the input data for the material constants required by the chosen material model. The third and final phase of the research activity has been dedicated to the study of the shield structure impact behavior by means of finite element analysis. The FEM simulation was performed with the explicit code PAM-Crash.

Delamination and Dynamic Response of Through-thickness Reinforced Delaminated Composites

Roberta Massabò[1] and Luigi Brandinelli[2]

[1]Department of Civil Engineering
McCormick School of Engineering and Applied Science
Northwestern University
Evanston, IL

[2]Department of Structural and Geotechnical Engineering
University of Genova
Genova, Italy

The paper deals with different aspects of the mechanical behavior of delaminated composites in the presence of bridging mechanisms such as those developed by a through-thickness reinforcement (stitching, z-pinning or weaving). We will present our recent work on the problems of mode I and mixed mode large scale bridging delamination and the dynamic response of through-thickness reinforced delaminated beams. The problem of mode I and mixed mode large scale bridging delamination is treated using the weight function method in terms of stress intensity factors at the crack tip. The model accounts for the orthotropy of the material and allows us to investigate problems characterized by very short cracks or bridging mechanisms acting close to the crack tip. The influence of the through-thickness reinforcement on the fracture behavior is investigated and unusual phenomena of crack arrests and crack propagation in the presence of regions of contact that have been observed in the experiments are predicted theoretically and explained [1]. A beam theory model has been formulated to analyze the role played by linear bridging mechanisms in reducing the delamination-induced degradation of the dynamic properties of laminated beams. The model follows the formulation proposed in [2] for

delaminated beams in the absence of bridging mechanisms. An application of the model to a typical stitched carbon epoxy-laminate shows that a low area fraction of through-thickness reinforcement can substantially reduce the degradation of the natural frequencies of the structure.

[1] Massabò, R., Brandinelli, L., and Cox B.N., (2002) Mode I Weight Functions for an Orthotropic Double Cantilever Beam, accepted for publication in Int. J. Engineering Science.

[2] Luo H., Hanagud S. (2000),Dynamics of delaminated beams, Internatinal Journal of Solids and Structures, Vol. 37, pp.1501-1519.

The authors were supported by the European Research Office of the US Army, Contract # N68171-01-M-5909, and by the Italian Department for the University and for Scientific and Technological Research.

Contact Between a Cylindrical Indenter and a Sandwich Beam with Functionally Graded Core

Nicoleta A. Apetre and Bhavani V. Sankar

Department of Aerospace Engineering
Mechanics and Engineering Science
University of Florida
Gainesville, FL 32611-6250

In this paper we analyze the problem of indentation of a sandwich beam by a rigid cylindrical indentor. The core is assumed to be functionally graded with stiffness properties varying through the thickness. The contact problem is solved using the assumed contact stress distribution method. Relations are derived for load-contact length, load-indentation, and maximum stresses and strains in the core for functionally graded cores as well as homogeneous core. The results will be useful in answering the question if FG cores have an advantage over homogeneous cores when a sandwich panel is subjected to low-velocity impact.

The core/ face sheet delamination is a major concern in sandwich laminate construction. The stiffness discontinuity at the face sheet and core interface results in a large increase in shear stresses. While the core material itself

15th ASCE Engineering Mechanics Conference
June 2-5, 2002, Columbia University, New York, NY

FREE VIBRATIONS OF THROUGH-THICKNESS REINFORCED DELAMINATED BEAMS

Luigi Brandinelli [1] and Roberta Massabò [2]

ABSTRACT

The dynamic behavior of laminated beam-type structures presenting delaminations is characterized by stiffness degradation, natural frequency shifts and opening modes during vibration. This paper investigates the influence of a through-thickness reinforcement on the natural frequencies of through-width delaminated beam. A model based on the theory of bending of beams is formulated where the reinforcements are modeled as a uniform distribution of linear springs able to react to longitudinal and transversal relative displacements between the surfaces of the delamination. The natural frequencies of a delaminated cantilever beam are predicted for different lengths of the delamination. The effectiveness of the through thickness reinforcement on the natural frequencies is demonstrated through the transition from damaged (unbridged) to intact beam values upon increasing the stiffness of the springs. An application of the model to a typical stitched carbon-epoxy laminate for aeronautical applications shows that low percentages of through-thickness reinforcements can substantially improve the dynamic response of delaminated beams.

Keywords: Through-thickness reinforcement, delamination, natural frequencies, beam theory, dynamics.

INTRODUCTION

Delamination is one of the most common failure mechanisms of laminate composite materials. Besides being known as major cause of stiffness and strength degradation, delamination is also known to cause a change in the dynamic behavior. Extensive experimental and theoretical investigations have demonstrated that delaminations can cause shifts and/or extra natural frequencies which can approach the exciting frequencies. Additionally, delaminations can cause changes in modal shapes. Conditions causing the opening of delaminated surfaces in modal shapes, so-called "opening modes", have been experimentally detected and theoretically reproduced (Wang et al., 1982; Shen and Grady, 1992; Luo and Hanagud, 2000).

The efficacy of the through-thickness reinforcement technology (stitching, z-pinning, weaving) in enhancing the delamination strength and damage tolerance of composite laminates has been abundantly documented in the last twenty years. In particular, it has been proven how small percentages of reinforcements can increase interlaminar fracture toughness, shear and compressive strength after impact (Dransfield et al., 1994). On the other hand, to the knowledge of the authors, the efficacy of through-thickness reinforcements in limiting the delamination-induced degradation of the dynamic properties has not yet been investigated. It is reasonable to assume that through-thickness reinforcements can reduce the degradation of the dynamic properties by opposing the relative displacements between the delamination surfaces.

[1] Dept. of Structural end Geotechnical Engineering, University of Genoa, Italy. E-mail: brandinelli@diseg.unige.it

[2] Dept. of Civil Eng., McCormick School of Engineering and Applied Science, Northwestern University, Evanston, IL 60208. E-mail: r-massabo@northwestern.edu

A simple model based on laminated beam theory has been devised in order to study the role played by through-thickness reinforcements on the dynamic response of delaminated composite beam. Following the approach described in Luo and Hanagud (2000), a through-width delaminated beam has been modeled by using four elementary beams connected at the delamination edges. The action of the reinforcement has been represented by a uniform distribution of linear elastic springs able to oppose longitudinal and transversal relative crack displacements (Massabò and Cox, 1999). The constitutive law of the springs describes the load transfer mechanisms from the reinforcements to the surrounding material and is assumed as a model input. Although a more general formulation of the model could be based on a nonlinear spring constitutive law, in the present work a linear relationship has been assumed, which is an acceptable assumption for most through-thickness reinforced laminates provided the crack displacements are not too high (Cox et al., 1997). The model assumes bending/extensional coupling in the laminate constitutive description, and accounts for the effect of inertia in the moment dynamic equilibrium equation of the beam. Shearing deformation effect is neglected. Through this approach, delaminations of different lengths and at different sites, both thickness-wise and length-wise, can be analyzed.

The model has then been used to predict the effect of through-thickness reinforcements for a wide range of geometric configurations, reinforcement stiffness values and material parameters of the composite laminate. Finally, an application of the model is presented to simulate the dynamic response of a stitched carbon-epoxy laminate for aeronautical applications. In this case, the appropriate stiffness value for the linear elastic springs has been deduced from the experimental data in Cox et al. (1997).

THEORETICAL MODEL

The model refers to the scheme shown in Fig.1 representing a laminated beam of length L and thickness t with a through-width delamination of length L_{del}. Linear bridging mechanisms acting along the surfaces of the delamination are represented in the model by means of uniformly distributed linear elastic springs, with stiffness k_v in the transverse direction and k_t in the longitudinal direction. Plane strain conditions parallel to plane x-y are assumed and the problem is solved by applying the theory of bending of beams.

The delamination identifies four beams, for $i = 1, \ldots 4$, of length L_i, thickness t_i, distance of the centroid from the delaminated surfaces h_i and cross sectional area and moment of inertia S_i and I_i. The generalized displacements are the transverse displacement, w_i, the axial displacement, u_i, and the bending rotation, ϕ_i, and the stress resultants per unit width are the normal force, N_i, shear force, Q_i and bending moment, M_i, for $i = 1,.., 4$ (Fig. 2).

Equations of motion and constitutive equations are defined for the four beams and a boundary value problem is set up in terms of the generalized displacements (see Appendix I). The problem generally requires a numerical solution. However, a closed-form solution can be obtained based on the following assumptions:

1) mid-plane delamination;
2) homogeneous material;
3) absence of opening modes: the transverse displacements of the two delaminated beams coincide, that is $w_2 = w_3 = w$.

Assumption 2 is evidently satisfied not only by all isotropic and orthotropic homogeneous materials but also by unidirectional lay-ups made of the same type of orthotropic lamina and

laminates with many layers and no bending/extensional coupling. Quasi-isotropic laminates typically used for aeronautical applications and cross-plies [0/90] belong to this category. Assumption 3, is usually satisfied if the delamination is not too close to the surface of the beam, as observed by Luo and Hanagud (2000), and is commonly referred to as "constrained model" assumption.

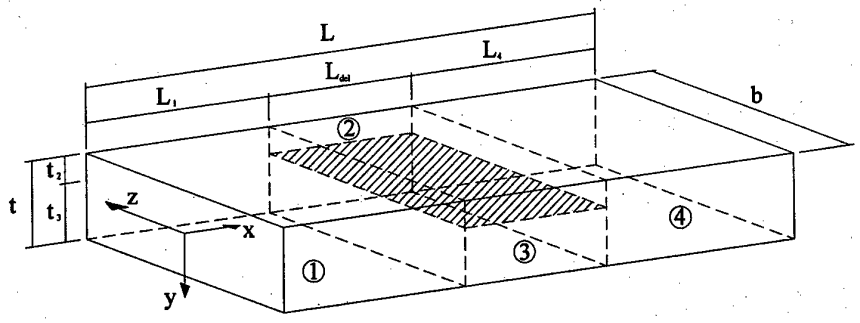

FIG. 1: Scheme of the four-beam model for a delaminated beam.

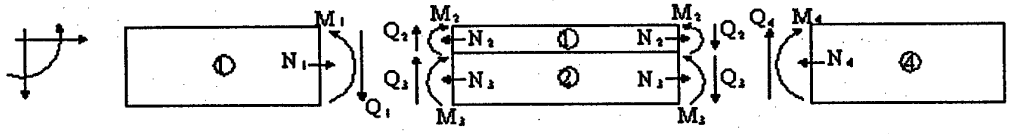

FIG. 2: Sign convention for stress resultants and displacements.

Assuming a free harmonic vibration characterized by a single angular frequency ω, $u_i(x,t)=u_i(x)e^{j\omega t}$ and $w_i(x,t)=w_i(x)e^{j\omega t}$ for i = 1, ..4, the problem is defined in terms of the relative axial displacement amplitude, $u_r = u_2 - u_3$, and the transverse displacement amplitude, *w*, of the beams 2 and 3 and by the axial and transverse displacement amplitudes of the beams 1 and 4.

It is convenient to formulate the problem in a dimensionless form introducing the normalized coordinate $\xi = x / t$ and the normalized amplitude displacements $\hat{u}_r = u_r / t$ and $\hat{w} = w / t$, for the delaminated beams, and $\hat{u}_i = u_i / t$ and $\hat{w}_i = w_i / t$, with i = 1,4, for beams 1 and 4. The other dimensionless variables are the spring stiffness β and the eigenvalue ψ defined as:

$$\beta = k_t t / E_1 \quad \text{and} \quad \psi = \frac{\rho\omega^2 t^2}{E_1} \tag{1}$$

where E_1 is the effective longitudinal Young's modulus of the beam and ρ is the density. The boundary eigenvalue problem is then defined by the following equations:

$$\begin{cases} \begin{cases} \hat{u}_1{}_{,\xi\xi} + \psi\hat{u}_i = 0 \\ \hat{w}_i{}_{,\xi\xi\xi\xi} + \psi\hat{w}_i{}_{,\xi\xi} - 12\psi\hat{w}_i = 0 \end{cases} & i = 1...4 \\ \hat{u}_r{}_{,\xi\xi} + (\psi - 4\beta)\hat{u}_r + 2\beta\hat{w}_{,\xi} = 0 \\ \hat{w}_{,\xi\xi\xi\xi} - (12\beta - \psi)\hat{w}_{,\xi\xi} - 48\psi\hat{w} = 24\beta\hat{u}_r{}_{,\xi} \end{cases} \qquad (2)$$

The continuity conditions at the first delamination edge $\xi = L_1/t$ are:

$$\hat{w}_1 = \hat{w}, \qquad \hat{w}_{1,\xi} = \hat{w}_{,\xi}, \qquad \hat{u}_2 = \hat{u}_1 + \frac{t}{4L}\hat{w}_{1,\xi}, \qquad \hat{u}_3 = \hat{u}_1 - \frac{t}{4L}\hat{w}_{1,\xi}$$

$$M_1 = M_2 + M_3 - \frac{t}{4}N_2 + \frac{t}{4}N_3, \qquad Q_1 = Q_2 + Q_3, \qquad N_1 = N_2 + N_3$$

while those at the other edge $\xi = L_2/t$ (with $L_2 = L_1 + L_{del}$) are:

$$\hat{w}_4 = \hat{w}, \quad \hat{w}_{4,\xi} = \hat{w}_{,\xi}, \qquad \hat{u}_2 = \hat{u}_4 + \frac{t}{4L}\hat{w}_{4,\xi}, \qquad \hat{u}_3 = \hat{u}_4 - \frac{t}{4L}\hat{w}_{4,\xi}$$

$$M_4 = M_2 + M_3 - \frac{t}{4}N_2 + \frac{t}{4}N_3, Q_4 = Q_2 + Q_3, \qquad N_4 = N_2 + N_3$$

The boundary conditions of a cantilever beam are:

$$\hat{w}_1 = 0, \qquad \hat{w}_{1,\xi} = 0 \qquad \text{at}\,\xi = 0$$

$$M_4 = 0, \qquad Q_4 = 0 \qquad \text{at}\ \xi = 1.$$

The solution procedure is outlined in Brandinelli and Massabò (2001). The natural frequencies and the corresponding modal shapes of the delaminated beam are calculated through the analytical integration of the eigenvalue problem (2). It is worth noting that for very low and very large values of β, the normalized stiffness of the ligaments, a high numerical precision is required in the solution.

Under these assumptions, the proposed model has been validated by referring to the asymptotic frequency values obtained by letting the spring stiffness vanish (thus simulating the absence of reinforcement) and indefinitely grow (absence of delamination). For a vanishing spring stiffness, the experimental tests of Shen and Grady (1992), on delaminated cantilever beams without a through-thickness reinforcement, have been successfully reproduced (Brandinelli and Massabò, 2001). Luo and Hanagud (2000) used the same tests to validate their beam model. For very high spring stiffness, the frequency values predicted by the model approach the values corresponding to an intact beam.

If assumption 1 (mid-plane delamination) is removed, the procedure outlined above is no longer applicable. It is still possible however to proceed with a numerical integration of the differential eigenvalue problem described in Appendix I, based on relaxation techniques (Keller, 1968). The system of differential equations (A4) is approximated by finite-difference equations and the multidimensional Newton-Raphson method is used for the iteration scheme.

FREE VIBRATIONS OF THROUGH-THICKNESS REINFORCED BEAMS

The model described in the previous section has then been used to systematically determine the role played by through-thickness reinforcements in reducing the delamination-induced degradation of the dynamic properties of through-width delaminated cantilever beams.

The dimensionless formulation of the problem allows the definition of the calculated natural frequency f of the delaminated beam, normalized with respect to the corresponding intact beam value f_0, as a function of the dimensionless stiffness of the ligaments $\beta = k_t t / E_1$, the normalized length of the delamination, L_{del}/L, the normalized length of the beam, L/t and a parameter describing the position of the delamination along the length, $(L_1 + L_{del}/2)/L$. The chart shown in Fig.3 refers to the first natural frequency, a mid-plane delamination, $L/t = 50$ and $(L_1 + L_{del}/2)/L = 0.5$. The three curves in the diagram refer to three different values (0.25, 0.50 and 0.75) of the L_{del}/L ratio. For very small values of β the curves tend to the normalized frequencies of the delaminated beam in the absence of through-thickness reinforcement. As expected, the curves show a transition from the damaged and unbridged values to the values corresponding to an intact beam upon increasing the elastic spring stiffness.

The diagram also shows the values of f/f_0 corresponding to a typical stitched carbon/epoxy laminate composite for aeronautical applications (Cox et al., 1997). The composite has a quasi-isotropic lay-up (48-plies [45/0/-45/90]) and a thickness of 7.2 mm. The reduced longitudinal Young's modulus is E_1 = 49 GPa, and in-plane Poisson's ratios are $\nu_{12} = \nu_{21}$ = 0.3. The laminate was stitched with doubled 3650 denier S-2 glass fiber tows on a square array of side 3.2 mm; the individual stitch area is 0.636 mm^2 and the total stitch area fraction is c_s = 0.062.

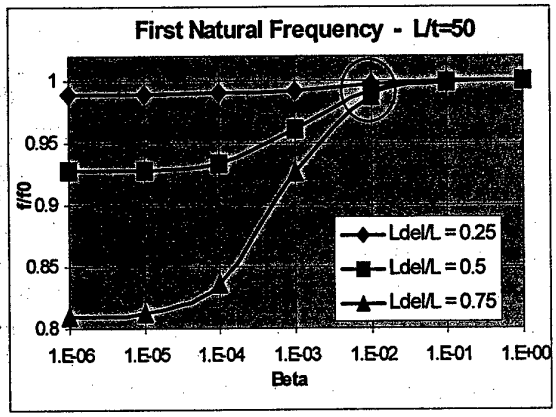

FIG. 3. Normalized first natural frequency as a function of the normalized stiffness of the reinforcement, $\beta = k_t t / E_1$, for three normalized delamination lengths.

Experimental shear tests have been performed by Cox et al. (1997) in order to define the constitutive relationship, load versus crack sliding displacement, of a single reinforcement. The experimental data showed a linearly increasing branch followed by a nonlinearly decreasing one at large sliding displacement corresponding to the failure of the reinforcement. Based on this observation the experimental data can be approximated with a linear bridging law describing the first branch. The equivalent normalized stiffness for

the spring distribution of the model has been calculated as being equal to $\beta \approx 0.01$.

In the diagram, a circle is used to highlight the solutions corresponding to this case. They show that low area fractions of through-thickness reinforcements can substantially reduce the delamination-induced degradation of the dynamic properties of the beam. For a delamination with L_{del}/L = 0.5, the through thickness reinforcement takes the value of the first natural frequency from 0.93 f_0 back to 0.994 f_0 with a 7% relative increment. Moreover, the effectiveness of the through-thickness reinforcements on the frequency heightens upon increasing the normalized length of the delamination. Analyses carried out for different values of the normalized length of the beam L/t show that the effectiveness of the reinforcement increases upon raising the L/t ratio.

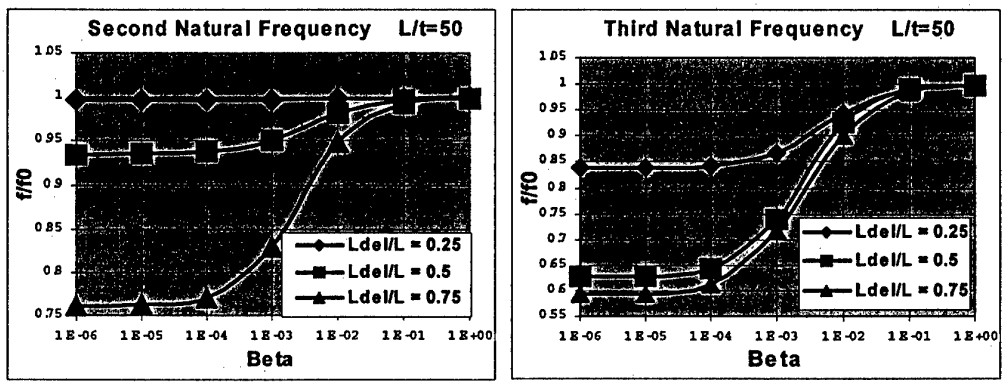

FIG. 4. Normalized second and third natural frequencies as a function of the normalized stiffness of the reinforcement, $\beta = k_t t / E_1$, for three different normalized delamination lengths.

Figure 4 shows diagrams of the second and third natural frequencies. As already noted in experimental tests on damaged composites (Kimpara et al. 1998) the damage primarily affects the frequencies of high-order vibration modes. For the case L_{del}/L = 0.5, for instance, the damaged value (unbridged) of the third natural frequency is 63% of the corresponding intact value, while the damaged value of the first frequency is 93% of the intact value. The model proposed here also shows how the influence of the bridging mechanisms acting along the crack is more evident on the frequencies of high-order modes. For the stitched-carbon epoxy laminate described above and L_{del}/L = 0.5, for instance, the through-thickness reinforcements induce a 43% relative increment on the damaged value of the third frequency and only a 7% increment on the first frequency. This observation can be useful for the design of dynamic experimental tests to investigate the properties of through-thickness reinforcements through the solution of an inverse model.

CONCLUSIONS

A theoretical model has been proposed to evaluate how the translaminar reinforcement can limit the effects of delaminations on the dynamic response of beam structures. The model is based on laminated beam theory and includes the effect of the inertia in the beam's moment dynamic equilibrium equations. Effect of shearing deformation is neglected. The action of

reinforcements is simulated through a uniform distribution of linear-elastic springs that are able to counteract the relative transversal and longitudinal displacements between the surfaces delineating the delamination. Assuming no extensional/bending coupling in the beam constitutive equations and absence of opening modes, the model has been applied to the case of a delaminated cantilever beam for different delamination lengths. The effectiveness of the through-thickness reinforcement on reducing natural frequency shifts has been demonstrated through the transition from damaged to intact beam values upon increasing the stiffness of the springs. The application of the model to a laminate composite reinforced through the thickness by stitching and previously tested by the authors, has shown that low percentages of through-thickness reinforcements can substantially improve the dynamic response of delaminated beams.

ACKNOWLEDGMENTS

The authors would like to acknowledge support from the European Research Office of the U.S. Army, contract number N68171-01-M-5909 to the University of Genoa, and from the Italian Department for the University and for Scientific and Technological Research.

REFERENCES

Brandinelli L. and Massabò R. (2001), "Dynamic response of delaminated beams in the presence of through-thickness reinforcements," (in Italian) proc. of the 15th AIMETA Conference of the Italian Association of Theoretical and Applied Mechanics, Taormina, Italy, ISSN 1592-8950.

Cox, B.N., Massabò, R., Mumm, D.R., Turrettini, A., Kedward, K., (1997), "Delamination Fracture in the Presence of Through-Thickness Reinforcement," Proceedings of ICCM, Gold Coast, Australia, 1-159 – 1-177.

Dransfield, K. Baillie, C., Mai, Y.W. (1994), "Improving the Delamination Resistance of CFRP by Stitching – a Review," Composite Science and Technology, **50**, 305-317.

Shen M.-H.H., Grady J.E. (1992), "Free vibrations of delaminated beams," AIAA Journal, **30** (5), 1361-1370.

Keller, H.B. (1968), Numerical Methods for Two-Point Boundary Value Problems, Waltham, MA: Blaisdell.

Kimpara, I, Kageyama, K, Suzuki, T and Ohsawa, I. (1998), "Simplified and unified approach to characterization of compressive residual strength of impact damaged CFRP laminates," Key engineering materials, Trans Tech Publications, Switzerland, **141-143**, 19-34.

Luo H., Hanagud S. (2000), "Dynamics of delaminated beams," International Journal of Solids and Structures, **37**, 1501-1519.

Massabò R., Cox B.N. (1999), "Concepts for bridged mode II delamination cracks," J. Mech. Phys. Solids, **47** (6), 1265-1300.

Massabò R., Mumm D., Cox B.N. (1998), "Characterizing mode II delamination cracks in stiched composites," Int. Journal of Fracture, **92** (1), 1-38.

Wang J.T.S., Liu Y.Y., Gibby J.A. (1982), "Vibration of split beams," Journal of Sound and Vibration, **84** (4), 491-502.

APPENDIX I.

The differential equations of axial, transversal and rotational motion for beams 1 and 4 can be simply written as

$$N_{i,x} = \rho S_i u_{i,tt} \qquad Q_{i,x} = \rho S_i w_{i,tt} \qquad -Q_i + M_{i,x} = \rho I_i \varphi_{i,tt} \qquad i = 1,4 \qquad (A1)$$

where partial differentiation with respect to the spatial variable x and time t is denoted by a comma. For the delaminated beams the equations of motion include the contribution of the action performed by the springs:

$$\begin{cases} N_{2,x} + k_t(u_3 - h_3\varphi_3 - u_2 - h_2\varphi_2) = \rho S_2 u_{2,tt} \\ N_{3,x} - k_t(u_3 - h_3\varphi_3 - u_2 - h_2\varphi_2) = \rho S_3 u_{3,tt} \\ Q_{2,x} + k_V(w_3 - w_2) = \rho S_2 w_{2,tt} \\ Q_{3,x} - k_V(w_3 - w_2) = \rho S_3 w_{3,tt} \\ -Q_2 + M_{2,x} + k_t h_2(u_3 - \varphi_3 h_3 - u_2 - \varphi_2 h_2) = \rho I_2 \varphi_{2,tt} \\ -Q_3 + M_{3,x} + k_t h_3(u_3 - \varphi_3 h_3 - u_2 - \varphi_2 h_2) = \rho I_3 \varphi_{3,tt} \end{cases} \tag{A2}$$

The constitutive equations of the laminated beam can be written in the following form:

$$N_i = A_i u_{i,x} + B_i \varphi_{i,x} \qquad M_i = B_i u_{i,x} + D_i \varphi_{i,x} \tag{A3}$$

where A_i and D_i represent the axial and bending stiffness respectively, and B_i is the extension/ bending coupling coefficient. Using the relation $\varphi_i = -w_{i,x}$, and introducing the quantities $m_i = \rho S_i$, $J_i = \rho I_i$, the governing equations of the model are

$$\begin{cases} \left.\begin{aligned} &A_i u_{i,xx} - B_i w_{i,xxx} = m_i u_{i,tt} \\ &D_i w_{i,xx} - B_i u_{i,xxx} - J_i w_{i,xxtt} + m_i w_{i,tt} = 0 \end{aligned}\right\} i=1,4 \\ A_2 u_{2,xx} - B_2 w_{2,xxx} + k_t(u_3 + h_3 w_{3,x} - u_2 + h_2 w_{2,x}) = m_2 u_{2,tt} \\ A_3 u_{3,xx} - B_3 w_{3,xxx} - k_t(u_3 + h_3 w_{3,x} - u_2 + h_2 w_{2,x}) = m_3 u_{3,tt} \\ D_2 w_{2,xx} - B_2 u_{2,xxx} - k_t h_2(u_{3,x} + h_3 w_{3,xx} - u_{2,x} + h_2 w_{2,xx}) - J_2 w_{2,xxtt} - k_v(w_3 - w_2) + m_2 w_{2,tt} = 0 \\ D_3 w_{3,xx} - B_3 u_{3,xxx} - k_t h_3(u_{3,x} + h_3 w_{3,xx} - u_{2,x} + h_2 w_{2,xx}) - J_3 w_{3,xxtt} + k_v(w_3 - w_2) + m_3 w_{3,tt} = 0 \end{cases} \tag{A.4}$$